Layer-by-Layer Design of Nanofiltration Membranes

Entwicklung von "Layer-by-Layer" Nanofiltrationsmembranen

Von der Fakultät für Maschinenwesen der
Rheinisch-Westfälischen Technischen Hochschule Aachen
zur Erlangung des akademischen Grades eines Doktors
der Ingenieurwissenschaften genehmigte Dissertation

vorgelegt von
Daniel Menne

Berichter:
Univ.-Prof. Dr.-Ing. Matthias Wessling
Adjunct Professor Dr.Ir. N.E. Nieck Benes

Tag der mündlichen Prüfung: 25.01.2017

für Claudia
für Nora und Ella

für meine Eltern

Abstract

In this thesis, a new kind of a stable nanofiltration membrane is discussed. The fabrication is based on polyelectrolyte (PE) adsorption in a sequential manner using a layer-by-layer (LbL) technique on porous ultrafiltration membranes of polymeric or ceramic nature. A new coating method involving constant flux permeation enables precise tailoring of the performance in terms of retention and permeability of the resulting membranes. The stability of the new membranes is superior to commercially available nanofiltration membranes and its performance is competitive. Regeneration, i.e. deconstruction and rebuilding of the polymeric LbL film, is demonstrated on a ceramic multichannel support. It allows the reuse of the highly stable but also expensive ceramic support.

Zusammenfassung

In dieser Arbeit werden neuartige Nanofiltrationsmembranen basierend auf Polyelektrolyt Adsorption untersucht. Hierbei werden negativ und positiv geladene Polyelektrolyte abwechselnd mittels des "Layer-by-Layer" (LbL) Verfahrens auf poröse Polymer- und Keramikmembranen aufgebracht. Die Trenneigenschaften und die Permeabilität der resultierenden Membranen lassen sich präzise einstellen indem die Polyelektrolyte bei konstantem Flux permeiert werden. Die sich ergebenen Membranen sind bei ähnlichen Trenneigenschaften in Bezug auf ihre Stabilität den heutzutage erhältlichen Nanofiltrationsmembranen überlegen. Des Weiteren wurde die Regenerierung von LbL Membranen untersucht, wobei der Polyelektrolyt Film vom keramischen Träger entfernt und anschließend wieder wird neu aufgebaut wird. Dadurch wird die Wiederverwendung des sehr stabilen aber auch teuren keramischen Trägers ermöglicht.

Contents

1 Introduction

One of the world's greatest challenges in the coming decades will be adequate water supply, even in regions considered "water-rich" [1]. Water treatment research focuses on not only salt retention but also on the separation of micropollutants such as pesticides, hormones, pharmaceuticals or endocrine disrupting compounds. An alternative for conventional water treatment methods is nanofiltration which successfully retains most of the micropollutants, thus preventing their accumulation during the production of drinking or produced water [2–7]. Today's membranes are thin-film composites made from polyamides assembled on a porous support by interfacial polymerization. However, the membranes suffer from low chemical stability, as the polyamides are not stable in the presence of hypochlorite which is commonly used for membrane cleaning. Furthermore, these membranes are mostly produced in flat sheet geometry and packed into spiral-wound modules. Such modules are often not backwashable, which is an additional desired strategy for membrane cleaning, and the packing density is lower than in hollow fiber membrane modules.

A promising alternative to conventional polyamide films is polyelectrolytes (PE) assembled using a layer-by-layer (LbL) technique. Due to the ionic nature, LbL films assembled onto porous support membranes show selective transport of monovalent over bivalent ions: Through the number of layers, their macromolecular nature, and their charge, PE multilayer membranes can be tailored to have the designed proper-

ties for water-softening applications, such as nanofiltration membranes [8–14].

Within this study a new coating method – coating at constant flux condition – for LbL assembly on polymeric hollow fibers is presented in Chapter 4. It is shown for the very first time that the mass of PE transported convectively towards the surface of the membrane determines the membrane properties. The method is used to tailor membrane performance in a precise way. Thus, the molecular weight cut-off, ion retention, and permeability of various coated LbL membranes are discussed in Chapter 5.

In Chapter 6 the newly demonstrated coating method presented in Chapter 4 is adapted to tubular ceramic monoliths as the support membrane. Due to the high stability of the LbL film and of the ceramic support, a new extremely stable nanofiltration membrane was fabricated. The stability of the LbL membranes is discussed further in Chapter 7. This chapter also discusses the regeneration – i.e. deconstruction and rebuilding of the LbL film – in an applicable manner for real treatment plants.

Finally, the use of LbL membranes for three separation tasks demonstrates their use as an adequate replacement for conventional nanofiltration membranes in Chapter 8.

2 State of the art

2.1 Layer-by-Layer technique with polyelectrolytes

Layer-by-Layer (LbL) assemblies comprise cationic and anionic polyelectrolytes (PE) adsorbed in a sequential manner into ultra-thin films, as shown in Fig.2.1 [17, 18]. The adsorbed single layers are in the range of a few nanometers. The thickness, structure, and thus the properties of the LbL films are tailored by various parameters: PE type, its molecular weight and concentration, the ionic strength and pH of the coating solution, adsorption time, coating method and number of layers. [19–26]. The following section gives an overview on various PEs, coating parameters and methods, and how they influence the layer build-up. The section is based on a review by Seantier and Deratani [27] and has been complemented with further studies.

Parts of this chapter have been either published in "Daniel Menne, Johannes Kamp, John Erik Wong, and Matthias Wessling. Precise tuning of salt retention of backwashable polyelectrolyte multilayer hollow fiber nanofiltration membranes. Journal of Membrane Science, 499:396–405, 2016" or in "Daniel Menne, Cagri Üzüm, Arne Koppelmann, John Erik Wong, Chiel van Foeken, Fokko Borre, Lars Dähne, Timo Laakso, Arto Pihlajamäki, and Matthias Wessling. Regenerable Polymer/Ceramic Hybrid Nanofiltration Membrane Based on Polyelectrolyte Assembly by Layer-by-Layer Technique. Journal of Membrane Science, 520:924 – 932, 2016"

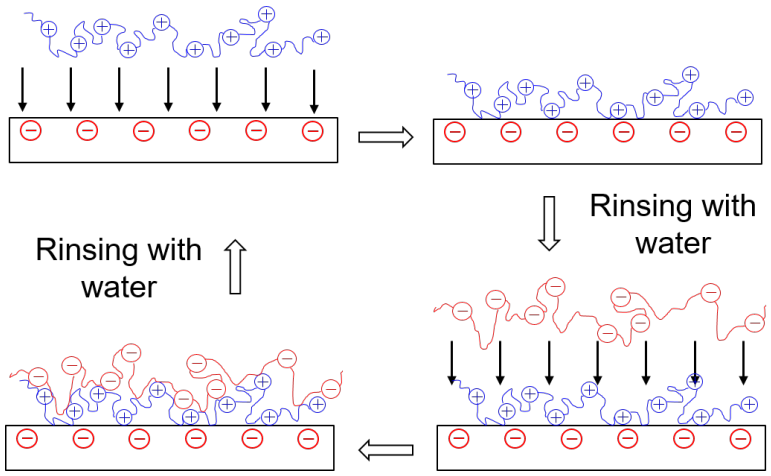

Figure 2.1: Alternating adsorption of polyelectrolytes on a negatively charged surface in sequential manner

Applied polyelectrolytes PEs are long-chain molecules with a molecular weight of several kDa that have a functional group within the repeating unit that dissociates in water to a polycation or polyanion – i.e. a positively or negatively charged PE. They can be grouped into strong and weak PEs: Strong PEs dissociate independently of pH, whereas the degree of dissociation is a function of pH for weak PEs. Regularly employed strong polyelectrolytes are polydiallyldimethylammonium chloride (PDADMAC) and polystyrene sulfonate (PSS). Commonly used weak PEs are poly(allylamine hydrochloride) (PAH), polyethylenimine (PEI), and polyacrylic acid (PAA). In this study, only PDADMAC as polycation and PSS as polyanion are employed.

PE multilayer film characterization As the film's thickness is just in the nanometer range, the characterization is not trivial. However, some techniques enable the characterization of PE multilayer films. Ellipsometry and reflectometry determine the refractive index and the mass per surface area that adsorbs on the surface. From this data, the layer thickness can be calculated [28–30]. Another commonly

used technique to detect the adsorbed mass is quartz crystal microbalance (QCM), as the adsorbed mass correlates with the frequency of the quartz crystal resonator [31–33]. With X-ray photoelectron spectroscopy (XPS) the elemental composition of the adsorbed film can be determined [31, 34, 35], while UV-VIS spectroscopy is applied to determine specific groups within the PE [31, 36]. Fluorescence spectroscopy, together with confocal laser scanning microscopy (CLSM), determines the distribution of a fluorescence-labeled PE within the PE film [37]. Finally, atomic force microscopy (AFM) fulfils two tasks: It provides data about the morphology of the film [38, 39] and it can be employed to quantify the interaction between the PE and the surface [40, 41].

Most of these techniques cannot be used with membranes. To assess the layer build-up on various materials, Rouster [42] worked on "mimicry" surfaces and compared the results with model surfaces such as silicon wafer. For instance, a thin film of Plexiglas (trademark of bulk poly(methylmethacrylate) (PMMA)) was coated onto a silicon wafer and this was used for LbL film assembly. During the first few layers, the growing behavior of LbL films on Plexiglas deviated slightly from the one on the silicon wafer, while the overall trend in the growing behavior was comparable.

Coating parameter and how it affects film properties Next to the PE type, the ionic strength within the coating solution is the most important parameter that defines the structure and morphology of the assembled film [20, 21, 24]. In case of low ionic strength, the charge compensation is between the polyanion and the polycation. This is called the intrinsic charge compensation. Increasing the ionic strength leads to extrinsic charge compensation. Now, the charge compensation is favored by the counter ions [43]. That means, in case of high

ionic strength, the charge screening of the PEs occurs predominantly through the counter ions, resulting in coiled and more flexible PE conformation (already in solution) [19]. The film assembly at high ionic strength accompanies with thicker, more open, and more mobile layers [26]. These open layers exhibit larger pores for permeation. According to the Hagen-Poiseuille equation (Equation 2.1), the permeability of the LbL film increases due to the bigger pores. However, higher ionic strength is also reflected in thicker layers. The layer thickness contributes to the resistance as well, which leads to a decrease in the permeability. Thus, it is hard to predict whether the permeability increases or decreases due to the ionic strength in the PE solution. Antipov et al. [20] reported for PSS/PAH multilayer films a decrease in permeability with increasing ionic strength whereas de Grooth et al. [30] observed the opposite for PDADMAC/PSS films.

$$J = \frac{{r_p}^2 \Delta p}{8\eta \frac{\Delta x}{A_k}} \tag{2.1}$$

For weak PEs, the pH of the coating solution is of major importance. Depending on the pH, weak polyelectrolytes are either fully or just partly dissociated, which defines the morphology and structure of the assembled film. Thereby, the observed layer thickness varied as a function of the pH between 0.5 and 8 nm for PAH/PAA films [44]. The pore size of PSS/PAH multilayer films was reported to be about 0.34 nm, assembled at pH 1.7 and without any additional salt [45]. At pH 2.6 with 0.5 mol/l of NaCl, the same PEs yielded a pore size of 0.8 to 1 nm [46], demonstrating the importance of pH, particularly for weak PEs.

Coating methods The generally used method for LbL film assembly is based on adsorption from a liquid phase by dipping, spin-coating, or

spraying [25, 27, 47–49]. Adsorption time is the major parameter that controls the layer build-up during dip coating. Due to electrostatic forces, the PEs are transported by diffusion to the surface, where they finally adsorb until the plateau of the adsorption isotherm is reached [26]. During spin coating, the surface is spinned while the PE solution is added to the surface. The rotating speed and the PE concentration significantly influence the layer thickness, and can even be predicted by a power law relationship [50]. In case of spraying, the major parameter that needs to be controlled is the spraying rate and time.

In considering membranes from flat geometries, all the mentioned coating methods could be applied. However, most studies involving flat sheet membranes focus on dip coating [35, 36, 38, 51–54], while spray [55] and spin coating [56, 57] are rarely employed. For hollow fiber and tubular membranes, as applied in this study, dipping can be employed when the film should be assembled on the outer wall of the membrane [30]. Tang et al. [55] demonstrated a combination of spray and spin coating by turning a ceramic tubular substrate and through simultaneous spraying of the PE solution onto the outer side of the membrane. For LbL films that should be constructed on the lumen side, none of the mentioned techniques is feasible. In this case, static and dynamic coatings come into play. Static coating is similar to dip coating, except that in the case of hollow fiber or tubular membranes, the coating solution must first be pumped into the lumen of the membrane and this must be followed by the adsorption step. After a certain adsorption time, the lumen is flushed with pure water to remove the PE solution and the excess PEs that are just loosely bound. During dynamic coating, an additional flow perpendicular to the membrane surface is applied [58]. Thus, the PEs are transported to the surface by not only diffusion but also convection. Dynamic coating is more

efficient, as fewer layers are required to achieve the same performance. In Chapter 4, a new coating method of constant flux is demonstrated. Controlling the flux rather than the pressure during dynamic adsorption, as it is found elsewhere [36, 38, 54, 58, 59], enables precise tailoring and engineering of the properties of the resulting membranes.

Three zone model The three zone model was developed to explain the growth behavior of PE multilayer films, which is either linear or exponential in thickness. Within the initial linear growth regime the PEs from the solution do not diffuse into film that is the already constructed (Zone I in Figure 2.2a). Thus, the increment of film thickness is just due to the additional adsorbed layer. After a certain number of linear assembled layers, some PE types cause exponential thickness growth (Figure 2.2b). Within this regime, PEs from the solution penetrate the film of Zone III. For some PEs, this exponential growth transforms, after some more layers, into linear growth for further assembled layers (Figure 2.2c). It was supposed that the PEs within Zone II hinder diffusion deeper into the film due to a restructuring process within Zone II. In this situation, Zone III does not grow further; rather, it moves upward as Zone II grows linearly [27, 60].

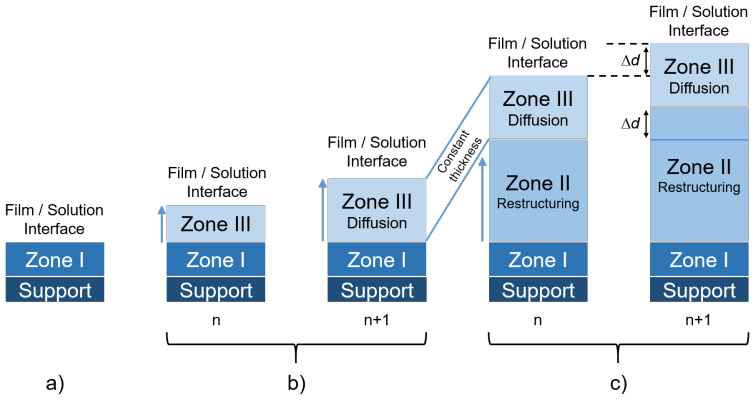

Figure 2.2: The three zone model for linear and exponential growth of LbL films. a) Linear growth for low layer numbers, impact of the surface still present. b) Exponential growth, impact of the surface is no longer present. c) Linear growth for many assembled layers. Adapted from Porcel et al. [60].

2.2 LbL in membrane application

Several techniques for membrane modification are commonly used. By grafting, the polymer backbone of the membrane is irreversibly chemically altered to enhance membrane performance and reduce fouling [61]. Using hydrogels or microgels, pH or temperature stimuli-responsive membranes are prepared [62, 63]. With plasma treatment, membranes can be hydrophilized, resulting in a lower affinity to fouling [64]. However, these methods are either not applicable on large scale or involve environmentally unfriendly chemicals. In contrast, LbL technology is based on aqueous soluble polymers and can be employed on every geometry, and potentially, on any scale.

LbL films on membrane supports can be sorted into three groups with various functions: a) LbL as a separation layer, b) LbL for fouling reduction [53], and c) LbL to incorporate additional functions, such as catalytic activity by use of metal nanoparticles or enzymes [65]. This

study deals with group a) only: the use of LbL technology to tailor the separation performance of a membrane. Hence, this section gives an overview about this topic only.

LbL films assembled onto porous support membranes show selective transport of monovalent over bivalent ions and are thus applied for nanofiltration [8–14, 25, 30, 38, 59, 66]. Depending on the chosen PEs and the coating parameters, even reverse osmosis [67], gas separation [68], and pervaporation membranes for water and alcohol separation [36, 54, 69] can be realized by LbL technique.

Recently, some new developments have emerged: The Vankelecom group demonstrated that the number of PE bilayers could be reduced to just a few to obtain already a defect-free layer, thus making a potential up-scaling feasible. In particular, the question of how quickly a membrane can be made has been addressed in order to reduce the number of processing steps from 20 to 80 down to six [70].

In terms of nanofiltration and reverse osmosis membranes, the stability of an LbL film is of great interest, as most of the existing nanofiltration membranes do not withstand oxidizing media, such as sodium hypochlorite (NaOCl), and can be employed in only a limited pH range (pH 3-10). De Grooth et al. [71] demonstrated that polyelctrolyte multilayer based on PDADMAC and PSS, the same system used in the present study, are stable in the presence of NaOCl. The Kentish group reports an LbL-based membrane with sulfonated polysulfone (sPSf)/ polyallylamine hydrochloride (PAH) and PSS/PAH layers crosslinked with glutaraldehyde (GA) [67]. In comparison to a standard polyamide-based nanofiltration or reverse osmosis membrane, the crosslinked membranes show much better stability toward NaOCl, with comparable performance in terms of flux and retention. Hence, LbL-based membranes are also relevant because of their potential chemical

stability during disinfection treatment.

As the stability of certain PE multilayer films is rather high, LbL was also employed for organic solvent nanofiltraiton. Therefore, PDADMAC/sulfonated poly(ether ether ketone) (SPEEK) and PDADMAC/PAA were assembled on a solvent-resistant support – polyacrylonitrile (PAN) – and used for the separation of Rose Bengal, Acid Fuchsine, and Bromothymol Blue from various organic solvents [35, 72, 73].

Another interesting approach is the use of LbL as so-called sacrificial layers. The LbL film can be regenerated by rigorous deconstruction and rebuilt afterward. Ahmadiannamini et al. [74] proposed an approach to dissemble PE films for polymeric flat sheet membranes: In case of weak PEs, low or high pH, followed by Triton X-100 (non-ionic surfactant to disrupt the non-ionic interactions between LbL film and substrate), should be applied, whereas strong PEs are removed just by Triton X-100. Ilyas et al. [75] demonstrated the effective removal of weak PEs by a trigger consisting of low pH (pH 3) and high ionic strength (3 M $NaNO_3$) from dense ultrafiltration membranes. However, the presented membrane was not pH stable. In Chapter 7 the regeneration of pH and backwash-stable ceramic LbL membrane is discussed.

2.3 Nanofiltration applications

Nanofiltration (NF) is a pressure driven membrane process that is located between ultrafiltration (UF) and reverse osmosis (RO). NF membranes have typically an MWCO between 200 and 1.000 Da and are selective for monovalent over multivalent ions [76]. The following section gives a brief overview about the most important NF applications and is based on the book "Nanofiltration: Principles and Applications"

written by A.I Schäfer, A.G. Fane, and T.D. Waite [7]

Water treatment More stringent regulations of drinking water productions among other things contributed to a growing interest in NF processes within the field of water treatment. Especially maximum contamination levels for trace components (small organic molecules, such as disinfection by-products, pesticides, endocrine disrupting compounds (EDC), and pharmaceutically active compounds) in the water resulted in a shift from coagulation processes to membrane filtration. These micropollutants can be retained by NF [77, 78] while they pass conventional water treatment plants [2, 3]. Thus nanofiltration can be applied not only for water softening [79–81] and removal of dissolved organic components (such as natural organic matters (NOM)) [80] but also for micropollutant rejection.

The membrane selection is done by the feed water quality. The most important parameters to characterize the quality of the feed water are pH, total dissolved solids (TDS), ion concentrations (sulfate, chloride, nitrate, calcium, etc.), color, total organic carbon (TOC), turbidity, and the silt density index ((SDI, for more information on the SDI follow reference [82–84]). Besides membrane performance, the process performance depends also on the system design, including recovery rates as well as pre- and posttreatment. The commonly used membrane modules for water treatment are spiral wound modules, whereas tubular membrane modules are preferably applied for small plants due to lower requirements for the pretreatment.

Food industry NF is commonly applied in the dairy [85] and the sugar [86, 87] industry. In the dairy industry, whey concentration by NF is the state of the art process and the most successful membrane application within the food industry. For sugar concentration

and purification, NF can have a significant economic advantage over conventional treatment processes, such as evaporation, crystallization, and ion-exchange chromatography. The requirements for the system design and the membranes for application in food industry differ from those for water treatment as special efforts for a sanitary design must be taken.

Industrial application Chemical [88], pulp and paper [89, 90], and textile [91, 92] industry are the major branches where NF is regularly applied. Within chemical industry, NF can be applied in the production process to separate the desired product from the side and waste products but also to discharge the pollutions flows from the production processes. In pulp and paper as well as in textile industry, a large amount of water is employed. Reuse of the water is desired due to the water scarcity in the world but leads to accumulation of the undesired substances. Thus the water must be treated before reuse which can be realized with NF. In pulp and paper industry, dissolved extractives, sugars, multivalent ions, and chloride must be removed from the water. Effluents from the textile industry contain a high loading of dyes together with salts at a high temperature of about 50-60°C at a pH of about 11.

2.4 Mass transfer in nanofiltration membranes – A model for membrane characterization

In 1997 Bowen et al. [93] proposed a model to characterize nanofiltration membranes. The model is based on the extended Nernst-Planck equation (Equation 2.2). It enables obtaining three parameters that

characterize the membrane: 1) the pore radius r_p, 2) the ratio of the effective layer thickness Δx to the porosity A_k, and 3) the charge density X. To obtain these parameters, a fit of the presented model to the measured retention and permeability is required.

$$j_i = -D_{i,p}\frac{dc}{dx} - \frac{z_i c_i D_{i,p}}{RT} F \frac{d\Psi}{dx} + K_{i,c} c_i J \tag{2.2}$$

j_i is the flux of species i while the terms on the right-hand side represent the transport by diffusion, electro-migration, and convection. In the present study, the model is used only for uncharged solutes; hence the electro-migration term can be neglected and Equation 2.2 can be simplified to Equation 2.3. Due to this simplification, only the parameters r_p and $\frac{\Delta x}{A_k}$ are obtained.

$$j_i = -D_{i,p}\frac{dc}{dx} + K_{i,c} c_i V \tag{2.3}$$

$$D_{i,p} = K_{i,d} D_{i,\infty} \tag{2.4}$$

The diffusive and convective transport is hindered by the pore size of the membrane. This reflects in the hindrance factors $K_{i,c}$ and $K_{i,d}$ both of which are functions of λ, the ratio of solute radius r_s to pore radius r_p. The hydrodynamic coefficients K^{-1} (enhanced drag coefficient) and G (lag coefficient) are based on a finite-element analysis [93].

$$\lambda = \frac{r_s}{r_p} \tag{2.5}$$

$$K^{-1}(\lambda, 0) = 1 - 2.3\lambda + 1.154\lambda^2 + 0.244\lambda^3 \tag{2.6}$$

$$G(\lambda, 0) = 1 + 0.054\lambda - 0.988\lambda^2 + 0.441\lambda^3 \tag{2.7}$$

These coefficients were used for $0 < \lambda < 1$. For $\lambda > 1$ – i.e. the solute is bigger as the membrane pore – full retention was assumed. Assuming

a fully developed parabolic flow profile within the pores the hindrance factors are determined with Equation 2.8 and 2.9 [93]:

$$K_{i,d} = K^{-1}(\lambda, 0) \tag{2.8}$$

$$K_{i,c} = (2 - \Phi)\ G(\lambda, 0) \tag{2.9}$$

$$\Phi = (1 - \lambda)^2 \tag{2.10}$$

Integrating Equation 2.3 from $x = 0$ to $x = \Delta x$ with the concentrations $c_{i,F}$ and $c_{i,P}$ at $x = 0$ and $x = \Delta x$ respectively, gives an expression for the retention R_{real} (Equation 2.11). R_{real} describes a theoretic retention without any impact due to concentration polarization. However, the retention used to fit the model was affected by concentration polarization. Thus, the fit must be conducted with the observed retention R_{obs}, as it takes into account limitations due to concentration polarization (Equation 2.12).

$$R_{real} = 1 - \frac{c_{i,P}}{c_{i,F}} = 1 - \frac{K_{i,c}\ \Phi}{1 - exp(-Pe_m)[1 - K_{i,c}\ \Phi]} \tag{2.11}$$

$$ln\left(\frac{1 - R_{obs}}{R_{obs}}\right) = ln\left(\frac{1 - R_{real}}{R_{real}}\right) + \frac{J}{k} \tag{2.12}$$

Where Pe_m the Peclet number is:

$$Pe_m = \frac{K_{i,c}}{K_{i,d}}\ \frac{V\Delta x}{D_{i,\infty}A_k} \tag{2.13}$$

$$\tag{2.14}$$

The mass transfer coefficient k for hollow fiber membranes can be determined with Equation 2.15 using the Reynolds number Re and the Schmidt number Sc [94].

$$k = 1.86 \left(\frac{Re\ Sc\ d}{l}\right)^{0.33} \frac{D_{i,\infty}}{d} \tag{2.15}$$

$$Re = \frac{\rho d v}{\eta} \tag{2.16}$$

$$Sc = \frac{\eta}{\rho D_{i,\infty}} \tag{2.17}$$

d and l are the diameter and length of the hollow fiber membrane, respectively. For ρ, the density, and η, the viscosity, values for pure water at 25°C were used. The measurements to fit the model were conducted using a polyethylene glycol (PEG) solution (Section 3.3). The diffusion coefficient $D_{i,\infty}$ and the hydrodynamic radius r_s of PEG are both functions of the molecular weight M_w. They were calculated by formulas 2.18 and 2.19 (r_s in Å), respectively [95, 96].

$$D_{i,\infty} = 9.82 \times 10^{-9} M_w^{-0.52} \tag{2.18}$$

$$r_s = 0.1912\ M_w^{0.559} \tag{2.19}$$

Beside the mass transport of the solute the transport of the solvent (water) must be considered. Thus the Hagen-Poiseuille equation (Equation 2.20) was applied to determine the flux J for a given transmembrane pressure (Δp)

$$J = \frac{{r_p}^2 \Delta p}{8\eta \frac{\Delta x}{A_k}} \tag{2.20}$$

Finally, the measured retention and flux was fitted to the calculated retention with Equation 2.12 and the calculated flux using the Hagen-Poiseuille equation (Equation 2.20) to obtain the pore radius r_p as well as the ratio of the effective layer thickness to the porosity $\frac{\Delta x}{A_k}$. The retention for several PEGs with various molecular weights was employed.

The fitting was done by the least-squares method in MATLAB using the "lsqnonlin" function.

3

Materials and methods

3.1 Support membranes

Polymeric hollow fiber membranes The support membrane employed for LbL modification is a polyethersulfone-based (PES) ultrafiltration membrane (HFs) provided by Pentair X-Flow (Netherlands). Ten of those fibers were potted with a two-component epoxy resin into a module housing (Polyamide (PA) tube with 9 mm inner diameter and 12 mm outer diameter). Each fiber had a length of 40 cm and an inner diameter of 0.8 mm, resulting in a total membrane area of about 0.01 m^2 per module (Figure 3.1). The membranes have a pure water permeability of about 120 LMH/bar (LMH: liter per square meter and hour) and a separation skin with pores of about 10 nm on the lumen side: Tthe separation skin is negatively charged.

Parts of this chapter have been either published in "Daniel Menne, Johannes Kamp, John Erik Wong, and Matthias Wessling. Precise tuning of salt retention of backwashable polyelectrolyte multilayer hollow fiber nanofiltration membranes. Journal of Membrane Science, 499:396–405, 2016" or in "Daniel Menne, Cagri Üzüm, Arne Koppelmann, John Erik Wong, Chiel van Foeken, Fokko Borre, Lars Dähne, Timo Laakso, Arto Pihlajamäki, and Matthias Wessling. Regenerable Polymer/Ceramic Hybrid Nanofiltration Membrane Based on Polyelectrolyte Assembly by Layer-by-Layer Technique. Journal of Membrane Science, 520:924 – 932, 2016"

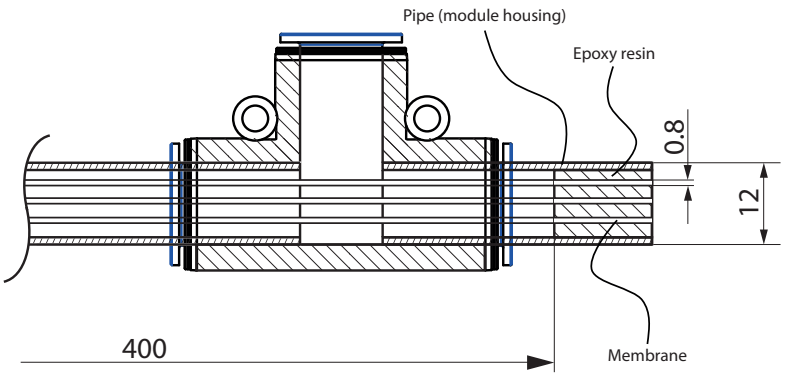

(a) Technical drawing of membrane module

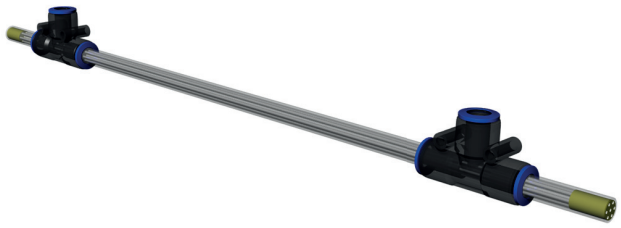

(b) 3D Drawing of membrane module

Figure 3.1: Membrane module with 10 PES membranes

Ceramic membrane monolith For LbL film assembly on ceramic membranes, a monolith produced by Metawater (Japan) and provided by RWB Water Services B.V. (Netherlands) was employed. The ceramic membrane is made from alumina with a nominal pore size of 100 nm. The untreated membrane shows a pure water permeability of about 1,100 LMH/bar. The monolith comprises 55 channels, each with a diameter of 2.5 mm and a length of 9.25 cm, resulting in a membrane surface of 0.04 m^2. Because of its material, the membrane

can withstand harsh chemical conditions, such as low and high pH, oxidizing agents, such as hypochlorite, and organic solvents. For usage, the monolith was mounted in a housing.

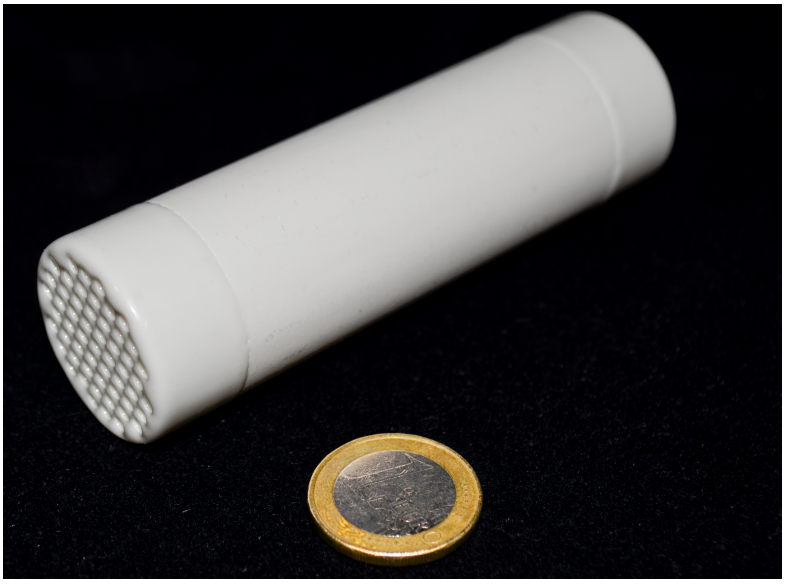

Figure 3.2: Ceramic membrane monolith comprising 55 feed channels

3.2 Coating

The polycation, polydiallyldimethylammonium chloride (PDADMAC) and the polyanion, poly(sodium 4-styrenesupolystyrene sulfonate (PSS) were purchased from Sigma Aldrich and Kemira. PDADMAC from Sigma Aldrich with a molecular weight of 400 to 500 kDa was used for the ceramic membrane while the one from Kemira with a molecular weight of 350 kDa was used for the polymeric HFs membrane. PSS with a molecular weight of 1000 kDa was used for both membranes. Furthermore, 1 g/l of the PE together with a certain amount of NaCl was diluted in ultra-pure water.

Before the coating was performed, the ceramic membranes were pretreated over-night with a 1,500 ppm sodium hypochlorite (NaOCl) so-

lution. The NaOCl cleaned and activated the surface to ensure better attachment of the first layer, leading to increased coating reproducibility. The polymeric membrane had to be wetted before coating. Therefore, the membrane module containing the hollow fiber membrane was submerged in a water and ethanol mixture (18 w%) for five hours.

In case of the ceramic membrane, the geometry of the membrane module accompanies a large dead volume on the feed and retentate side. To avoid complex formation between the polycation and the polyanion, the module had to be completely drained before and after each coating step. The coating procedure was conducted with the membrane module in vertical mode, with feed and retentate at the bottom and top, respectively. Due to this configuration, the module could be drained easily with an airflush at low pressure of less than 0.1 bar from retentate (top) to feed (bottom) (Figure 3.3a). The draining steps were executed immediately before and after each coating step, and were mandatory to ensure a perfectly reproducible coating. The exact procedure of preparing the LbL film is important and it needs to be performed with care [15]:

1. The lumen of the membrane is flushed at 3.5 l/h for 3 min for the polymeric and 5 min for the ceramic membrane with the first PE solution without any transmembrane pressure. The flow rate and time was optimized to ensure that the lumen is completely filled with the PE solution. However, this step must not be too long because as soon as the first PEs enter the lumen of the membrane the diffusive adsorption (static) starts.

2. Adsorption step of polyelectrolyte:

    a) In the case of diffusive coating (static) the PE solution remained for 10 min within the lumen of hollow fiber mem-

brane.

b) In the case of convective adsorption a constant flux – variable pressure – dead-end permeation with convection of the PEs to the surface of the membrane for a defined time at a defined flux was applied.

c) In the case of constant pressure – variable flux – adsorption the feed side of the membrane was connected to a constant pressure reservoir filled with the PE solution while the permeate flow rate was measured with a flow meter. The coating time was adjusted to pass a defined permeate volume.

d) In case of crossflow coating, a crossflow filtration with a certain feed, retentate, and permeate flow rater was conducted.

3. Only for ceramic membranes: Airflush from retentate (top) to feed (bottom) to drain the system in order to avoid complex formation.

4. Rinsing of the membrane's lumen from feed to retentate with deionized water to remove the excess PE at 8.5 l/h for 20 min. During this period, the PE present inside the lumen and loosely bound to the surface of the membrane will be removed. The conductivity of the deionized water used for this step and the next step was frequently measured. It was always between 1 and 2 μS/cm.

5. Permeation with deionized water to determine the pure water permeability / resistance after each deposited layer at constant flux for 10 min. The transmembrane pressure was measured and it reached, within this period, a plateau value to determine a

steady-state permeability.

6. Only for ceramic membranes: Airflush from retentate (top) to feed (bottom) to drain the system before the next PE is flushed into the module.

7. Repetition of the above steps but with the oppositely charged PE.

The coatings were performed with an OSMO Inspector built by Convergence Industry B.V. (Netherlands) (Figure 3.3a and 3.3b). The setup is equipped with Coriolis mass flow meter from Bronkhorst Cori-Tech B.V. (Netherlands) with an accuracy of about 0.2 %. The system is based on the work published in [97]. The temperature of the PE solution was not controlled but measured immediately before the PE entered the membrane module. It was always between 23 and 25 °C.

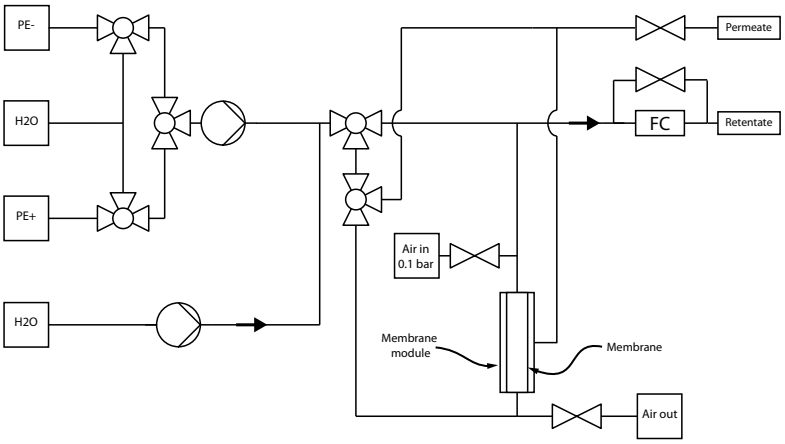

(a) Flowsheet

(b) OSMO Inspector

Figure 3.3: a) Flowsheet and b) picture of the OSMO Inspector as it was used for preparation of the LbL membranes.

Every coating – i.e. every set of parameters – was repeated at least twice or thrice times. In case of bigger deviations more repetitions were carried out. The error bars, as found in the figures, and the deviation, as stated in the tables, refer to the repetition of the coating on a new membrane module and not to a repetition of a single measurement. The emerging trends presented in the figures hence indicate the high quality and precision of the method described.

3.3 Retention and molecular weight cut-off (MWCO) measurements

The salt retention properties of the resulting membrane were determined through crossflow filtration with 5 mmol/l $MgSO_4$. This was performed at a crossflow rate of 1,000 l/h (Reynolds $\approx$ 3000) to ensure turbulent conditions and an absolute retentate pressure of 3.5 bar. By measuring conductivity of feed and permeate, the retention for $MgSO_4$ was calculated using $R = 1 - \frac{c_p}{c_f}$. As the correlation between the conductivity and the concentration is linear, the feed and permeate concentration (c_f, c_p) could be replaced by the conductivity of the feed and permeate, respectively. For the cut-off measurements, polyethylene glycol mixtures (PEG) with various molecular weights (200, 300, 400, 600 1000, 1500, 2000, 4000 Da, each 1 g/l) were used. The PEG's molecular weight distribution was brought allowing to determine a reliable cut-off – defined as the molecular weight that is retained by 90% – between 150 and 6,000 Da. The filtration for collecting the feed and permeate sample was conducted in the same way as explained above for the salt retention. The sample collection was carried out after four hours of continuous filtration and was analyzed using size exclusion chromatography (SEC) with water as the eluent. The retention curve was determined for each measured molecular weight.

$$R = 1 - \frac{c_p}{c_f} \tag{3.1}$$

3.4 Permeability

The permeability was monitored during the coating procedure after each layer at a constant flux 50 LMH, as explained in the detailed

description of coating process. The pure water permeability was measured as well before and after coating, and after each stability and regeneration method. The feed side was connected to a pressure vessel at 0.5 bar that was filled with deionized water, while the permeate was collected and weighted continuously. The temperature of the feed and permeate was determined as well. It was used for a viscosity-depended temperature correction of the permeability.

3.5 Stability measurements and methods for layer deconstruction

The stability of the coated membranes during backwashing was evaluated at a backwash pressure of 6 bar for 1 min. This reverse pressure level is significantly higher than during permeation. After each fifth backwash, the pure water permeability was re-measured. To further increase the shear forces, the backwash was superimposed with a simultaneous airflush on the lumen side of the membrane at 3 bar.

The chemical stability with regard to high pH was studied by submerging the membrane within a NaOH solution for a certain period. The concentration of the NaOH varied between 0.1 (pH 13) and 1 mol/l (pH 14). After a defined exposure time, the pure water permeability was re-measured to evaluate the stability.

The stability towards salt was evaluated by the filtration of a salt solution. The salt concentration was increased step-wise from 0.1 to 3 mol/l. Subsequent to the salt filtration, a pure water filtration was conducted to obtain irreversible changes of the membrane due to the salt filtration in advance.

More harsh treatment for the desired layer removal was performed with a highly concentrated 5 mol/l NaCl solution, and with cationic

and anionic surfactants, 2 mmol/l cetyltrimethylammonium bromide (CTAB) and 10 mmol/l sodium dodecyl sulfate (SDS), respectively. The surfactant concentration was above the critical micelle concentration (CMC) as it is suggested to be necessary for an effective layer disassembly [33]. The layer removal was studied in three ways: 1) rinsing of the chemical solution on the lumen side, 2) a backwash, meaning a filtration from permeate to feed, and 3) a backwash with a simultaneous air-flush on the lumen side of the membrane. For all treatment methods, 0.75 liters of solution were applied. To ensure a similar treatment time for the different methods, the rinsing was interrupted as soon as the module was completely filled with the treatment solution and paused for 5 min. After this period, the rest of the solution was flushed through the channels. The backwash and the simultaneous airflush were performed in the same way as explained above for the backwash stability measurement. More harsh treatment to fully recover the support membrane was achieved by RCA cleaning [98]. 450 ml water are mixed with 100 g 30% hydrogen peroxide and 150 g 20% ammonium hydroxide for the treatment of five ceramic supports. The ceramic supports are submerged with the solution for 15 min at 85 °C.

3.6 Scanning electron microscopy

Scanning electron microscopy (SEM) images were produced using a Hitachi S4800. The polymeric fibers were broken in liquid nitrogen, dried over-night, and sputtered with tungsten.

3.7 Benchmark study (Chapter 8.1)

To evaluate the performance of LbL membranes, a benchmark study on real waste water was conducted. The effluent from the waste water treatment plant in Kaarst (Germany) was brought to Aachen and filtered for a week. The facility in Kaarst is equipped with an ultrafiltration module for downstream processing; thus, the effluent that was used as feed in this study is the permeate of an ultrafiltration membrane. Three different membranes were tested: 1) LbL on a polymeric support, 2) LbL on a ceramic support, and 3) as the benchmark a commercially available spiral wound module NF270-2540 from DOW Filmtec. The LbL membrane based on the polymeric support (HFs) was coated at a flux of 30 LMH with 0.5 mol/l of NaCl in the PDADMAC/PSS solution. In total four bilayers were assembled. The ceramic LbL membrane comprised three bilayers coated at 30 LMH without salt in the PDADMAC/PSS solution followed by two bilayers with 0.5 mol/l NaCl in the coating solution coated at the same flux. The coatings were conducted as explained in Section 3.2

The filtration was conducted at 20°C, and the permeate and retentate have been recirculated to the feed reservoir. During one week of filtering, several feed and permeate samples were taken and analyzed for the following substances or parameters: total organic carbonate (TOC), anions (Cl^-, $SO_4{}^{2-}$), cations (Na^+, Mg^{2+}), and four different micropollutants (Table 8.2). The permeability was regularly measured to assess the flux decline due to fouling. The three different membranes were tested successively; hence, the feed water had to be renewed after each run. This resulted in fluctuations of the initial concentrations (Table 3.1). The highest initial concentrations were observed for the experiment with the NF270. The difference in the initial concentration might also influence the performance. Thus, the comparison just by

Table 3.1: Initial concentration for all analyzed compounds for the three conducted tests with the different membranes

	NF270	LbL/Ceramic	LbL/Polymeric
TOC [mg/l]	9.5	8.4	9.1
Na^+ [mg/l]	110	62	36
Mg^{2+} [mg/l]	25	17	11
Cl^+ [mg/l]	142	90	51
$SO_4{}^{2-}$ [mg/l]	125	68	40
Benzotriazole [μg/l]	1.33	3.84	2.34
Carbamezepine [μg/l]	0.79	0.38	0.26
Sulfamethoxazole [μg/l]	0.28	0.18	0.1
Diclofenac [μg/l]	3.96	1.32	1.19

this study might be misleading.

As the geometry of the three membranes differs a lot, the process parameters had to be adjusted to ensure comparable conditions. The initial transmembrane flux was 20 LMH for all membranes, resulting various transmembrane pressures due to the different pure water permeabilities of the membranes (Table 3.2). To ensure an equal flow pattern within the lumen of the membranes is rather difficult. Thus the crossflow rate was discussed with the manufacture of the support membranes.

Table 3.2: Process parameters for the three different membranes

	NF270	LbL/Ceramic	LbL/Polymeric
Module type	Spiral-wound	Tubular	Hollow fiber
Membrane area [m^2]	2.6	0.04	0.01
Feed flow [l/h]	650	400	9
Feed flow velocity [m/s]	0.19*	0.41	0.5
Reynolds	157*	1152	447
Feed pressure [bar]	2.5	2.2	2
Initial permeation flux [LMH]	20	20	20

* Determined by neglecting the spacers within the spiral-wound module that further increase turbulences.

4

Constant flux coating: A new coating method for precise membrane fabrication

Here, we report a systematic and rigorous description of a new constant flux LbL-fabrication process in the lumen of a polymeric hollow fiber membrane. The method is applicable for single and multiple bilayer polyelectrolyte (PE) films supported on the lumen side of hollow fiber membranes, based on controlled convective transport of PEs toward the surface of the membrane. The evidence reported below proves that the amount of PE transported to the membrane surface determines membrane properties, such as permeability and retention for bivalent ions. Controlling the flux rather than the pressure, as it is found elsewhere [36, 38, 54, 58, 59], enables the precise tailoring and engineering of the properties of the resulting membranes. The methods applied in the former mentioned studies and the method that is presented here share a common feature: Dynamic adsorption – i.e. a convective flow of PE toward the membrane surface – is involved. However, this study is the first one that performs the convective adsorption at constant flux. Furthermore static – i.e. without convective flux – and constant pressure coatings were applied for a comparison between the conventional coating method and the new suggested method at constant flux conditions.

This chapter is adapted from Daniel Menne, Johannes Kamp, John Erik Wong, and Matthias Wessling. Precise tuning of salt retention of backwashable polyelectrolyte multilayer hollow fiber nanofiltration membranes. Journal of Membrane Science, 499:396–405, 2016.

Table 4.1: Permeability and retention for $MgSO_4$ for static coatings – i.e. without convective flow – of a single bilayer made from PDADMAC and PSS at different polyelectrolyte concentration during the diffusive adsorption step.

PE concentration [g l^{-1}]	Pure water permeability [$\frac{LMH}{bar}$]	Retention for $MgSO_4$ [%]
1	45.8 ± 4	12.6 ± 2.7
10	39.5 ± 3.5	14.8 ± 2
15	37.4 ± 2.6	16.3 ± 1
25	41.3 ± 8.9	15.9 ± 0.6

4.1 Diffusive (Static) adsorption

The diffusive adsorption of PEs was studied as a benchmark experiment, as most of the prior literature used this method. PE concentration was between 1 and 25 g/l, and the adsorption time for all experiments was 10 min. The resulting membranes show nearly the same permeability and retention for $MgSO_4$ independent of the applied PE concentration. Results on planar surfaces suggest that the plateau region of the adsorption isotherm – i.e. maximum surface coverage – starts at low PDADMAC concentrations of about 1 g/l [21, 99], which was in this study the lowest applied concentration. Table 4.1 clearly shows that an increasing PE concentration does not influence the transport characteristics of a single bilayer. In order to increase the rejection properties of such membranes, normally multiple coatings of bilayers are required, with each of them causing the retention to increase while the flux decreases.

4.2 Convective (dynamic) adsorption in dead-end mode

Dead-end permeation at constant flux is a unique feature of the proposed fabrication method. The OSMO membrane system used allows the monitoring of the transmembrane pressure (TMP) rise that is established by the system in order to maintain the preset constant flux. The pressure increase can be recalculated into an apparent membrane resistance (Equation 4.1) as a function of the coating time. This is shown for three different coating fluxes (10, 20, and 30 LMH) in Figure 4.1.

The coating at a flux of 30 $\frac{l}{m^2\ h}$ (LMH) leads to a stronger increase in the overall resistance than the coating at 10 and 20 LMH. After the first convection cycle of the positively charged PDADMAC the lumen is flushed free of the PE solution and the resistance is measured again but now with deionized water to determine the resistance after the first layer deposition. The resistance during pure water filtration is significantly lower than the final resistance at the end of the previous coating step, suggesting that the origin of the resistance increase was partly removed. The subsequent pure water flux measurements, however, reveal a resistance significantly higher than the original unmodified membrane. We interpret this increased resistance as the fingerprint of the adsorbed PE. In fact, this remaining resistance for the pure water flux after the PE filtration scales with the flux used during the deposition period.

During the dead-end filtration of the PE solution, the concentration of the PE within the lumen of the fiber increases in time as a consequence of its rejection. For a coating at 30 LMH, the PE concentration increases to about 25 g/l in a time span of 10 min, assuming that all

PE chains are retained at the membrane wall and remain in solution. The static coatings applied at varied PE concentrations showed that this concentration increase does not affect the layer buildup if only diffusion is the origin of PE adsorption.

The increase in apparent resistance during filtration is related to the retention of the PE during filtration. Assuming that the PE system is fully dissociated, that all PEs and their counter ions remain in solution, and that they contribute ideally to the osmotic pressure, a rough estimation of the osmotic pressure can be taken (Equation 4.2). While the number of polymer chains is low, the number of counterions determines the magnitude of the osmotic pressure. The osmotic pressure would increase from 0.15 to 3.8 bar and from 0.12 to 3 for the PDADMAC and the PSS solution, respectively. The measured TMP at the end of the coating step was 4.6 for PDADMAC and 4.9 for the PSS (data not shown), which is in the same order of magnitude as the calculated osmotic pressure. This growing osmotic pressure during filtration of the PEs reduces the effective driving force (Equation 4.3): It also causes the membrane resistance to increase only apparently as shown in Figure 4.1, if not accounted for.

The above interpretation is only indicative: and the real situation is much more complicated. For strong PEs, such as PDADMAC and PSS, a large part of the counterions may be condensed on the polymer surface, as the distance between charges is smaller than the Bjerrum length (0.7 nm for room temperature). Hence, PDADMAC and PSS solutions deviate strongly from ideal behavior depending on polymer and salt concentration with measured osmotic coefficients between 0.1 and 0.6 [100–103]. The real osmotic pressure will be much lower than the theoretically calculated osmotic pressure above but it will still be in an order of magnitude that is not negligible. To perform a reliable cor-

rection of the apparent resistance for the osmotic pressure (Equation 4.3), a rigorous thermodynamic experimental analysis needs to be performed. Furthermore, concentration-dependent viscosity data would need to be incorporated, as first measurements showed a viscosity increase by a factor of four over the concentration range applied during PE filtration (data not shown). With these concentration-dependent solution properties, an instationary model could be developed by incorporating convective and diffusive flow in the lumen of the hollow fiber, and normally to the membrane surface.

During the second deposition step the resistance rises in a comparable manner and to a comparable degree. After the final flushing of the lumen, the resistance has significantly increased from about 2x10^{12} m^{-1} to 0.7x10^{13} - 3x10^{13} m^{-1}, depending on the coating flux. This increased resistance is the fingerprint of the deposited PE bilayer as it remains on the membrane because of the convective adsorption process. Later, backwashing data will show that this deposited layer is sufficiently strong for realistic membrane filtration applications.

$$R_{app} = \frac{TMP}{J\ \eta} \tag{4.1}$$

$$\pi = (c_{PE,polymer} + c_{counter\ ions})\ R\ T \tag{4.2}$$

$$R_{real} = \frac{TMP - \pi}{J\ \eta} \tag{4.3}$$

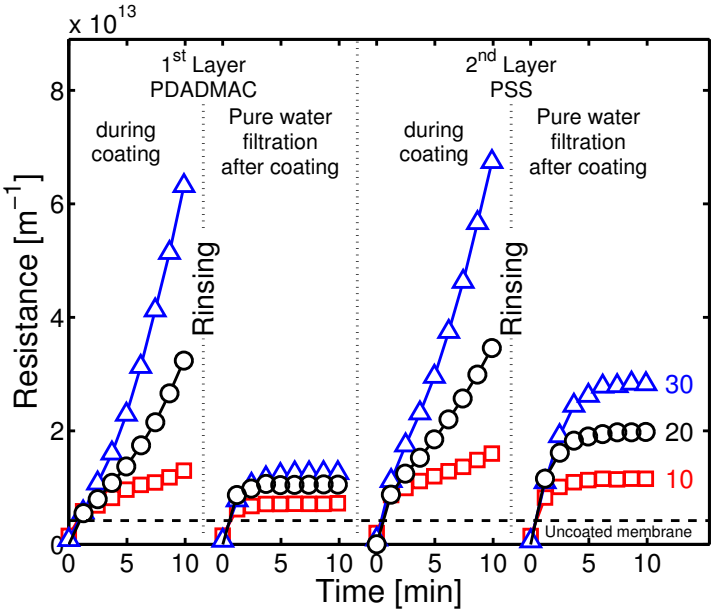

Figure 4.1: Membrane resistance as a function of time during coating and during pure water filtration after coating for varied coating fluxes of 10, 20, and 30 LMH over a constant coating time of 10 min. The dashed line represents the resistance of an uncoated membrane. The pure water resistance was measured for all coatings at a constant permeation flux of 15 LMH.

The data in Figure 4.1 is plotted as a function of time at different flow rates, but not as a function of the total permeated volume. In fact, it is instructive to represent this data as a function of the amount of PE retained inside the lumen of the hollow fiber as calculated with Equation 4.4, where J is the flux, t the coating time, and c_p the PE concentration in the feed solution. Three parameters can be varied to obtain the same amount of PE retained: flux, deposition time, and polyelectrolyte concentration. New measurements at different fluxes and at different permeation times are presented in Figure 4.2 for the (a) transmembrane pressure rise and (b) the resulting resistance. The intermediate pure water resistance measurements are not shown here. While the TMP-rise is a function of coating flux and time, the resis-

tance values coincide on a master curve for both PE. The apparent resistance during filtration scales with the mass of PE that is transported into the lumen of the hollow fiber, but is independent of the coating flux or coating time. Moreover, the feed-pressure level can be neglected as a potential parameter for the layer build-up since the pressure evolution differs for the coatings at the different flux levels. Possible compressing effects during layer build-up due to the pressure gradient between feed and permeate can, thus, be excluded.

To compare the results with the conventional coating methods, constant pressure coatings at 2 and 3 bar feed pressure were performed. Here, the permeation time was adjusted so that the permeated volume was identical to the coatings mentioned above. Also for constant pressure coatings the key driver is the retained PE mass. The resistance for the coatings at 2 and 3 bar constant coating pressure follows the same master curve as was observed for the constant flux coatings (Figure 4.2b).

With this surprisingly precise development of the overall resistance, we can now proceed to characterize the salt-retention properties of the new PE bilayer hollow fiber membranes.

$$\dot{m}''_{PE} = J\ t\ c_{PE} \tag{4.4}$$

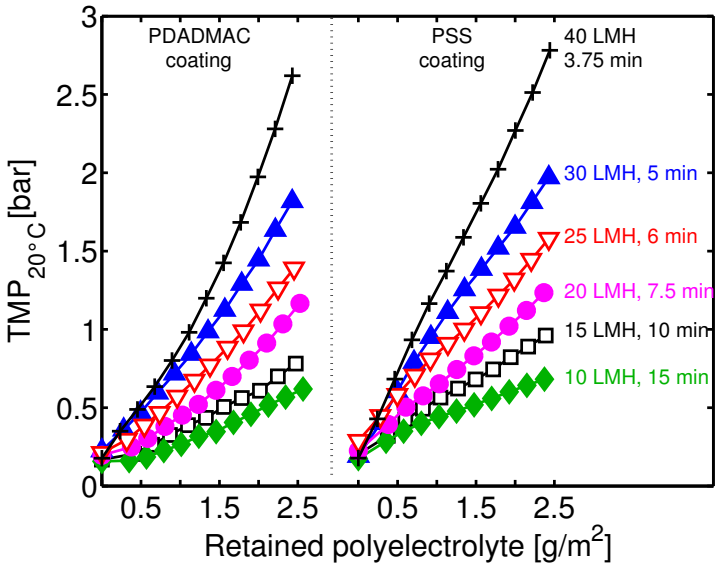

(a) TMP evolution during coating

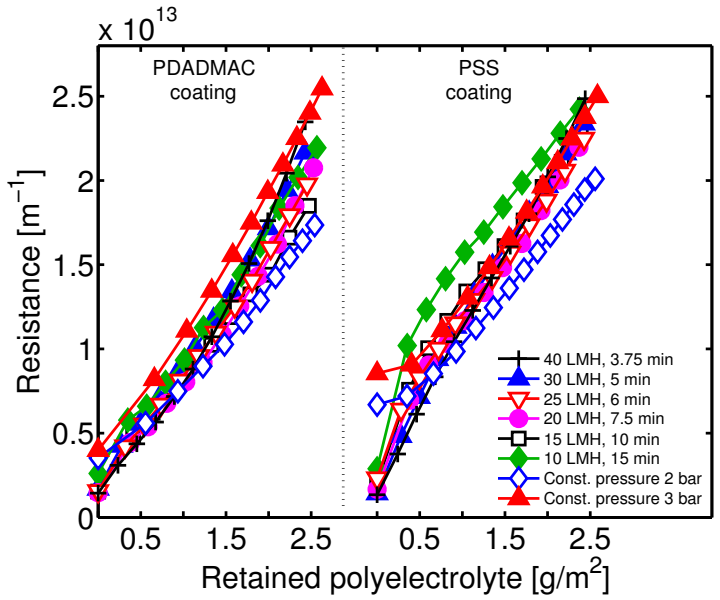

(b) Membrane resistance during coating

Figure 4.2: a) TMP evolution during coating as a function of the polyelectrolyte mass retained in the membrane lumen per membrane area. b) Development of membrane resistance during coating as a function of the polyelectrolyte mass retained in the membrane lumen per membrane area.

The membrane modules are exposed to a crossflow filtration with 5

mmol/l $MgSO_4$ and a retentate pressure of 3.5 bar (at turbulent condition at Reynolds $\approx$ 3000). The retention and pure water permeability of the LbL-modified membranes are shown in Figure 4.3. In Figure 4.3a, a set of experiments is shown where the coating time was kept constant at 10 min, but the permeation flux was varied between 0 and 30 LMH. Figure 4.3b depicts coatings at a constant permeation flux of 30 LMH, with a changing coating time between 2 and 10 min. In both cases, increasing coating flux and coating time result in increasing retention and decreasing permeability of the membrane. In Figure 4.4, the same data is represented but now as a function of the PE mass retained inside the lumen of the hollow fiber as calculated with Equation 4.4. Remarkably, the permeability (Figure 4.4a) and the retention (Figure 4.4b) develop similarly for varying flux and varying time. It also becomes clear that the properties of membranes prepared without convection adsorption (plotted in a first approximation as zero amount retained) are significantly different, having lower retentions and higher permeabilities. In order to obtain better retentions, convection is apparently a critical benefactor.

As already observed for the resistance during coating (Figure 4.2), the properties of the resulting membranes depend only on the mass of PE retained in front of the membrane surface. Therefore, we hypothesize that coating flux and coating time are interchangeable as long as the mass retained in front of the surface remains equal. To prove the unprecedented accuracy of our fabrication method, we characterized the membranes prepared for Figure 4.2. A predefined amount of PE was set through either a variation of flux or permeation time within a large window of preparation conditions. Furthermore, constant pressure coatings at 2 and 3 bar with the same amount of PE were applied (Figure 4.2b). The retention for $MgSO_4$ of these mem-

branes was 18.3±9.6% and 30.1±3.2% for the membrane coated at 2 bar and at 3 bar, respectively. These results are similar to the retention determined at constant flux condition (Table 4.2), suggesting that the key driver is the retained PE amount also for constant pressure coatings as well.

The results presented above are not in line with the accepted theory of charge compensation being the sole driving force for adsorption and determining the amount of PE that adsorbs onto the surface [26, 29, 34, 104]. At a membrane surface, but particularly under convective conditions, the mechanisms governing the thickness of the layers seem different. The amount of PE that adsorbs on the surface depends not only on the PE and substrate charge density but also on the amount that is convectively transported to the surface. According to the scanning electron images (Fig 4.5), the layers built up at 30 LMH resulted in a 20 to 30 nm thicker layer as compared to the static coated layers – i.e. more mass adsorbed. However, the layers are rather thick, as compared to values from other studies investigating layers assembled on flat surfaces, such as silicon wafers. The expected layer thickness of one bilayer is about 5 to 10 nm [26, 29]. The SEM images show a thickness of about 55 nm and 82 nm for the static coated and the constant flux coated membrane, respectively. One explanation for this discrepancy might be that the first (bi)layer penetrates into the porous structure, which is more pronounced for the dynamic coating resulting in a deeper penetration and thus a thicker layer. By assuming a thickness of 10 nm for one bilayer, the penetration depth would be about 40 nm and 70 nm for the static coating and the constant flux coating, respectively. The 16 layers give a total membrane thickness of about 140 nm. According to the literature a value of about 90 to 100 nm for PDADMAC/PSS layers at 0.5 mol/l NaCl can be expected

[26, 29]. Subtracting the penetration depth determined for the bilayer coating from the layer thickness of the 16-layer membrane result in a reasonable layer thickness of about 70 to 100 nm. However, from the SEM images, no direct conclusion about a potential penetration of the first bilayer can be drawn. Yet the thickness development of the subsequent coatings is very much in line with data from the literature.

The thicker layers of the dynamic-coated membrane, compared to the static-coated membrane correlates, appropriately with the highly reproducible retention and permeability results. The retention for layers built at dynamic conditions is higher while the permeability is lower. Furthermore, the SEM images suggest that the layer built up at dynamic conditions is denser and smoother than the layer assembled under static conditions. The constant flux coating should be self-regulating, forming quite a uniform layer. During the coating, the resistance might vary locally, leading to lower flux at locations of higher resistance, while there will be an increased flux at locations of lower resistance. As a consequence, the transport of PEs to the membrane surface will be more pronounced in parts where the resistance is still low, thereby increasing the resistance due to the adsorbing PE. This self-regulating mechanism might explain that the layer formed at constant flux permeation seems to be more uniform and dense as well as and smoother than the layer formed under static conditions. The increased thickness and greater uniformity, will contribute to better retention. This self-regulation mechanism may even have the potential to be used as a repair mechanism for aged reverse osmosis or nanofiltration membrane modules.

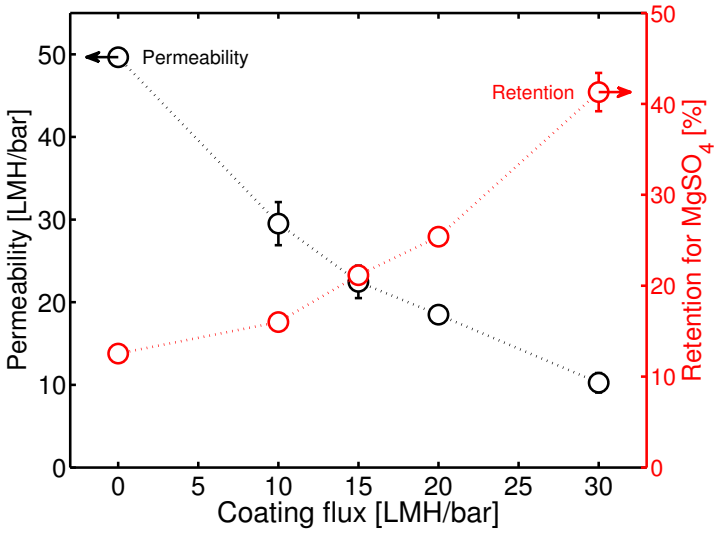

(a) Various coating fluxes

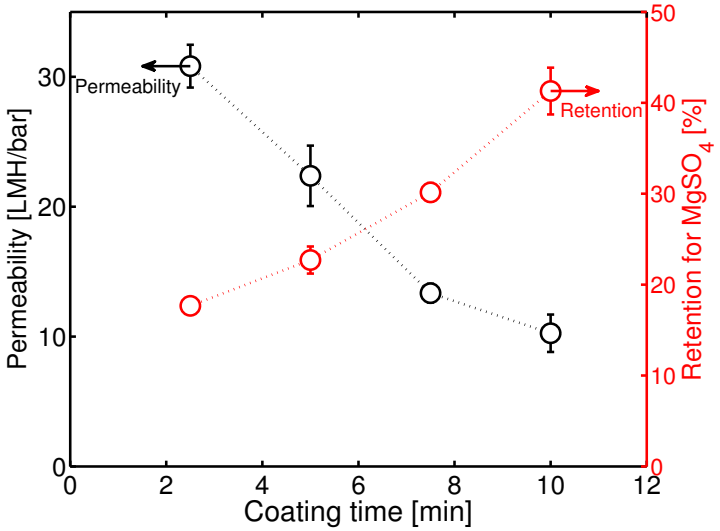

(b) Various coating times

Figure 4.3: a) Permeability and retention as a function of the coating flux for a constant coating time of 10 min. b) Permeability and retention as a function coating time for a constant coating flux of 30 LMH.

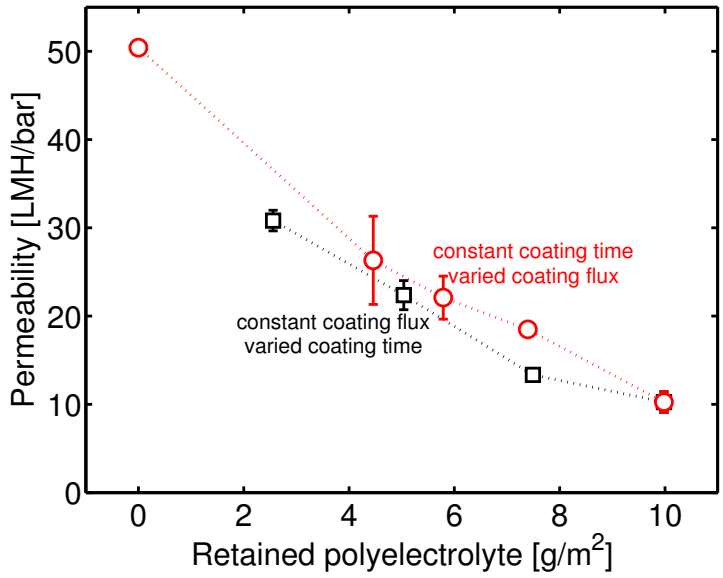

(a) Permeability

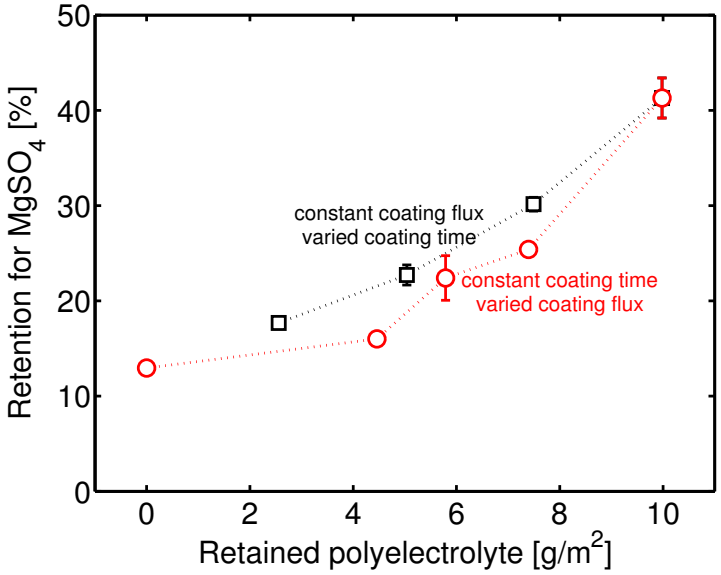

(b) Retention for $MgSO_4$

Figure 4.4: a) Permeability as a function of the total retained polyelectrolyte mass in the membrane lumen per membrane area as calculated with Equation 4.4. b) Retention as a function of polyelectrolyte mass retained per bilayer in the membrane lumen per membrane area as calculated with Equation 4.4. Red circles: constant coating time of 10 min and various coating fluxes between 0 and 30 LMH. Black squares: constant coating flux of 30 LMH and various coating times between 2.5 and 10 min

Table 4.2: Permeability and retention for $MgSO_4$ for coatings with various coating fluxes and coating times with the same amount of polyelectrolyte (PE) mass per bilayer retained in the membrane lumen per membrane area as calculated with Equation 4.4.

Coating flux [LMH]	Coating time [min]	PE mass retained per membrane area $[\frac{g}{m^2}]$	Pure water permeability $[\frac{LMH}{bar}]$	Retention for $MgSO_4$ [%]
10	15	5	22.5 ± 1.6	23.7 ± 2.8
15	10	5	21.2 ± 0.8	22.4 ± 2.0
20	7.5	5	21.5 ± 1.6	23.6 ± 0.8
25	6	5	21.5 ± 2.2	21.9 ± 0.2
30	5	5	22.8 ± 1.1	22.4 ± 1.7
40	3.75	5	24.6 ± 0.8	19 ± 0.5

In summary, the data shows that just one bilayer of polyanion and polycation is sufficient to prepare membranes with $MgSO_4$ retentions up to 45%.

4.3 Multilayer assembly at static and dynamic conditions

One can now extend the question and apply the methodology described above to multilayers instead of just a single bilayer. Static coatings and dynamic coatings at 10, 20, and 30 LMH were performed, but this time one to 10 bilayer were built up. The coating time was always 10 min. A plateau value of 80 to 90% for the retention for $MgSO_4$ is observed for all the different coatings (Figure 4.6a). For coatings at higher flux,

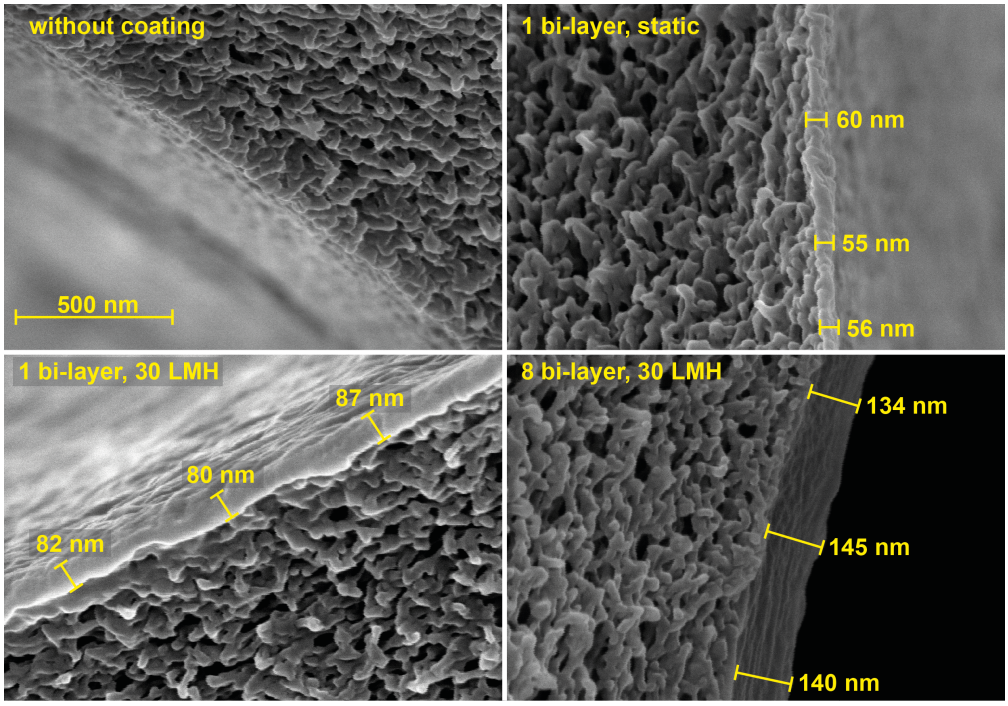

Figure 4.5: Scanning electron microscopy images of four different membranes: Upper left: without coating; upper right: one bilayer coated in static mode with an adsorption time of 10 min; bottom left: one bilayer coated in dynamic mode at 30 LMH for 10 min; bottom right: eight bilayers coated in dynamic mode at 30 LMH for 10 min

this plateau starts with fewer layers than coatings at lower flux or with just diffusive mass transport. An exact but inverse behavior can be observed for the pure water permeability (Figure 4.6b)). With a coating at high flux, the permeability drops after one bilayer to the plateau value while more layers are needed at lower flux or static coating to reach the same plateau.

The same data but now as a function of PE mass retained are depicted in Figure 4.7. The concept of the amount of PE transported to the surface to be the key parameter holds for multilayer coatings as well. Between 0 and about 20 g/m^2 retained PE mass, the development of the retention and permeability is rather similar regardless of

whether the coating was performed at high flux and with fewer layers or at lower flux and with more layers. Above 20 g/m^2, all coatings reached the plateau value for the retention. The permeability shows a minimum at about 20 to 30 g/m^2, whereas above this amount the permeability increases again. This might be explained by the overcompensation of PDADMAC, whereas PSS barely compensates charges in the subsequent adsorption step [29]. As a consequence, the positive fixed charge based on PDADMAC is enriched in the multilayer. Since PDADMAC is more hydrophilic and swells more in water than PSS [28], the permeability of the resulting layer might increase as well. However, at the same time, the layer thickness grows with each newly deposited layer, which should further increase the resistance and, thus, decrease the permeability.

The results above demonstrate that the many required layers assembled at static or low flux conditions can be replaced with just a few layers coated at higher flux. This reduces the potential production effort considerably, as each layer has to be prepared with care. After each layer, the membrane must be rinsed and the coating setup must be cleaned in order to prevent complex formation of the polycation and polyanion. These complexes would cause blockages within the setup and would be rinsed into the membrane during the next coating step, where they finally lead to non-reproducible coatings. These steps are mandatory for a successful and reproducible layer build-up but they are rather time and water intensive processes. With higher flux during coating, the number of layers can be reduced; hence, the rinsing and cleaning steps are minimized as well. This leads to a faster and more reproducible production of an LbL membranes.

Table 4.3 compares the developed LbL membrane with several different commercially available nanofiltration membranes. The retention

of the LbL membrane is just slightly lower than most of the existing membranes. In terms of pure water permeability, the LbL membrane outperforms most of the commercially available nanofiltration membranes. Due to good retention with high permeability, in combination with the good cleaning opportunities (see Chapter 7), the developed membranes are especially attractive because their properties can be precisely tuned inside the module. In fact, it is not always desirable to have the highest possible retention. For instance, in drinking water production from surface water, the salt balance of the water should be kept constant, which would not be possible with the classical nanofiltration membranes. Yet, the presented new type of nanofiltration membrane can be precisely tailored to the needs of the separation task by varying the many process conditions at which the membranes are prepared.

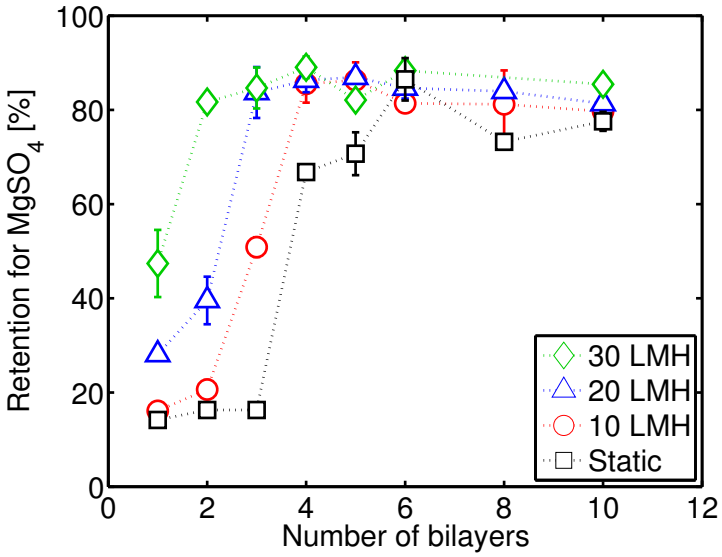

(a) Retention for $MgSO_4$

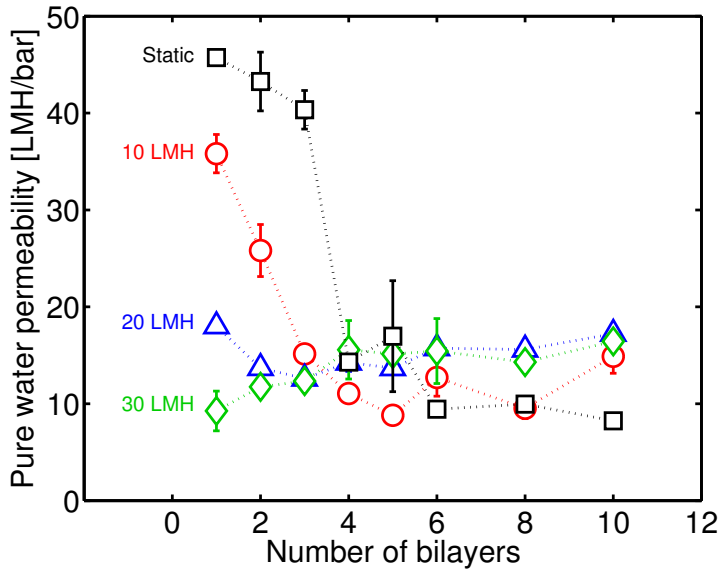

(b) Pure water permeability

Figure 4.6: a) Retention for $MgSO_4$ and b) pure water permeability as a function of bilayer number. Green diamonds: coating at 30 LMH; blue triangles: coating at 20 LMH; red circles: coating at 10 LMH; black squares: static coating. All coating times were 10 min.

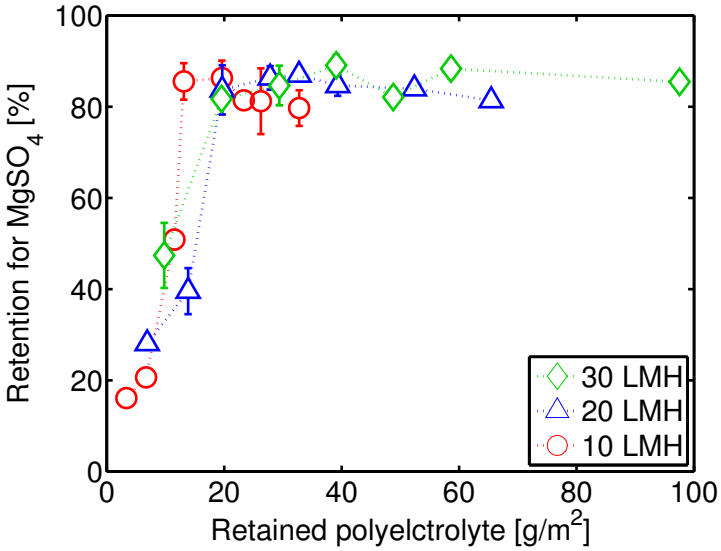

(a) Retention for $MgSO_4$

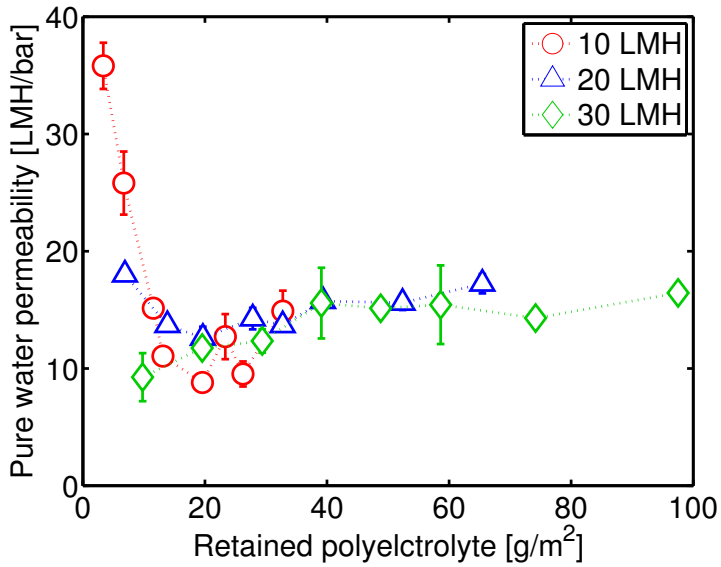

(b) Pure water permeability

Figure 4.7: a) Retention for $MgSO_4$ and b) pure water permeability as a function of the retained polyelectrolyte mass for as calculated with Equation 4.4 for 10 bilayers. Green diamonds: Coating at 30 LMH; blue triangles: coating at 20 LMH; red circles: coating at 10 LMH. All coating times were 10 min.

Table 4.3: Pure water permeability and retention for $MgSO_4$ for commercially available nanofiltration membranes as found in the literature.

Membrane	Pure water permeability [LMH] [$\frac{LMH}{bar}$]	Retention for $MgSO_4$ [%]	Source
NTR7450 (Nitto Denko)	6.3 - 23	40 - 53	[105–108]
NF270 (Dow)	11 - 13.5	97 - 100	[105, 109, 110]
NF90 (Dow)		100	[110]
NF40 (Dow)	9.4	100	[107, 108]
NF30F (Microdyn Nadir)		40	[110]
NP030 (Microdyn Nadir)	4.4		[105]
NFT50 (Alfa Laval)	5.9	95	[111]
CA30 (Hoechst)	23.2	56 - 60	[107, 108]
Desal 5DK (GE)	4.5	98	[105, 112]
Desal 5HL (GE)	11.6	98	[105, 113]
LbL (30 LMH, 4-10 bilayer)	≈15	85 - 90	Present study

4.4 Coating at crossflow conditions

Superimposed to the convective flow perpendicular to the membrane surface due to permeation, an axial flow (crossflow) was applied. The permeation flux was kept constant at 30 LMH for all experiments, while the crossflow velocity was varied (Figure 4.8). During coating, the resistance (determined with Equation 4.1 with the measured TMP that was necessary to maintain a constant permeation flux) reached a maximum before it flattened out to a plateau value. By increasing the crossflow velocity, the maximum was shifted to shorter filtration times.

We hypothesize that during LbL film assembly under crossflow conditions, adsorption and desorption occurred. In the beginning of the coating procedure, the adsorption was dominating, which resulted in increasing resistance. As soon as the maximum is reached, either desorption or restructuring of the PEs due to the shear forces, became dominating, leading to decreasing resistance. In the plateau region, adsorption and desorption were either in equilibrium or neither of them occurred.

The crossflow velocity during coating determined the final resistance of the subsequent pure water permeation. Increasing the crossflow velocity resulted in lower resistance. Thus, the pure water permeability of the coated membranes increased with the crossflow velocity (Figure 4.9b) while the retention decreased (Figure 4.9a).

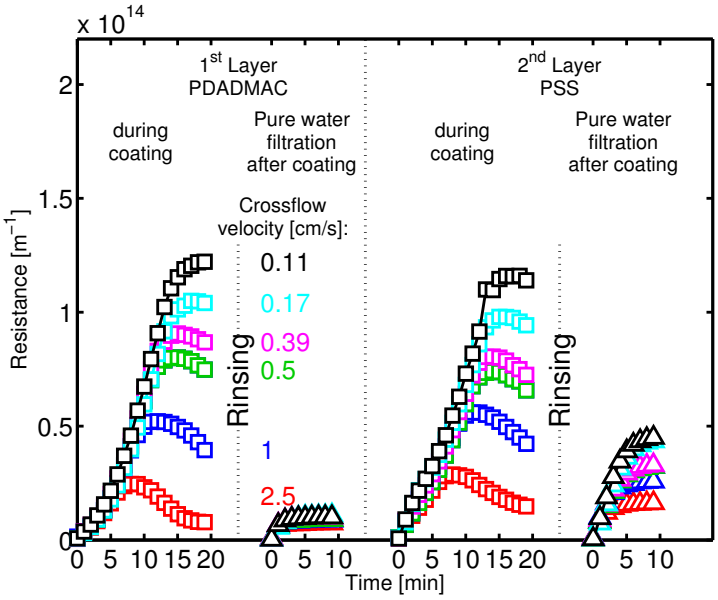

Figure 4.8: Membrane resistance as a function of time during coating and during pure water filtration after coating. The coating flux was 30 LMH for all coatings while the crossflow velocity was varied.

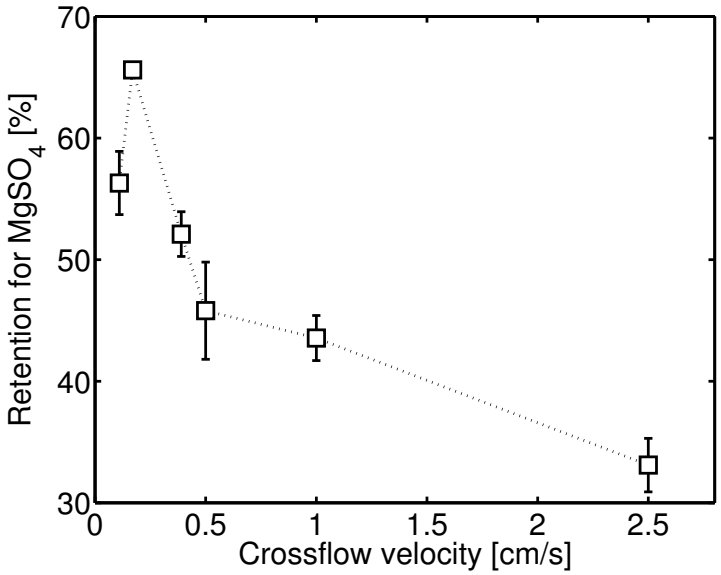

(a) Retention for $MgSO_4$

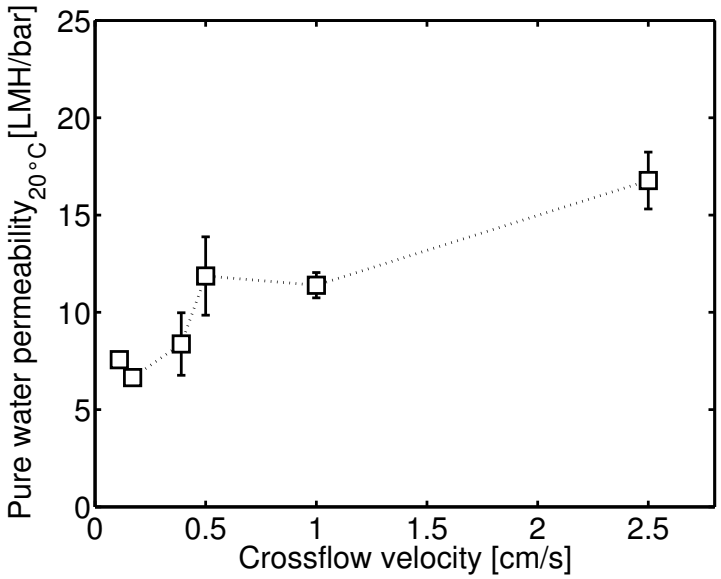

(b) Pure water permeability

Figure 4.9: a) Retention for $MgSO_4$ and b) pure water permeability as a function of the crossflow velocity applied during coating.

To further study the plateau region, experiments at different coating times (10 and 15 min) and higher crossflow rates were conducted (Figure 4.10). The coating time was chosen to ensure that all coatings reached the plateau region. The retention and the pure water

permeability did not differ significantly between the two coating times 4.11. Thus, it can be concluded that as soon as the plateau region was reached either, adsorption and desorption were in equilibrium or no further adsorption and desorption occurred at all.

The correlation between crossflow velocity and membrane properties suggests that the LbL film thickness is controlled by the crossflow velocity. For spin coating, such a correlation was drawn by Cho et al. [50]. A power law relationship described the LbL film thickness as a function of rotating spin (shear forces at the interface between the surface and the coating solution) and PE concentration. In case of crossflow coating, the crossflow velocity will influence both, the shear forces at the interface and the PE concentration. While the shear forces correlate directly with crossflow velocity, the concentration at the interface results from an equilibrium between convective mass transport of the PEs toward the surface due to permeation and their diffusive back-transport of those to the bulk phase due to a concentration gradient. Increasing the crossflow velocity will increase the diffusive back-transport while the convective transport remains constant, as it is controlled by the permeation rate. Therefore, the concentration at the interface will decrease with increasing crossflow velocity. Thus, adopting the mentioned power law for spin coating to crossflow coating predicts a thinner layer for increasing crossflow velocity. As this power law was fitted for spin coating, it can not be adopted for crossflow coatings on porous supports. Rather, it might demonstrate the likely relation between crossflow velocity and layer thickness.

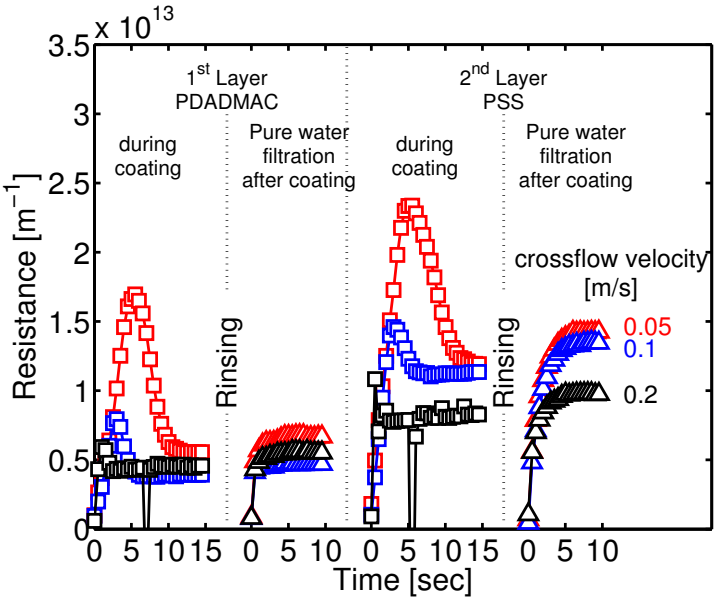

Figure 4.10: Membrane resistance as a function of time during coating and during pure water filtration after coating. The coating flux was 30 LMH for all coatings while the crossflow velocity was varied.

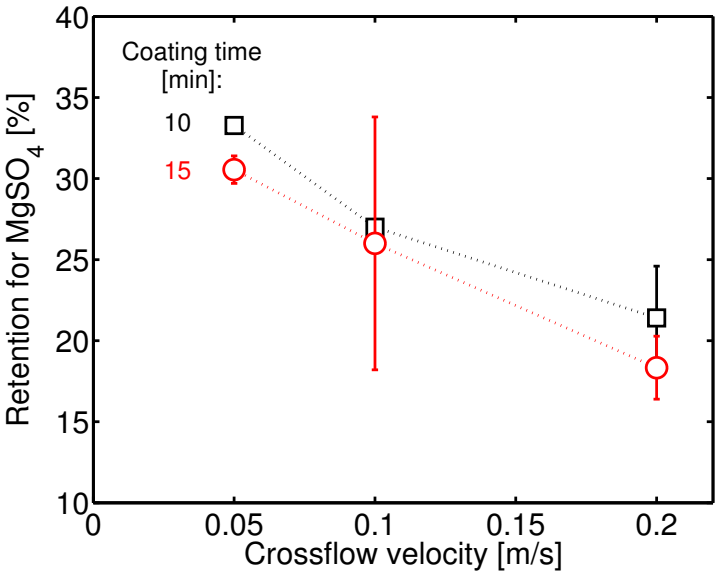

(a) Retention for $MgSO_4$

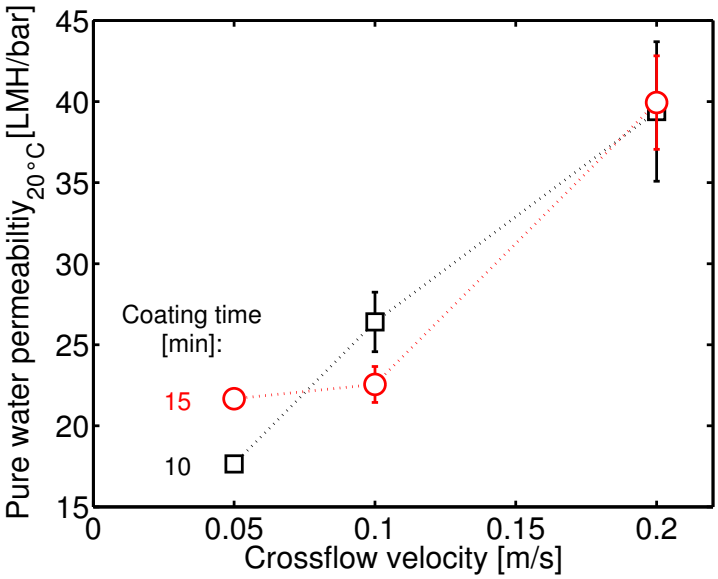

(b) Pure water permeability

Figure 4.11: a) Retention for $MgSO_4$ and b) pure water permeability as a function of the coating time and the crossflow velocity applied during coating.

4.5 Conclusion

In this chapter, a new convective adsorption method of PE assembly at constant flux, with a surprisingly precise development of the membrane resistance was presented. The properties of the resulting membranes scale with the amount of PE that is transported to the surface, whereby coating flux and time span are interchangeable. This enables easy production of membranes with tailored properties: Even a single bilayer can result in nanofiltration properties. By adding more bilayers, a retention for $MgSO_4$ of about 90% is feasible; thus, the membrane is flux- and retention-wise competitive with existing nanofiltration membranes. On using a superimposed axial flow during coating – i.e. crossflow – a further parameter for membrane tailoring can be used.

The developed membrane has advantages over existing thin-film composite nanofiltration membranes. It is an inside-out hollow fiber with the active separation layer on the lumen side. This enables controlling the flow pattern within the lumen, which is highly desirable for ensuring long-term sustainable flux and retention performance. Moreover, the developed membrane can be easily fabricated onto existing hollow fiber membrane modules. As the packaging density of a hollow fiber membrane module is much higher than the one of a spiral-wound module, the demonstrated membranes have significant viability to become a new, realistic membrane product.

5

Coating parameters tailor membrane transport properties

In this chapter, we employed the new coating method presented in Chapter 4 to study the effect of various coating parameters on membrane performance. The NaCl concentration within the polyelectrolyte (PE) solution, coating flux, coating time, and layer number were varied and evaluated by the molecular weight cut-off (MWCO), ion retention, and permeability. In total, 65 combinations of the above-mentioned parameters have been tested. While only a few of them are shown in the figures of this chapter, all coatings and the corresponding performance data are presented in Table 5.2. This table can be employed to determine the optimal coating conditions for a certain separation task.

5.1 Molecular weight cut-off

Figure 5.1 depicts MWCO and permeability as a function of layer number and salt concentration in the PE solution. Irrespective of the salt concentration in the coating solution, a rather low MWCO of about 250 Da was achieved (Figure 5.1a and 5.2a). Astonishingly, for more layers, the cut-off increased, though one would have expected the cut-off to decrease further. For 0.25 mol/l NaCl in the coating solution, no MWCO could be determined for the coatings comprising eight and 10 bilayers, as the biggest applied PEGs, about 6,000 Da, are retained by the membrane to less than 90% (Figure 5.2b). At the same time,

the solution permeability of these membranes with very high MWCOs differed just slightly from one of the membranes with very low cut-offs.

An increase in the MWCO is accompanied by an increase of the pore size, which was confirmed by fitting the model for nanofiltration membrane characterization to obtain pore radius r_p and the ratio of active membrane thickness Δx to porosity A_k (Section 2.4). The fitting revealed a pore radius of 0.46 and 3.41 nm for the membrane with three and 10 bilayers, respectively (Table 5.1). Remarkably, the pore radius for three bilayers determined by the fitting is comparable to the one experimentally determined by Jin et al. [45] of 0.41 nm for a PDADMAC/PSS film.

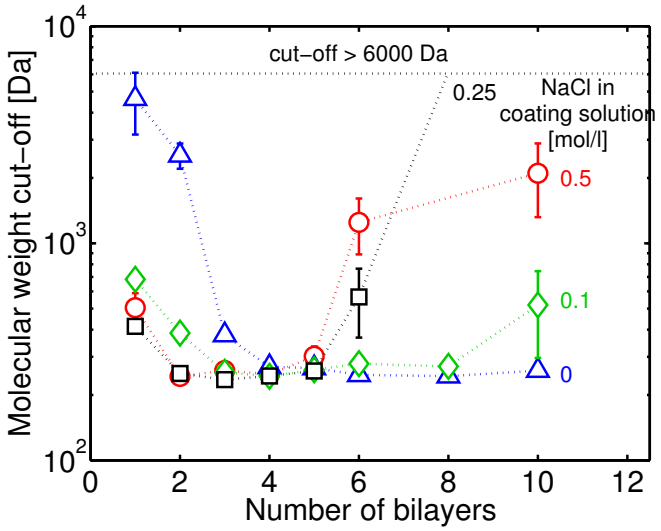

(a) MWCO

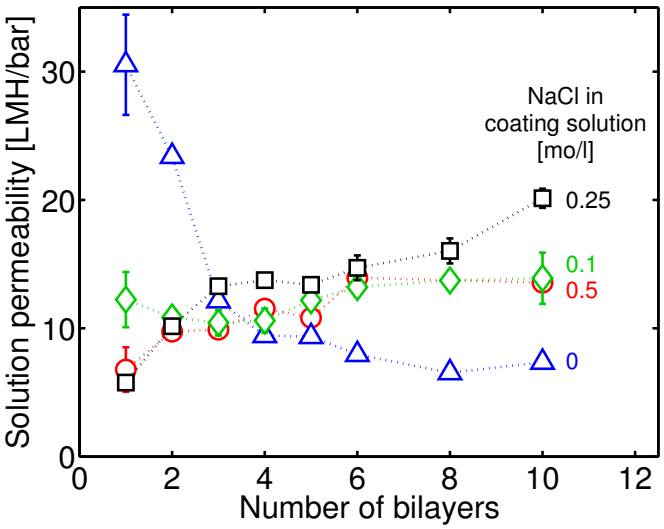

(b) PEG solution permeability

Figure 5.1: a) MWCO as a function of salt concentration within the coating solution and layer number and b) PEG solution permeability measured during the MWCO determination.

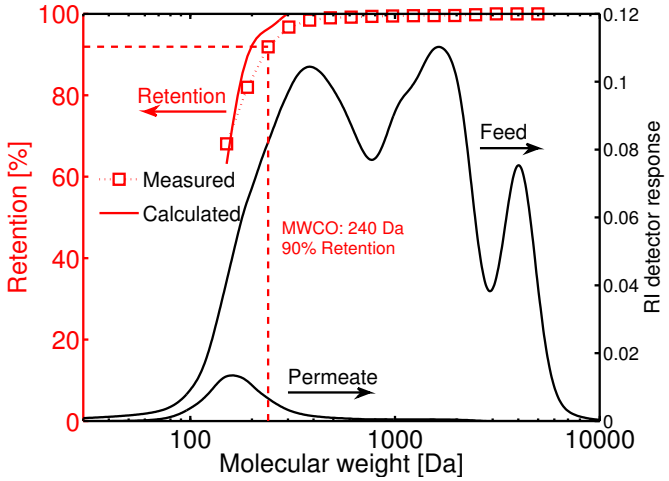

(a) 3 bilayer, 0.25 mol/l NaCl within the coating solution

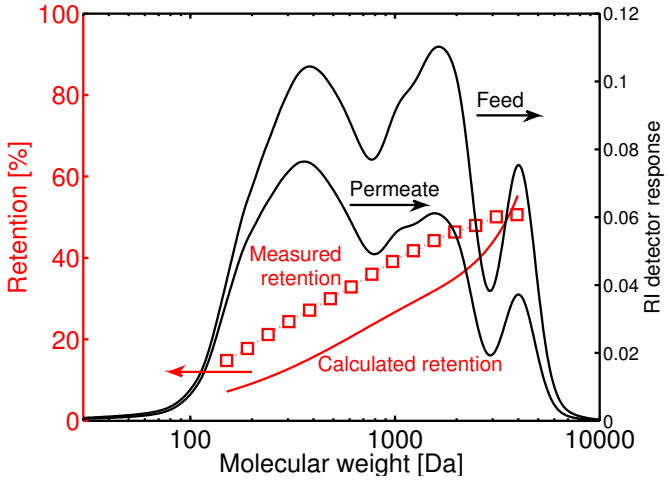

(b) 10 bilayer, 0.25 mol/l NaCl within the coating solution

Figure 5.2: Left y-axis: retention for PEG; right y-axis: refractive index detector response for feed and permeate sample. a) Three bilayers coated with 0.25 mol/l NaCl within the coating solution. The dotted line represents the retention at 90 % which is defined as the MWCO. b) 10 bilayers coated under the same condition as used for a). The MWCO could not be determined, as the retention did not exceed 90%. The markers represent the measured retention. The solid line is the calculated retention using the model for membrane characterization (Section 2.4) with the best-fitted parameters (Table 5.1).

To explain the increased pore size for high layer numbers, one has to

Table 5.1: r_p and $\frac{\Delta x}{A_k}$ for the membranes determined by the model for membrane characterization (see Section 2.4)

Coating	r_p [nm]	$\frac{\Delta x}{A_k}$ [μm]
3 bilayers	0.46	0.77
10 bilayers	3.42	49.2

consider the charge (over)compensation of PDADMAC/PSS multilayer assemblies and the characteristics of those two PEs. Ghostine et al. [29] showed that the theory of charge overcompensation is wrong for PDADMAC/PSS multilayers. In fact, PDADMAC overcompensates the charge, whereas PSS merely compensates. Thus, PDADMAC will accumulate more and more within the multilayer film with increasing layer number. PDADMAC is more hydrophilic than PSS and shows stronger swelling in water [28]. Hence, the swelling of the PDADMAC-enriched film might open the pores, which would result in a higher cut-off for more assembled layers.

As the pore size of the film comprising three bilayers is lower than the one assembled from 10 bilayers, the latter assembled layer must have influenced the film underneath. This can be explained with the three zone model (Section 2.1, Figure 2.2). For PEs which exhibit an exponential growth behavior (Figure 2.2b)), such as PDADMAC/PSS, the PEs from the solution diffuse into Zone III but cannot penetrate into Zone I. Thus, the film of Zone I must be very open, as it cannot be affected by the latter assembled layers. Zone III must have been dense for low layer numbers but it became more open as the number of assembled layers increased. The diffusion of the additional PEs – particularly PDADMAC – from the solution into the LbL film opened the layer, thus resulting in a lower MWCO.

5.2 Ion retention

The salt retention for the membranes coated at 0.25 mol/l NaCl in the coating solution, which showed a sharp increase in the MWCO with increasing layer number (black line 5.1a), is depicted in Figure 5.3a. The salt retentions were determined with single salt measurements and not with salt mixtures. While the MWCO increased above five bilayers, the salt retention for NaCl, $MgCl_2$, and $MgSO_4$ remained unchanged with increasing layer numbers. Thus, the membranes can be tailored to be selective for big uncharged solutes ($M_w > 6000$) while ions are retained. The ionic nature of each assembled layer repelled the ions even though the pore size increased dramatically as shown with fitting of the model for membrane characterization (Section 2.4).

Only the Na_2SO_4 retention decreased with increasing layer number. At low layer numbers (one to three bilayers), the membranes retained Na_2SO_4 very well (>90%) while the retention decreased successively to less than 50% for 10 bilayers. At the same time, the retention for $MgCl_2$ increased to above 90 % during the first three bilayers and remained constant for further layers. These results can be explained by a shift in membrane charge from negative to positive. At low layer numbers, the membranes appeared to be negatively charged; hence, the bivalent anion ${SO_4}^{2-}$ was retained very well [1]. With increasing layer number, the positive charge became dominating; thus, $MgCl_2$ is retained better than Na_2SO_4. The dominating positive charge contradicted that the last assembled layer is from anionic nature as was PSS. However, as explained above, PDADMAC accumulates within the multilayer film and, thus, Adusumilli and Bruening [115] measured a positive zeta potential of PSS-terminated PDADAMAC/PSS multilayer films for

[1] Na_2SO_4 was retained better than $MgSO_4$ as the attraction effect between cation and membrane is higher for bivalent than for monovalent cations [114].

more than seven bilayers. Therefore it is very likely that charge reversal was initiated by the accumulation of PDADMAC within the multilayer film.

Moreover, the permeability increased with layer number (Figure 5.3b), which might be explained as well with the accumulation of PDADMAC in the film. The strong swelling of the PDADMAC-enriched film resulted in improved water transport, and thus, higher permeability.

For low layer numbers, the solute permeability was lower than the pure water permeability, which is the result of concentration polarization. For high layer numbers it is reversed: The solute permeability (for NaCl,$MgCl_2$, and $MgSO_4$) is higher than the pure water permeability. As no obvious explanation can be found for this observation, it is very likely that the salt – although its concentration was low (5 mmol/l) – affected the LbL film. At the same time, the retention for the mentioned salts remained constant with increasing layer numbers, which leads to impressive performance. For instance, the retention for NaCl was greater than 50% with a measured solution permeability of about 27 LMH/bar at 10 bilayers.

Figure 5.4 depicts the salt retention and solution permeability as well, but only for the membranes coated at 0.1 mol/l NaCl (instead of 0.25 mol/l) in the coating solution. The overall trend for the retention of these membranes was comparable, as observed for the membranes coated at 0.25 mol/l in the coating solution (Figure 5.4a (0.1 mol/l NaCl) and 5.3a (0.25 mol/l NaCl)). However, the permeability varied significantly between the two salt concentrations. While the permeability increased with layer number for the coatings at 0.25 mol/l NaCl, it is independent of layer number for the coatings assembled at 0.1 mol/l NaCl (Figure 5.4b [0.1 mol/l NaCl] and 5.3b [0.25 mol/l NaCl]). Af-

ter the deposition of the first bilayer, the permeability reached a high plateau value of about 17 LMH/bar, which remained constant for more assembled layers.

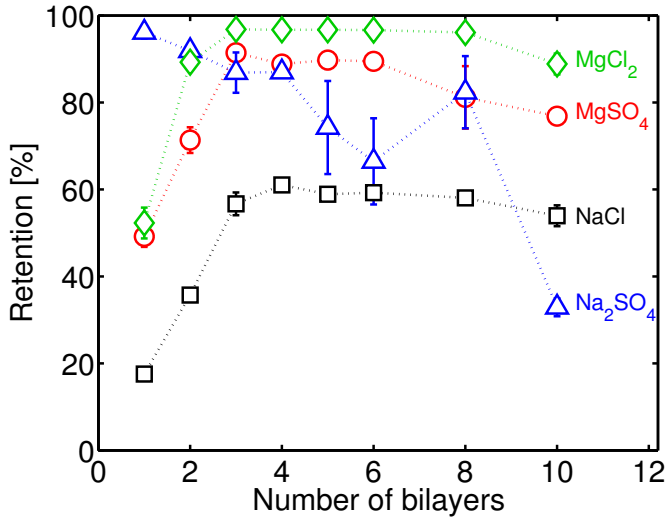

(a) Retention

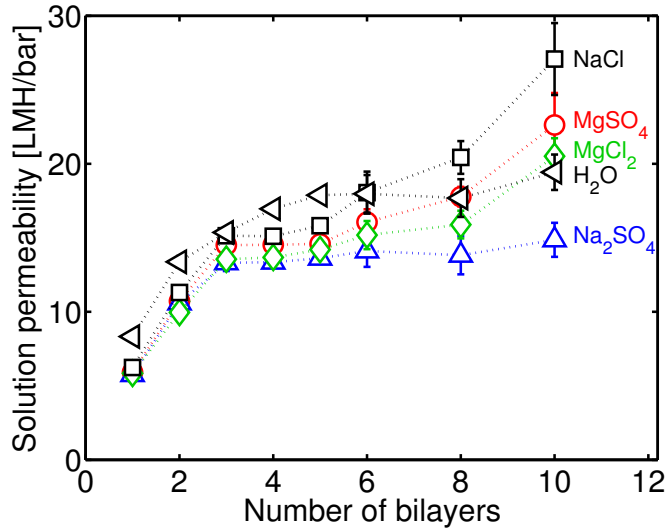

(b) Solution permeability

Figure 5.3: Membranes were coated with 0.25 mol/l NaCl within the coating solution. a) Retention for $MgCl_2$ (green diamonds), $MgSO_4$ (red circles), NaCl (black squares), and Na_2SO_4 (blue triangles). The retention was determined with a single salt and not a mixture of the mentioned salts. b) Solution permeability measured during the salt retention measurement plus the pure water permeability (black left-pointing triangles).

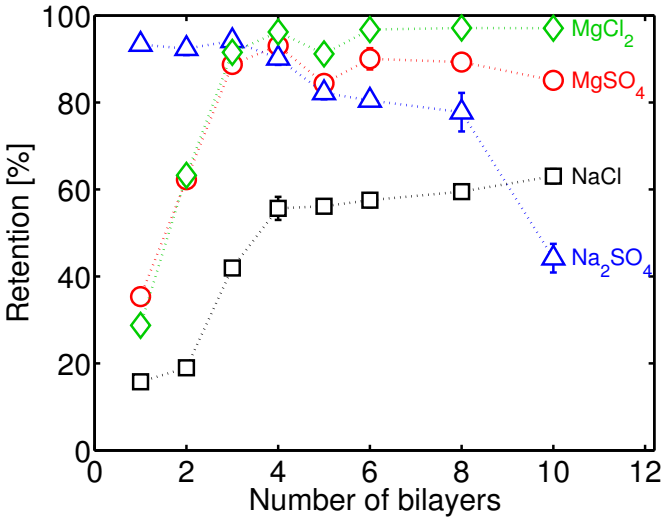

(a) Retention

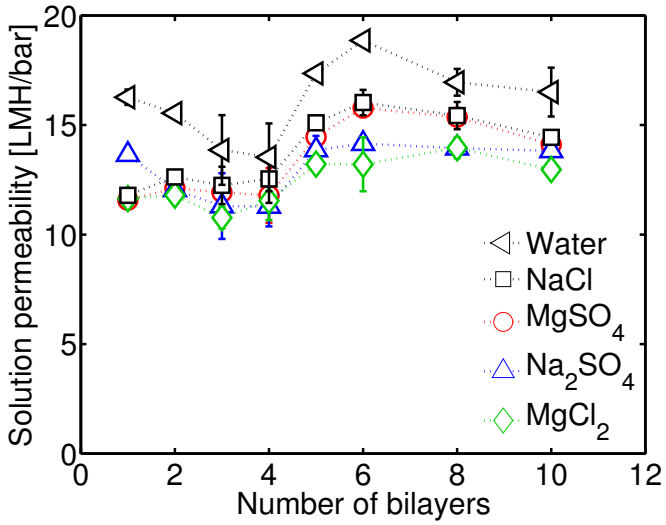

(b) Solution permeability

Figure 5.4: Membranes were coated with 0.1 mol/l NaCl within the coating solution. a) Retention for single measured salts: $MgCl_2$ (green diamonds), $MgSO_4$ (red circles), NaCl (black squares), and Na_2SO_4 (blue triangles). b) Solution permeability measured during the salt retention measurement plus the pure water permeability (black left-pointing triangles).

5.3 Choosing the right coating parameters

Figure 5.5 depicts the retention for $MgSO_4$, and the permeability for membranes coated at 0, 0.1, 0.25, and 0.5 mol/l NaCl as a function of layer number. These coatings demonstrate clearly how diverse PDADMAC/PSS films can be. From four bilayers on, the retention for $MgSO_4$ was approximately the same, irrespective of salt concentration in the PE solution. However, the permeability differed between 7 and 22 LMH/bar. This example emphasizes the flexibility of the LbL technology to tailor the membrane with a retention that meets the requirements of the separation task with the best possible permeability. Therefore, Table 5.2 presents 65 different coatings at various salt concentrations, coating fluxes, coating times, and layer numbers. The table provides information about the MWCO determined with polyethylene glycol, single salt retentions for Na_2SO_4, $MgSO_4$, $MgCl_2$, and NaCl, and the pure water permeability. The table can be used to find the optimal membrane for a certain separation task.

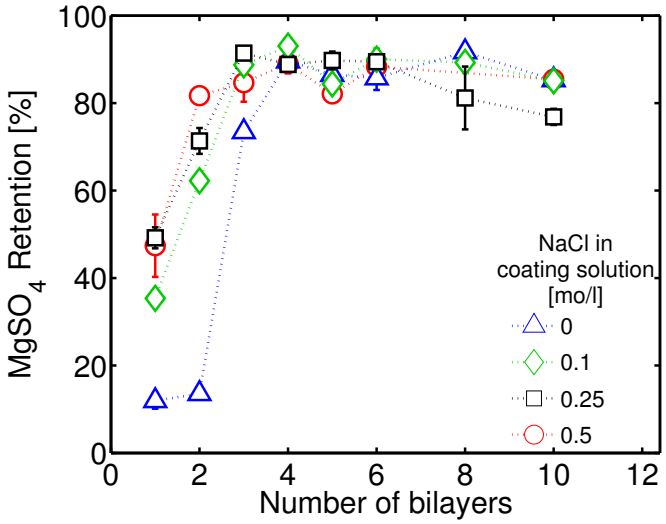

(a) Retention for $MgSO_4$

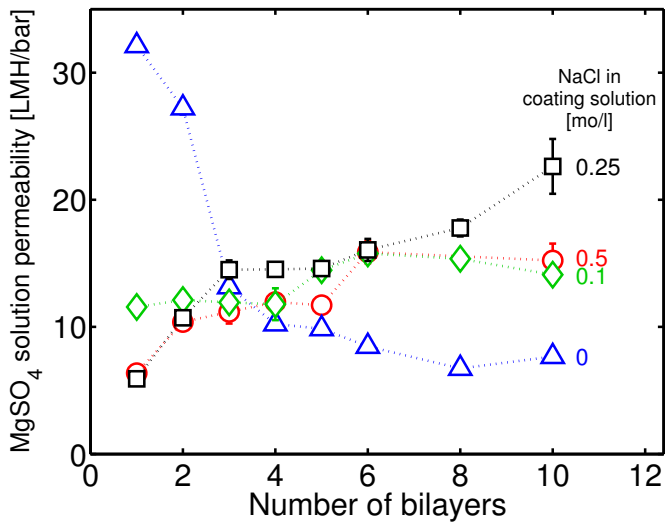

(b) MgSO4 solution permeability

Figure 5.5: a) Retention for $MgSO_4$ and b) $MgSO_4$ solution permeability as a function of NaCl concentration within the PE solution and layer number. NaCl within the coating solution in mol/l: 0 (blue triangles), 0.1 (green diamonds), 0.25 (black squares), and 0.5 (red circles).

Table 5.2: MWCO, salt retention ($MgSO_4$,Na_2SO_4,$MgCl_2$, and NaCl), and pure water permeability for various coating parameters: c_{NaCl}: NaCl concentration within the coating solution; $J_{coating}$: flux applied during coating in dead-end operation mode; $t_{coating}$: coating time; and n: number of layers. MWCO and salt retention determined by crossflow filtration with Reynolds ≈ 3,000 with a feed and retentate pressure of 4.8 and 3.5 bar, respectively. MWCO was measured with various polyethylene glycols (MW: 200, 300, 400, 600, 1000, 1500, 2000, 4000 Da, each 1 g/l). Salt retention was measured a with single salt solution of 5 mmol/l. The table is sorted in ascending order for the following columns: 1. c_{NaCl} 2. $J_{coating}$ 3. $t_{coating}$ 4. n.

c_{NaCl} [mol/l]	$J_{coating}$ [LMH]	$t_{coating}$ [min]	n	MWCO [Da]	Retention				Pure water permeability [LMH/bar]
					$MgSO_4$	Na_2SO_4	$MgCl_2$	NaCl	
0	30	10	2	4638.5 ± 1468.5	11.9 ± 1.8	59 ± 6.5	6.6 ± 4.2	4.7 ± 1	49.9 ± 0.6
0	30	10	4	2543 ± 339.4	13.6 ± 1.4	59 ± 6.5	14.5 ± 0.1	5.3 ± 0.8	37.5 ± 1.5
0	30	10	6	377.8 ± 18.1	73.5 ± 0.1	89.9 ± 0.6	75.9 ± 1.6	15.6 ± 0.4	12 ± 1.2
0	30	10	8	269.4 ± 10.2	89.6 ± 0.1	89.4 ± 1.4	93.4 ± 0.1	37.9 ± 0.1	14 ± 0.4
0	30	10	10	266.1 ± 2.8	86.5 ± 1.6	82.4 ± 2.2	86.8 ± 2.9	29.8 ± 0.3	12.9 ± 0.1
0	30	10	12	247.7	85.8 ± 2.8	86.6 ± 3.6	83.2 ± 5.9	31.5	13.3 ± 0.9
0	30	10	16	244.2 ± 3.3	91.7 ± 0.5	87.6 ± 2.8	93.3 ± 0.4	42.3 ± 1.9	8.5
0	30	10	20	259.2 ± 5.3	85.3 ± 0.3	75.7 ± 4.8	96.8 ± 0.1	65.2 ± 0.4	9
0.1	30	10	2	682 ± 4.2	35.4 ± 0.3	93.3 ± 0.6	28.8 ± 1.8	15.8 ± 0.3	16.3 ± 0.4
0.1	30	10	4	385.4 ± 13.1	62.3 ± 1.8	92.4 ± 1.5	63.3 ± 1.5	19 ± 0.6	15.5 ± 0.1
0.1	30	10	6	254.6 ± 2.4	88.8	94.2 ± 0.4	91.5 ± 0.4	42 ± 1.4	13.9 ± 1.6
0.1	30	10	8	243.9 ± 5.3	93 ± 1.2	90.2 ± 1.5	96.2 ± 0.6	55.7 ± 2.7	13.5 ± 1.5
0.1	30	10	10	261 ± 0.8	84.4 ± 1.5	82.2 ± 1.5	91.2 ± 1.6	56.1 ± 0.2	17.4 ± 0.1
0.1	30	10	12	278.7 ± 12	90.1 ± 2.5	80.5 ± 0.1	96.8 ± 0.4	57.5 ± 1.6	18.9
0.1	30	10	16	271 ± 7.5	89.3 ± 0.1	77.8 ± 4.4	97.1 ± 0.1	59.5 ± 0.8	17 ± 0.6
0.1	30	10	20	519.9 ± 223.7	85.1 ± 0.2	44.2 ± 3.3	97.1 ± 0.1	63.1 ± 1.6	16.5 ± 1.1

c_{NaCl} [mol/l]	$J_{coating}$ [LMH]	$t_{coating}$ [min]	n	MWCO [Da]	Retention				Pure water permeability [LMH/bar]
					$MgSO_4$	Na_2SO_4	$MgCl_2$	NaCl	
0.25	30	10	2	414.1 ± 22.1	49.2 ± 2.4	96.1 ± 1.4	52.3 ± 3.5	17.6 ± 1.5	8.3 ± 0.3
0.25	30	10	4	251.1 ± 8.4	71.4 ± 2.9	91.9 ± 0.9	89.3 ± 1.1	35.7 ± 1.1	13.4 ± 0.4
0.25	30	10	6	235.4 ± 6.1	91.4 ± 1.3	86.9 ± 4.6	96.8 ± 0.2	56.7 ± 2.6	15.4 ± 0.1
0.25	30	10	8	244.6 ± 2	88.9 ± 0.6	87 ± 1.2	96.7 ± 0.4	61.1 ± 0.3	17
0.25	30	10	10	258 ± 18	89.8 ± 2	74.3 ± 10.7	96.7 ± 0.2	58.9 ± 0.6	17.9 ± 0.2
0.25	30	10	12	565.8 ± 198.2	89.5 ± 1.5	66.5 ± 9.9	96.6 ± 0.2	59.3 ± 0.2	18 ± 1.3
0.25	30	10	16	>6000	81.2 ± 7.2	82.4 ± 8.3	96.1 ± 0.3	58.1 ± 0.6	17.7 ± 1.3
0.25	30	10	20	>6000	76.9 ± 1.9	32.9 ± 2.1	88.9 ± 2.4	54 ± 2.4	19.4 ± 1.2
0.5	0	10	2	2193.4 ± 758.4	14.2 ± 0.2	61.6 ± 1	8.3 ± 5.5	6.5 ± 1.2	45.7 ± 0.7
0.5	0	10	4	4758.8 ± 1729.2	16.3 ± 0.3	65.6 ± 14.6	7.5 ± 2.2	3.7 ± 0.1	43.3 ± 3
0.5	0	10	6	4502.2 ± 1774.1	16.3 ± 1.1	72.3 ± 11.6	15 ± 3.6	5 ± 1.9	40.3 ± 2
0.5	0	10	8	391.1 ± 32.5	66.8 ± 0.4	94.9 ± 0.4	69.2 ± 1.2	12.2 ± 1.6	14.3 ± 0.4
0.5	0	10	10	420 ± 115	70.7 ± 4.5	90.5 ± 0.8	72.1 ± 6.7	15.8 ± 0.1	17 ± 5.7
0.5	0	10	12	246.3	86.5 ± 4.5	72 ± 1.4	92.1 ± 2.8	30.5 ± 6.1	9.4 ± 0.7
0.5	0	10	16	317 ± 7	73.2 ± 0.3	31.2 ± 0.2	90.7 ± 0.2	43.9 ± 0.2	10 ± 0.1
0.5	0	10	20	318.3	77.6 ± 2	34.5 ± 1.8	93 ± 1.3	50.8	8.2 ± 0.4
0.5	10	10	2	2511.1 ± 1193.3	16.1 ± 1	57.2 ± 3.5	21.3 ± 3.8	14.1 ± 5.9	35.8 ± 2
0.5	10	10	4	2727.8 ± 356	20.7 ± 2	80.2 ± 5.4	19.5 ± 2.4	11.1 ± 1	25.8 ± 2.7
0.5	10	10	6	817 ± 84.4	50.9 ± 2.1	85.7 ± 3.2	50.6 ± 3.8	16.2 ± 2.3	15.1 ± 0.6
0.5	10	10	8	243 ± 5.6	85.6 ± 4	85.2 ± 2.6	86.4 ± 0.7	33.2 ± 2.4	11.1 ± 0.4
0.5	10	10	10	319.2 ± 48.1	86.3 ± 3.8	79.9 ± 0.1	86.9 ± 6.4	39.3 ± 6.4	8.8 ± 0.5
0.5	10	10	12	407	81.4 ± 1.2	48.5 ± 16.4	84.7 ± 8.4	52.1 ± 2	12.7 ± 1.9
0.5	10	10	16	272.4 ± 3.9	81.2 ± 7.2	46.1 ± 0.2	96.4 ± 0.3	62.3 ± 0.1	9.5 ± 1.1
0.5	10	10	20	294.7	79.7 ± 3.9	42.6 ± 14.4	95.5 ± 1.6	57.5 ± 9.7	14.9 ± 1.7
0.5	10	15	2	856.3 ± 46.4	23.8 ± 1.1	62.6 ± 2.2	34 ± 5.9	12.1 ± 0.1	23.2 ± 1.7

c_{NaCl} [mol/l]	$J_{coating}$ [LMH]	$t_{coating}$ [min]	n	MWCO [Da]	Retention				Pure water permeability [LMH/bar]
					$MgSO_4$	Na_2SO_4	$MgCl_2$	NaCl	
0.5	15	7.5	2	913.9 ± 135.1	21.5 ± 1.3	61.7 ± 1.5	27.7 ± 4.1	13.1 ± 1.1	25.9 ± 3.5
0.5	20	7.5	2	690.3 ± 96.9	23.2 ± 2.1	71.2 ± 8.3	39.4 ± 8.7	14.6 ± 0.1	23.4 ± 1.5
0.5	20	10	2	667.4 ± 23.8	28.1 ± 0.1	73.3 ± 1.5	32.7 ± 3.9	15.4 ± 0.1	18 ± 0.4
0.5	20	10	4	380.4	39.6 ± 5.1	87	45 ± 5.6	18.5 ± 1.3	13.7 ± 0.2
0.5	20	10	6	253.1 ± 5.5	83.7 ± 5.4	93.3 ± 1.4	90.9 ± 2.3	41.4 ± 7	12.6 ± 1
0.5	20	10	8	275.1 ± 12.4	86.3 ± 2.6	74.6 ± 7.4	95.2 ± 2.9	58.8 ± 4.5	14.3 ± 0.9
0.5	20	10	10	268.6 ± 0.3	86.9 ± 0.9	70.9 ± 7.8	96.6 ± 0.1	59.9 ± 1.2	13.7 ± 0.4
0.5	20	10	12	312.7 ± 10.3	84.7 ± 2.3	52.3 ± 6.4	93.7 ± 2.3	57.6 ± 0.3	15.7 ± 0.6
0.5	20	10	16	305.3 ± 12.8	84 ± 1.3	50.8 ± 6.8	96.9 ± 0.1	63.8 ± 0.4	15.6 ± 0.6
0.5	20	10	20	309.6 ± 5.5	81.4 ± 0.1	63 ± 3.3	96.9 ± 0.1	62.9 ± 0.4	17.2 ± 0.8
0.5	25	6	2	655.9	23.2 ± 2.8	71 ± 5.3	31.3 ± 2	18 ± 3.3	26.2 ± 3.8
0.5	30	2.5	2	2556.1 ± 1050.6	18.9 ± 0.8	60.4 ± 8.3	-	9.9 ± 2.1	30 ± 1.4
0.5	30	5	2	745.2 ± 32	25.2 ± 2.2	69.1 ± 0.5	29.2 ± 4.7	12.4 ± 1	22 ± 2.7
0.5	30	7.5	2	522.9 ± 37.2	31.3 ± 0.3	75 ± 1.6	41.8 ± 11.5	-	13.1 ± 0.2
0.5	30	10	2	509.3 ± 96.4	50.7 ± 4.9	92.8 ± 2.3	39.2 ± 3.5	21.3 ± 1.6	8.2 ± 1.2
0.5	30	10	4	243.5 ± 0.1	81.7 ± 0.5	85.1 ± 0.6	95 ± 0.5	51.7 ± 1.2	11.7 ± 0.2
0.5	30	10	6	259.5 ± 6.3	84.7 ± 4.4	71.1 ± 7.2	93.1 ± 3.6	56.6 ± 5	12.3 ± 1
0.5	30	10	8	249.1	89.1 ± 2.3	73.1 ± 12.7	95.8 ± 1.1	52.2 ± 2.9	14.5 ± 1.6
0.5	30	10	10	301.6 ± 32.9	82.1 ± 1	74.1 ± 0.6	96.9 ± 0.1	62.2 ± 0.6	15.1 ± 0.5
0.5	30	10	12	1248.2 ± 359.3	88.3 ± 2.1	52.8 ± 14.5	96.5 ± 0.2	57.1 ± 8	17.1 ± 1.3
0.5	30	10	20	2102.6 ± 783.7	85.5 ± 1	59.9 ± 3.4	96.4 ± 0.2	63 ± 1.1	16.4 ± 0.6
0.5	40	3.75	2	649.1 ± 66.3	25.7 ± 0.3	74.2 ± 1.9	30.7 ± 10	12.1 ± 0.8	19.8 ± 1.3

5.4 Conclusion

The new coating method involving constant flux conditions, as presented in Chapter 4, was applied to study LbL membranes prepared with various coating parameters. To evaluate their performance, the MWCO, the salt retentions for four different single salts, and the permeability were determined. Using this data enables tailoring the membrane that meets the requirements for a certain separation task with the best possible permeability. The most unexpected result was the development of the MWCO with increasing layer number. Instead of a further decrease in the MWCO with an additional assembled layer, an increase in the MWCO was observed, particularly for the coatings with 0.25 and 0.5 mol/l NaCl in the PE solution. The observations have been associated with the selective accumulation of PDADMAC in the LbL film and, hence, accounts for the strong swelling of the film. While the cut-off increased, the retention of ions remained constant. Thus, the LbL membrane can be tailored to be selective for big organic compounds (M_w >6000) while ions are retained. It is to the best of our knowledge, the first membrane of its kind.

6

LbL on ceramic tubular multichannel monoliths

Better mechanical, chemical, and thermal resistance can be expected for ceramic membranes. Ceramic micro- and ultrafiltration membranes are successfully established, for instance, in waste water treatment [116, 117], drinking water production ([118, 119]), produced-water treatment [120, 121], and skim milk production [122]. The situation is different for nanofiltration membranes. Although recent developments report nanofiltration membranes with a molecular weight cut-off (MWCO) below 500 Da, with possible use at harsh chemical conditions – i.e. high and low pH or organic solvents [123, 124] – the membranes are not established in the market yet. Preparing them defect-free is still difficult and cumbersome, and they are too expensive to be competitive to polymeric nanofiltration membranes: Their production is time- and material-intensive due to many successive production steps.

A layer-by-layer (LbL) assembly based on PEs from aqueous solution [17] on a more open, but affordable, ceramic support [55, 125, 126] is suggested to be a viable alternative to the all-ceramic NF membranes. Thus, the coating method presented in Chapter 4 was adapted for ceramic monolith membranes. We were faced with two fundamental

Parts of this chapter have been either published in "Daniel Menne, Cagri Üzüm, Arne Koppelmann, John Erik Wong, Chiel van Foeken, Fokko Borre, Lars Dähne, Timo Laakso, Arto Pihlajamäki, and Matthias Wessling. Regenerable Polymer/Ceramic Hybrid Nanofiltration Membrane Based on Polyelectrolyte Assembly by Layer-by-Layer Technique. Journal of Membrane Science, 520:924 – 932, 2016"

as well as applied questions: 1. Is it possible to cover and close a 100 nm pore with an LbL system in a reasonable number of coating steps? 2. Is it possible to perform the LbL membrane build-up in a monolithic module?

6.1 Membrane fabrication

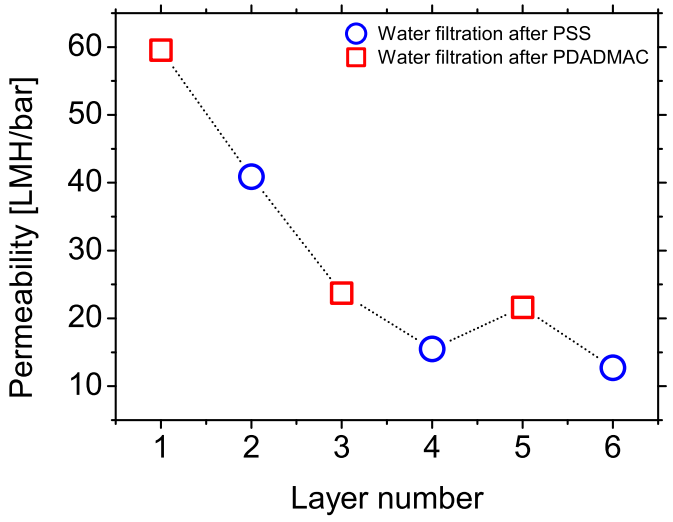

(a) Without supporting layers

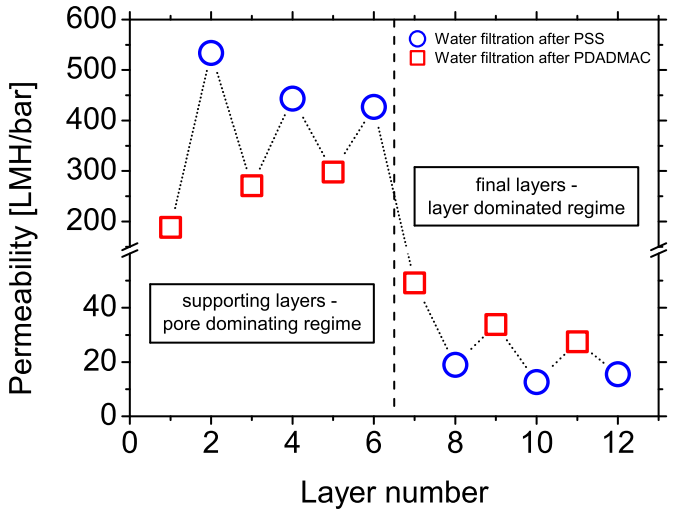

(b) With supporting layers

Figure 6.1: a) Pure water permeability as a function of assembled layers built up at a flux of 30 LMH with 0.1 mol/l NaCl in the coating solution and b) pure water permeability as a function of layer number for the coating with six supporting layers, assembled at a flux of 15 LMH without any salt in the coating solution, followed by six final layers built up at a flux of 30 LMH with 0.1 mol/l NaCl in the coating solution (same as in a).

Two different coating sequences are studied: a) direct assembly of the six layers at 30 LMH with 0.1 mol/l NaCl in the coating solution (Figure 6.1a) and b) six supporting layers without salt in the coating solution and assembled at low flux conditions of 15 LMH, followed by six final layers with 0.1 mol/l NaCl in the coating solution applied at 30 LMH (the same conditions as applied in a)) – i.e. in total 12 layers (Figure 6.1b). Generally, the amount of adsorbed PE mass depends among other things on the ionic strength of the PE solution [24, 30, 127] and the flux used for the coating [15]. As both the ionic strength and the coating flux is low for the supporting layers, the permeability decreases less than in the direct assembly of the separation layers (Figure 6.1, Table 6.1). Furthermore the ionic strength affects the conformation of the PE chains: at high ionic strength the PEs are coiled and stretched at low ionic strength. We hypothesize that the stretched PEs during the assembly of the salt-free supporting layers did not cover but narrowed the pores of the support. Thus, the succeeding separation layers do not penetrate that deep into the porous structure. In fact, this reflects in the final permeability of the membranes. Although the membrane with the supporting layers has, in total, twice the number of assembled layers, it shows a higher pure water permeability (22 LMH/bar) than the one without these supporting layers (15 LMH/bar) (Table 6.1).

Figure 6.1b supports the recently discovered "inverting odd-even"effect [30]. The "odd-even" effect describes the increase in the permeability by assembling an additional layer, although, intuitively, one would expect that the permeability should decrease due to the additional resistance caused by the new additional layer. In Figure 6.1b, the permeability increases by adding a PSS layer on top of the PDADMAC-terminated film during the first six layers; however, we observe the opposite for

the last six layers and the permeability of the PSS-terminated layer increases upon addition of the next PDADMAC layer.

To understand the observations, one needs to distinguish between the pore and the layer-dominating regime and take the swelling characteristics of the PEs into account. In the pore-dominating regime, the PEs adsorb mainly at the wall inside the pore of the support, while the PEs cover the pore in the layer-dominating regime. PDADMAC-terminated films swell four times more than PSS-terminated ones [28]. Thus, the PDADMAC-terminated layers in the pore-dominating regime during the first six layers, constricts the pore due to strong swelling; hence, the permeability is lower than the permeability of the PSS-terminated films. Transport resistance in the pore-dominating regime is convection-determined. As soon as the PE film covers the pores (last six layers), water transport is taken over by the resistance of the layer and the resistance through the swollen polymer network. Thus, the "odd-even" effect is now inverted: The more swollen layer has a lower resistance (Figure 6.1b). We pose the hypothesis that for a PE pair with unequal swelling characteristics, such as PDADMAC and PSS, a plot of permeability as a function of layer numbers is suited to judge whether the PEs cover the pores at all and can even be used to determine the first pore-covering layer. Such delicate balance between pore and top layer dominated resistance was recently also observed for microgel filtration. The discussed simultaneous measurements of electric impedance and hydraulic resistance may help to learn more about the crossing over between the two regimes [128]

6.2 Retention

Both membranes, with and without supporting layers, retain bivalent ions well with a slightly higher retention for the membrane without the supporting layers. With 80 to 90% retention for $MgSO_4$, the membranes are comparable to commercially available nanofiltration membranes. The MWCO is only determined for the membrane without the supporting layers. It has a value of about 240 Da (Figure 6.2, Table 6.1). It must be explicitly mentioned that such MWCO values are extremely difficult to attain for ceramic-only NF membranes. However, for the LbL-ceramic hybrid membranes, we succeed to attain these values reliably. Below we will show that this new hybrid monolith NF membrane also possesses remarkable mechanical and chemical integrity.

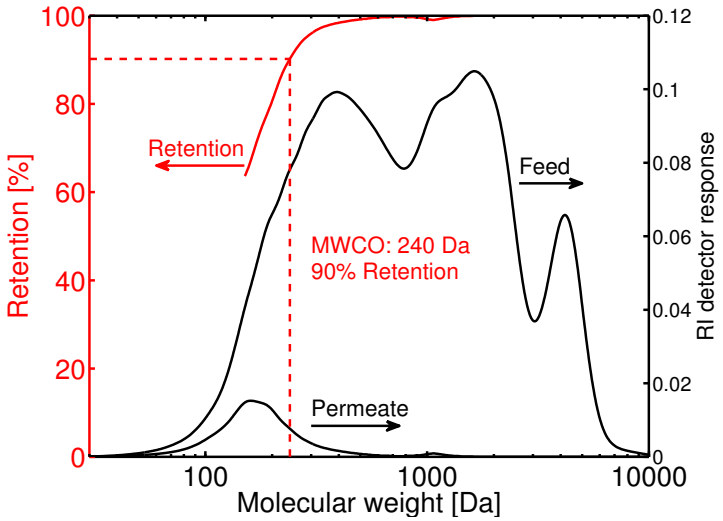

Figure 6.2: Molecular weight cut-off measurement with polyethylene glycol mixture for the coating comprising 3 bilayers coated at 30 LMH for 10 min with 0.1 mol/l NaCl in the PE solution (without supporting layers). Left axes in red: retention; right axes in black: refractive index detector response for feed and permeate.

Table 6.1: Permeability, retention for $MgSO_4$, and molecular weight cut-off determined with polyethylene glycol of various molecular weights for the ceramic membranes with the two different coatings.

Coating	Pure water permeability $[\frac{LMH}{bar}]$	Retention for $MgSO_4$ [%]	MWCO [Da]
6 Layer, 30 LMH, 0.1 M NaCl	15 ± 2	87.9 ± 3	240
6 Layer, 15 LMH, without NaCl	≈ 400	0	-
+			
6 Layer, 30 LMH, 0.1 M NaCl	22.3 ± 1.9	83.8 ± 1.9	-

6.3 Conclusion

The mass transport properties of the membrane – i.e. permeability and retention – are comparable to existing nanofiltration membranes; the permeability is even higher than that of conventional nanofiltration membranes. For fabrication just three bilayers were needed, although a pore of 100 nm had to be covered and closed. Using a supporting layer comprising three bilayers coated at low flux and without salt in the PE solution constricted the pore. As a result, the final separation layers did not penetrate that deep into the porous structure which revealed a final higher permeability.

7

Stability and regeneration of LbL membranes

PE films, assembled from PDADMAC and PSS, also exhibit chemical stability in the presence of hypochlorite as well as low and high pH [31, 71]. Hence, they fulfill the prerequisites of a stable nanofiltration membrane. Besides chemical stability, back-washability is highly desired to ensure fouling migitation and better cleaning. The concept of a backwashable hollow fiber nanofiltration membrane was already addressed by Frank et al. [129] in 2001. The membrane was fabricated by interfacial polymerization. However, the retention behavior was difficult to tune and the production involved non-aqueous solvents. De Grooth et al. [71] demonstrated a backwashable hollow fiber nanofiltration based on LbL technology and proved that the backwash is only non-destructive if the support membrane exhibits sufficient negatively charged groups at the membrane surface.

An issue rarely considered is the regeneration of membranes: it may be considered as a sustainable concept that could potentially minimize polymer consumption. In case of a ceramic support with an LbL film as separation skin, only the LbL film may be regenerated. Thus, regeneration would potentially compensate for the initially costly ce-

Parts of this chapter have been either published in "Daniel Menne, Cagri Üzüm, Arne Koppelmann, John Erik Wong, Chiel van Foeken, Fokko Borre, Lars Dähne, Timo Laakso, Arto Pihlajamäki, and Matthias Wessling. Regenerable Polymer/Ceramic Hybrid Nanofiltration Membrane Based on Polyelectrolyte Assembly by Layer-by-Layer Technique. Journal of Membrane Science, 520:924 – 932, 2016"

ramic membrane support as the more expensive ceramic support but also more stable support could be reused. The life span of such a ceramic support is about ten to 15 years and thus two to five times longer as compared to polymeric membranes. The regeneration would be executed as soon as a) the LbL film is damaged or b) the overall performance of the membrane falls below a certain threshold. By removing the LbL film, potential irreversible fouling would be removed as well, as it is attached to the polymeric LbL assembly [130]. On flat non-porous surfaces, the deconstruction was shown by the use of a highly concentrated salt solution [39, 131] and ionic surfactants (CTAB and SDS) [33, 37, 132]. Ahmadiannamini et al. [74] proposed a route for dissembling PE films for polymeric flat sheet membranes: in case of weak PEs, low or high pH followed by Triton X-100 (non-ionic surfactant) should be applied, whereas strong PEs are removed just by Triton X-100. Ilyas et al. [75] demonstrated the effective removal of weak PEs by a trigger consisting of low pH (pH 3) and high ionic strength (3 M $NaNO_3$) from dense ultrafiltration membranes; however, the presented membrane was not pH-stable. In general, understanding of such destruction process is shallow requiring more systematic research.

This chapter should answer three major scientific questions: 1. Does the LbL film show mechanical and chemical properties that are equal or superior to today's nanofiltration in terms of backwashing and pH resistance? 2. Is it possible to deconstruct such layers while they were specifically made to be chemically and mechanically stable? 3. Is it possible to identify construction and deconstruction systems that resolve this intrinsic contradiction to regenerate the membranes inside the module by complete deconstruction of the used LbL film and, subsequently, rebuild a new native LbL film?

7.1 pH

To study the stability in high pH, a ceramic membrane monolith with three bilayers, assembled at 30 LMH with 0.1 mol/l NaCl in the coating solution, is submerged for a certain time in a NaOH and HCl solution. The permeability is regularly checked and this is depicted in Figure 7.1a and 7.1b. The membranes withstand low and high pH. During the acidic treatment the permeability slightly increases in the beginning and decreases back to the original value after the treatment at pH 0. Thus, the presented membranes are more stable than most existing commercial nanofiltration membranes, which can be employed only within a pH range between 2 and 10 [133]. A comparison with explicitly pH-stable nanofiltration membranes, commercially available and from literature, leads to the conclusion that the presented membrane exhibits a very low MWCO with an extraordinarily high permeability (Table 7.1). Dalwani et al. [134] presented a pH-stable membrane based on sulfonated poly(ether ether ketone) (SPEEK), which was also tested up to pH 14. However, even this approach yielded lower permeability with a higher MWCO than the presented LbL membrane on a ceramic support.

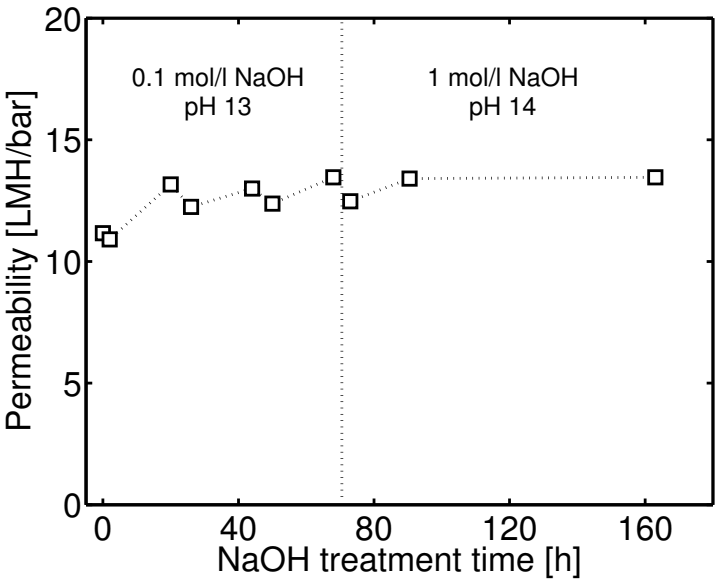

(a) NaOH

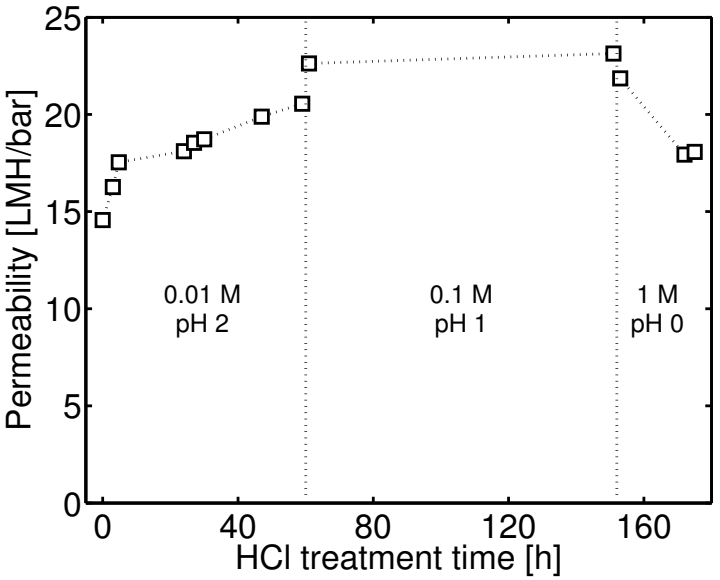

(b) HCl

Figure 7.1: a) Permeability as a function of NaOH treatment time at pH 13 and 14, and b) Permeability as a function of HCl treatment time at pH 0,1, and 2

Table 7.1: Permeability and MWCO for several pH-stable nanofiltration membranes as stated by the manufacturer.

Membrane	Permeability $[\frac{\text{LMH}}{\text{bar}}]$	MWCO [Da]
NP030 (N30F)	>1[a]	400
NF-PES-10	15.4[a]	1000
NTR 7450	11[b]	600-800
MPS-34	2	200
Desal 5 DK	5.4[c]	200
NF based on SPEEK [134]	1- 4.5[d]	≈ 500
LbL on ceramic support (this study)	15 ± 2[d]	240

[a] 40 bar, stirred cell (700 rpm), 5 g/l Na_2SO_4

[b] 10 bar, 2 g/l NaCl, 20-35% recovery

[c] 6.9 bar, 2 g/l $MgSO_4$, 10% recovery

[d] Pure water permeability

7.2 Backwash

A polymeric membrane module coated with four bilayers at 30 LMH was exposed to 30 backwash cycles each at 6 bar for 1 min. After each fifth backwash step, the permeability was measured while the retention was measured only once before backwashing and once after the 30 backwash steps. The permeability as a function of backwash steps is depicted in Figure 7.2a. The permeability did not change due to the backwash procedure. The measured retention for $MgSO_4$ remained unchanged at about 89 % before and after 30 backwashing steps.

The mechanical stability was evaluated for the ceramic support with the same coating as mentioned in Chapter 6 (coating without supporting layers). A backwash – even a superimposed airflush on the lumen side to amplify the shear forces – could not remove the LbL film as

shown in Figure 7.2, thus enabling good cleaning strategies to free the membrane from fouling. Unfortunately, such significant backwash stability may potentially counteract a potential ease of regeneration. De Grooth et al. [71] postulated and proved that a non-destructive backwashing of LbL membranes is possible only for support membranes containing sufficient negatively charged groups at the membrane surface, which would enable a strong interaction between the support membrane and the LbL film. The ceramic membrane employed in the present study is most likely, if at all, slightly negatively charged. Due to geometry reasons, the zeta potential measurements could not be conducted. Rezwan et al. [135] even reported a positive charge for alumina particles below pH 10 while Huisman et al. [136] determined an iso-electric point (IEP) of 8.5 for an α-alumina membrane. Nevertheless, the first applied layer in this study was a polycation. Thus, the good back-washability of the presented membrane contradicts the results from De Grooth et al. [71]. Therefore we hypothesize that the PE film is interlocked in the porous structure and that it cannot be removed by backwashing due to steric reasons rather than due to strong adsorption.

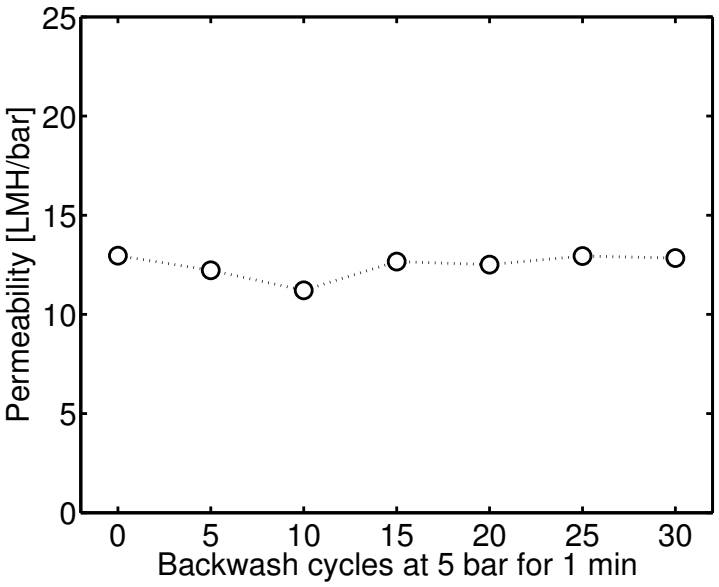

(a) Polymeric support

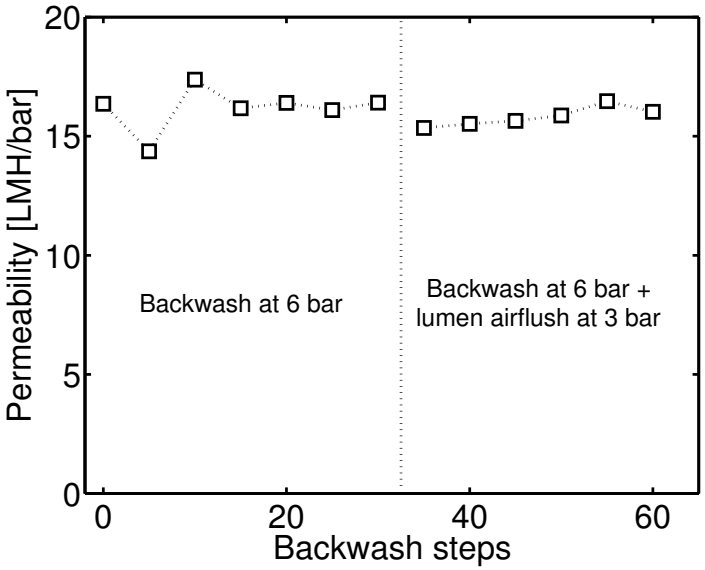

(b) Ceramic support

Figure 7.2: Permeability as a function of backwash steps at 6 bar for a) LbL on the polymeric support and b) LbL on the ceramic support. For the ceramic support, the shear forces have been further increased by a superimposed airflush on the lumen side at 3 bar.

7.3 Electrolytes

Highly concentrated electrolytes diminish the electrostatic interaction between the polycation and polyanion; hence they can be used to remove the layer [39, 131]. For deeper stability analysis of the LbL membranes, salt solutions of stepwise increasing NaCl concentration were filtered through an LbL membrane (red triangles in Figure 7.3). Subsequent to the salt filtration, pure water filtration was conducted to obtain irreversible changes of the membrane due to the salt filtration in advance (black squares in Figure 7.3). The employed membrane was a polymeric hollow fiber (HFs from Pentair X-Flow) with an LbL film comprising four bilayers coated at a flux of 30 LMH with 0.5 mol/l NaCl in the coating solution.

At low salt concentrations, the resistance during salt filtration increased with salt concentration, while it remained constant during the subsequent pure water filtration. The increase of the resistance during salt filtration is most likely induced by concentration polarization and not by an alteration of the LbL film, as NaCl is partly retained and it accumulates at the surface. Above 0.5 mol/l NaCl, the resistance observed during salt filtration decreased again. The electrolytes interfered with the electrostatic interaction within the LbL film, which resulted in lower retention for NaCl and, thus, the impact of concentration polarization diminished. In addition, the resistance observed during pure water filtration decreased. Thus, a salt concentration above 0.5 mol/l altered the membrane in an irreversible manner. Above 1.5 mol/l NaCl, the resistance during pure water filtration increased while the resistance during salt filtration further decreased. For this behavior no reasonable explanation could be found. The retention for $MgSO_4$ decreased from 89% to 53% due to the salt filtration, which underlines the destructive impact of highly concentrated salt on the LbL film.

To put these results in context, one has to look at the salt concentration of seawater, which is about 3.5 w%. Assuming that only NaCl is present in the seawater would reveal a concentration of about 0.6 mol/l. Thus, the presented membrane is not applicable for seawater filtration even if concentration polarization and concentration along the fiber are neglected.

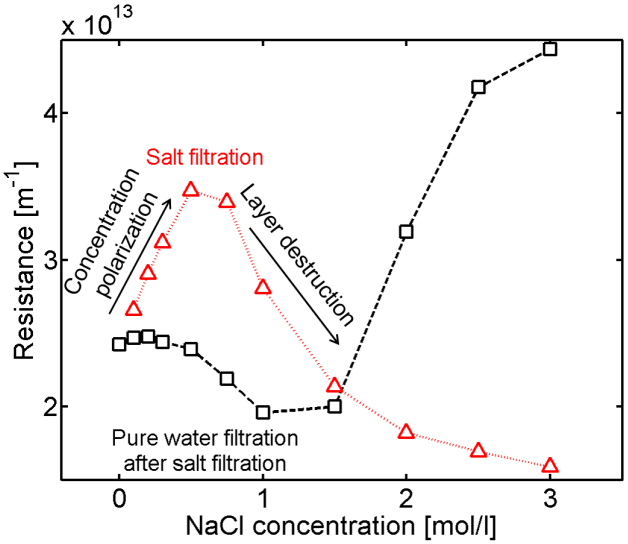

Figure 7.3: Membrane resistance as a function of NaCl concentration used for the filtration. Red triangles: filtration at with salt solution at a certain NaCl concentration. Black squares: pure water filtration after salt filtration.

7.4 Layer deconstruction for regeneration

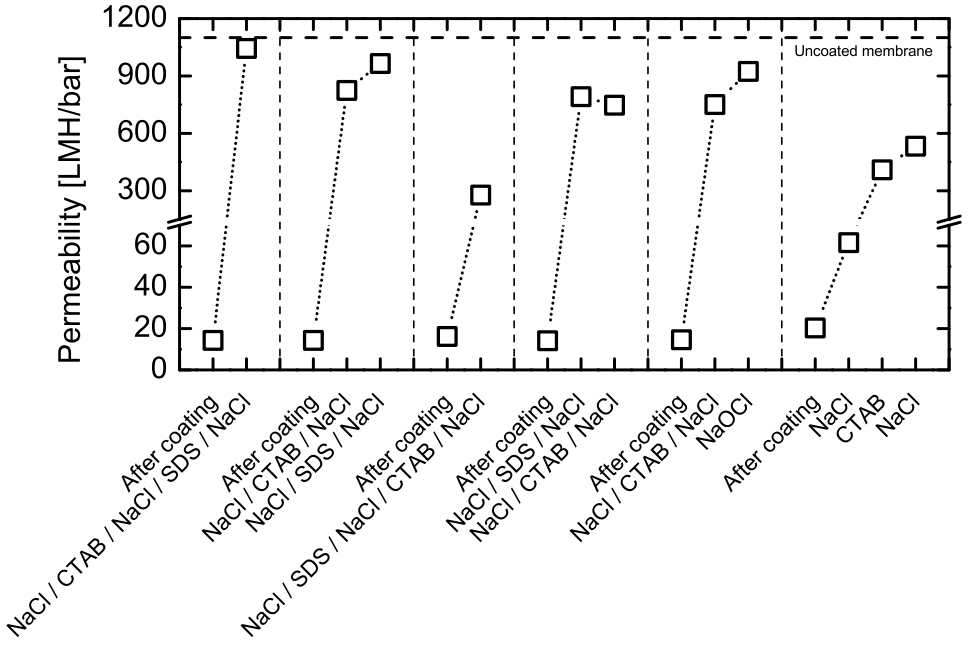

Figure 7.4: Permeability before and after treatment with various chemicals. All treatment steps were performed in backwash operation mode. NaCl / CTAB / NaCl means that the membrane was treated with NaCl, CTAB, and again with NaCl. Between each step, the membrane was not flushed with water. For each layer-removal test, a freshly coated membrane was employed.

The layer removal for membrane regeneration is studied using four different solutions: 1) highly concentrated NaCl solution (5 mol/l), 2) CTAB, a cationic surfactant, 3) SDS, an anionic surfactant, and 4) NaOCl, an oxidizing agent. All methods for layer removal are applied within the membrane module, meaning that dismounting of the membrane from the membrane module is not necessary. It underlines the potential applicability of the regeneration on-site in a real treatment

plant, where dismounting of the membrane is rather elaborate and not desired.

Cationic and anionic surfactants directly in succession, with salt in advance, in between, and as the last step (NaCl / CTAB / NaCl / SDS / NaCl) disassembles the LbL film most effectively. (In this experiment, the membrane is not flushed with water after each step; therefore the pure water permeability after each treatment step cannot be determined.) By this cleaning method, the permeability is almost completely recovered to a value of 1,040 LMH/bar (1,100 LMH/bar for the uncoated membrane). The highly concentrated salt solution screens the charges of the PE, thus diminishing the the electrostatic interaction of the polycation and polyanion. In addition, the cationic surfactant CTAB formed strong complexes with the polyanion (PSS) while the anionic surfactant SDS complexes with the polycation (PDADMAC). The CTAB-PSS and SDS-PDADMAC complexes should be neutral or just slightly charged; thus, the electrostatic interaction of polycation and polyanion vanishes, enabling the removal of the LbL film.

However, on swapping the cationic and the anionic treatment steps, which means that the treatment with SDS was applied first (NaCl / SDS / NaCl / CTAB / NaCl), the permeability increases only to about 280 LMH/bar . Most likely, the SDS-PDADMAC complexes, which are formed during the exposure to SDS, are not flushed out during the subsequent salt treatment. By applying CTAB, large PDADMAC-SDS-PSS-CTAB complexes might be formed that can not be removed from the membrane due to steric reasons. Furthermore, the effect of SDS on PDADMAC/PSS films might be less significant than the effect of CTAB [33, 37]. So, the removal strength of the PDADMAC/PSS layers depends on the application order of CTAB and SDS. If SDS is added as the first surfactant, it competes with the PSS, whereas if it is

the second surfactant, it can easily complex with the PDADMAC, as PSS is already trapped by the CTAB. It should be noted, however, that a longer or second salt treatment between SDS and CTAB exposure could have removed the PDADMAC-SDS complexes, which would have prevented the complex formation of PDADMAC-SDS-PSS-CTAB.

Sodium hypochlorite (NaOCl) as a subsequent treatment to the treatment with NaCl / CTAB / NaCl is another very effective cleaning strategy. It is known that PDADMAC and PSS is considerably stable with respect to hypochlorite [31]. However, after the NaCl / CTAB / NaCl treatment the remaining PSS is mainly present as PSS-CTAB complexes. These complexes can be attacked by the free chlorine radical or the strong oxidizer hypochlorite was removed easily and, thus, the permeability increases to 930 LMH/bar.

The treatment with NaCl / CTAB / NaCl increases the permeability to about 830 LMH/bar. The same treatment steps, although now with water flushing and permeability determination after each step, result in a permeability increase to only 530 LMH/bar. In other words, intermediate water flushing decreases the treatment's effectiveness. A potential explanation is the complexation degree of CTAB with PSS under various ionic strengths. In general, CTAB can complex at every single monomer within the large PSS chain. At low ionic strength, the degree of complexation should be high, resulting in large and non-charged complexes. As they are neutral, the complexes might aggregate among each other due to increased hydrophobic interactions. These aggregates are sterically entangled in the membrane pore and, thus, cannot be removed from the porous structure. Using highly concentrated salt solution directly after CTAB might result in only partial complexation of the CTAB and the PSS. As a result, the PSS-CTAB complexes are still partially charged, thus diminishing the complex

aggregation. Therefore, the complexes might be smaller when using salt directly, leading to a more effective treatment. Additionally, once PDADMAC/PSS layers are disassembled and the CTAB/PSS complex is formed, the highly concentrated salt solution might even partially decompose the CTAB/PSS complex, fastening its removal from the pores.

Despite its disadvantage for the layer-removal performance, this treatment with water flushing in between enables the evaluation of each single treatment step as the pure water permeability after each step could be measured. Due to the first salt treatment, the permeability increases from 15 to 60 LMH/bar. The high ionic strength screens the charges of the PE removing the film partly. The remaining PE film swells due to the salt treatment. Furthermore, the swelling allowed better penetration of the CTAB molecules into PE film during the next treatment step. This treatment increases the permeability further to about 400 LMH/bar.

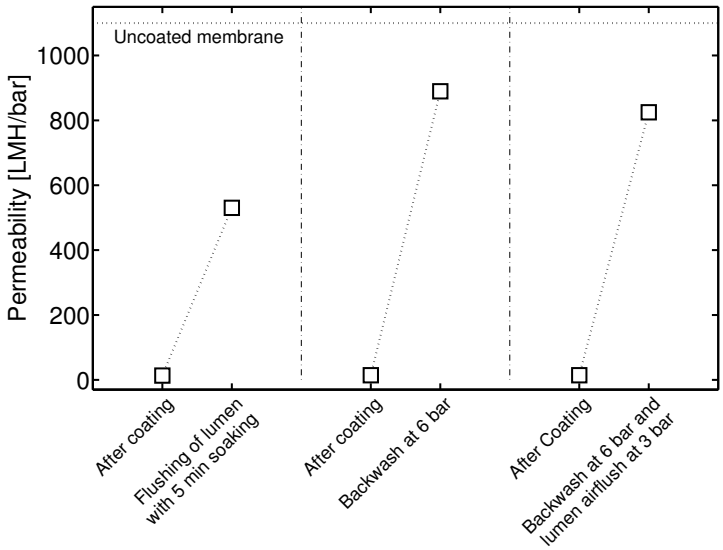

Figure 7.5: Pure water permeability as a function of different treatment methods for the treatment with salt and cationic surfactants (NaCl / CTAB / NaCl). Each layer removal method was applied on a freshly coated membrane.

The cationic treatment consisting of three steps – NaCl / CTAB / NaCl (without water flushing in between) – is performed in three different ways (Figure 7.5): a) rinsing of the chemicals on the lumen side of the membrane with a waiting step (to ensure a similar treatment time as compared to the two latter options), b) a backwash of the treatment solution with a permeate pressure of 6 bar, and c) a backwash of the chemicals at 6 bar with simultaneous airflush at 3 bar on the lumen side to further boost the shear forces. Rinsing on the lumen increases the permeability to only 530 LMH/bar, while backwashing with or without simultaneous lumen airflush recovers the permeability to a value between 800 and 900 LMH/bar. The PEs penetrates into the porous structure of the support during the coating procedure; thus, a treatment only on the lumen side of the membrane is not sufficient. The airflush do not improve the layer removal, as the permeability was almost the same as compared with the backwash-only treatment.

7.5 Regeneration cycles

For the layer removal and layer rebuilding cycles, the cationic treatment with a subsequent hypochlorite treatment was chosen. As soon as the permeability is recovered to a value above 900 LMH/bar, the layers are rebuilt. The properties, pure water permeability (Figure 7.6) and retention for $MgSO_4$ (Figure 7.7), do not change due the regeneration process as it always regained the same values after coating. After the third rebuilding step, the layer removal does not work as well as for the first three times, suggesting that, with each regeneration, a small amount of the PE remains on the support. This remaining part might accumulate on the surface, with each regeneration cycle affecting the new layer properties. Hence, the method requires more extensive fine-tuning. Yet, the retention properties remain high and reproducible. Additionally to the cleaning methods with surfactants, oxidants and salts, a more harsh cleaning, called RCA (named after the founder the Radio Corporation of America), involving hydrogen peroxide and ammonium hydroxide at 85 °C is applied. This method is commonly applied for semiconductor processing to clean silicon wafer and was adopted here to ceramic membranes. With this method the permeability could be recovered completely to its original value. However, this method is not applicable on site in a membrane plant as harsh chemicals are involved and thus its practical relevance is limited. Nevertheless, a strategy could pursue to regenerate the modules as often as possible on site before the membranes are exchanged and recovered with the RCA method at an off-site facility.

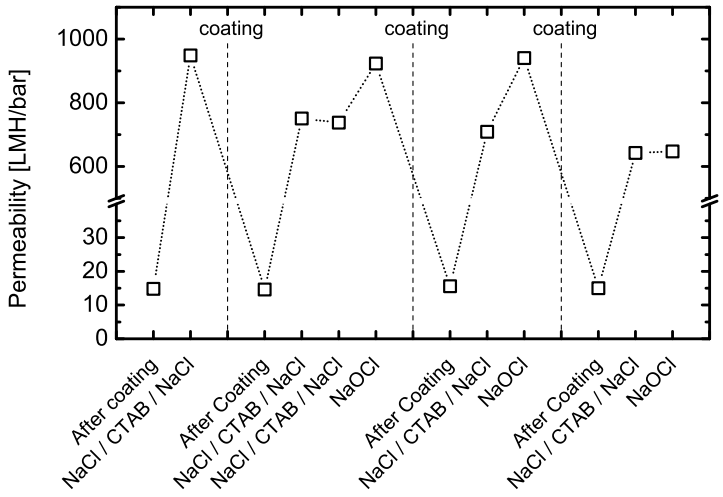

Figure 7.6: Permeability as a function of regeneration cycles.

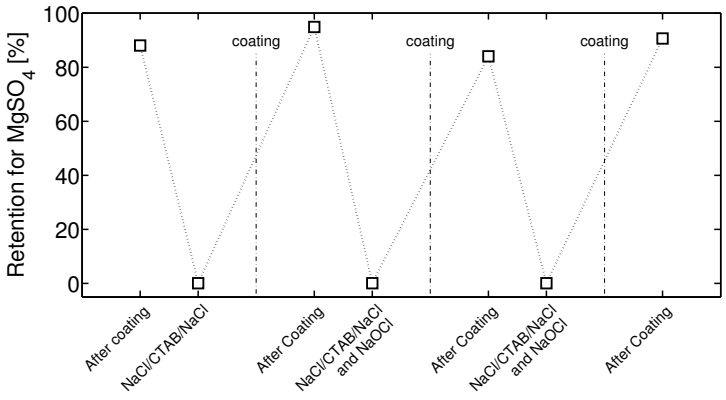

Figure 7.7: Retention for $MgSO_4$ as a function of regeneration cycles.

7.6 Conclusion

The membrane shows excellent stability with respect to backwashing (with and without simultaneous airflush) and high pH. Therefore, it can be employed in harsh environments where conventional nanofiltration membranes are not suitable. Furthermore, due to the membrane's good physical and chemical stability, a wide range of cleaning strategies can be applied to free the membrane from any performance-decreasing fouling. The polymeric LbL film is regenerable: It can be disassembled and rebuilt. Regeneration could be conducted as soon as the polymeric film is damaged or once the performance decline due to irreversible fouling falls below a certain threshold. In the second case, the disassembly of the polymer layers would automatically remove the foulants that are attached to the LbL film, increasing the permeability close to the original values of an uncoated membrane. The more expensive ceramic support can be reused, which improves the economic competitiveness of such a hybrid ceramic/polymeric membrane system. In real treatment plants, the regeneration can be performed on-site without dismounting the membrane modules from the plant as only environmental friendly chemicals are used.

8

Application of LbL membranes

8.1 Benchmark study to compare LbL-coated membranes with commercially available nanofiltration membrane at real test conditions

To evaluate the performance of LbL membranes, a benchmark study on real waste water was conducted. The effluent from the waste water treatment plant in Kaarst (Germany) was brought to Aachen and was filtered for one week. The facility in Kaarst is equipped with an ultrafiltration module for downstream processing; thus, the effluent that was used as feed in this study is the permeate of an ultrafiltration membrane. Three different membranes were tested: 1) LbL on a polymeric support, 2) LbL on a ceramic support, and 3) as benchmark, a commercially available spiral-wound module NF270-2540 from DOW Filmtec. Feed and permeate samples have been taken to determine the retention for TOC, various ions, and micropollutants. The permeability was measured regularly to observe the flux decline due to fouling. The detailed experimental procedure and information about the various applied membranes can be found in Section 3.7. As explained in Section 3.7, the feed concentration fluctuated quite a lot and the different geometries of the membranes resulted in various flow patterns in the feed channel. Thus, a comparison of the LbL and commercially

Table 8.1: Pure water permeability and $MgSO_4$ retention before real water filtration.

	NF270	LbL/Ceramic	LbL/Polymeric
Permeabilitiy [LMH/bar][a]	9	15	10
Retention $MgSO_4$ [%][b]	99	74	85

[a] Determined with pure water at constant feed pressure level of 0.5 bar in dead-end mode

[b] Determined at 3.5 bar retentate pressure under turbulent conditions – i.e. $Re \approx 3{,}000$ as explained in Chapter 3.3

available nanofiltration membrane based just on this study might be misleading.

Pure water permeability and $MgSO_4$retention Before real water filtration, the pure water permeability and the retention for $MgSO_4$ was measured (Table 8.1). The commercially available NF270 showed the lowest permeability with the highest retention for $MgSO_4$.

Permeability decline and TOC retention The LbL membranes retained about 50% of the TOC and performed almost as well as the NF270 (Figure 8.1a). The retention of TOC was surprisingly low for all membranes, showing that the water contained many really small molecules, such as micropollutants.

Only the NF270 membrane showed more or less no permeability decline and, hence, no fouling (Figure 8.1b). The membrane had feed spacers that introduced turbulences, which increased the shear forces at the surface. Thus, the flux decline due to fouling was less pronounced. However, these turbulences also caused a pressure loss in the axial direction of about 0.4 bar. The pressure loss measured for the LbL membranes was – with 0.1 and 0.01 bar for the polymeric and the ceramic support, respectively – considerably lower. The pressure loss

has to be compensated by the feed pump, leading to higher energy consumption for the NF270. The shear forces induced by the laminar flow pattern in the hollow fiber (polymeric) / tubular (ceramic) LbL membranes were too low, thus resulting in fouling. However, these membranes can be cleaned by backwashing, pH, and oxidizing media (Section 7), which is not an option for the NF270.

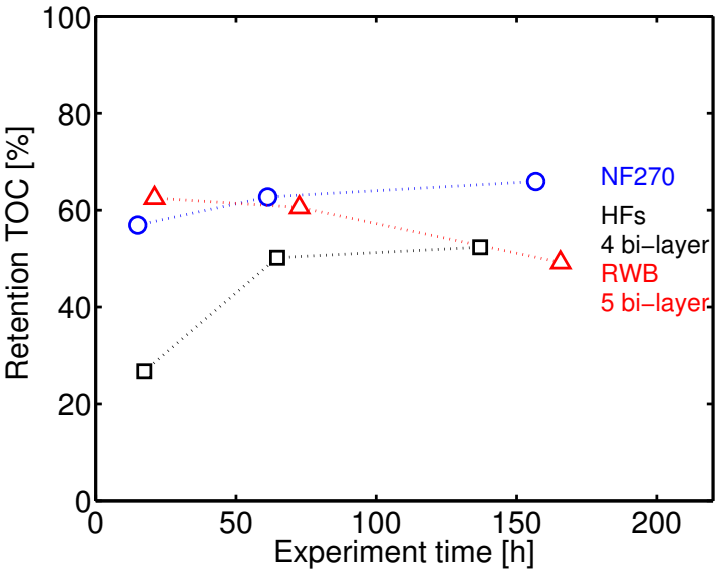

(a) TOC Retention

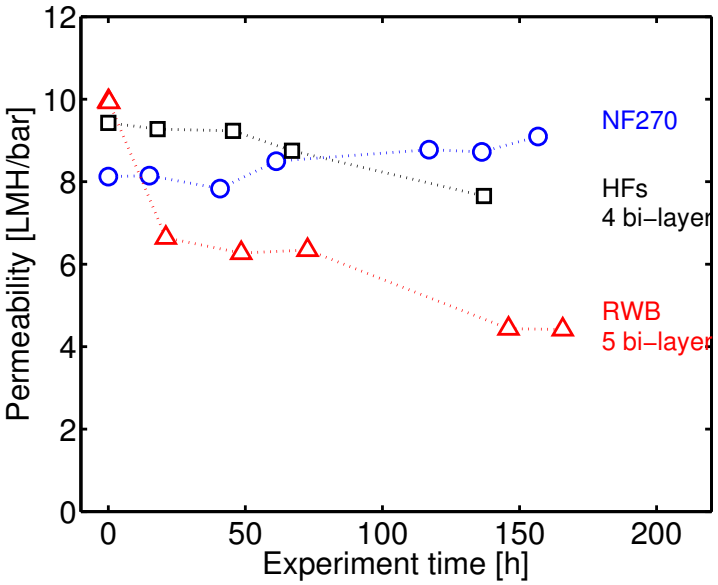

(b) Permeability

Figure 8.1: a) TOC Retention and b) permeability as a function of experiment time.

Ion retention Feed and permeate samples were analyzed to determine the concentration of four different ions: Cl^-, $SO_4{}^{2-}$, Na^+, and Mg^{2+}. The retention of the monovalent ions Cl^- and Na^+ was low for

all tested membranes. While the retention of Cl^- was similar for all membranes (Figure 8.2a), the Na^+ rejection was slightly higher for the NF270 (Figure 8.3a). The retention of bivalent ions was high irrespective of the applied membrane. ${SO_4}^{2-}$ was retained by the NF270 by nearly 100%, while the LbL membranes showed a retention of about 80 to 90% (Figure 8.2b). The strong negative charge of the NF270 is responsible for the high retention. The retention of bivalent cations, such as Mg^{2+}, was comparable for all tested membranes (Figure 8.3b). Since the LbL membranes' retention of monovalent cations was worse than the NF270, the selectivity for monovalent over bivalent cations was higher for the LbL membranes.

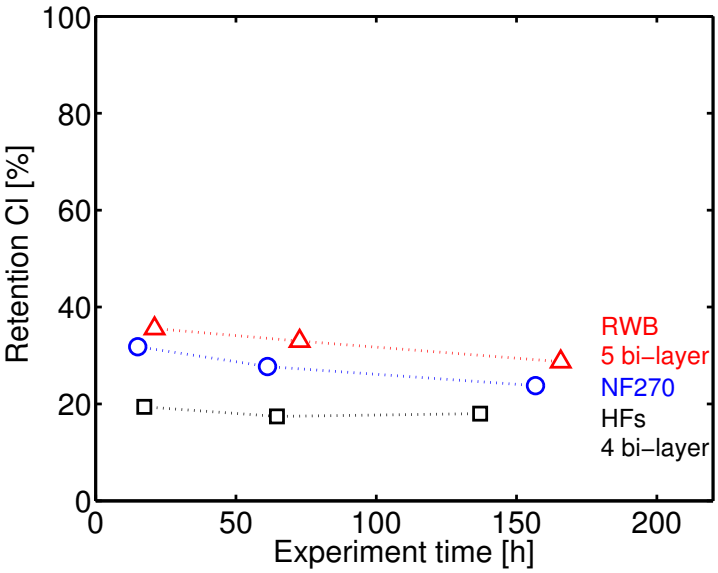

(a) Retention for Cl^-

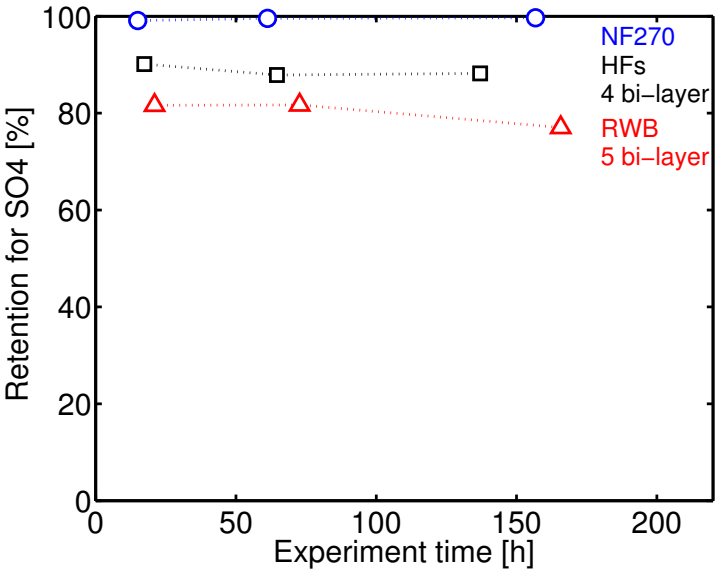

(b) Retention for SO_4^{2-}

Figure 8.2: Retention for anions as a function of experiment time: a) Cl^- and b) SO_4^{2-}.

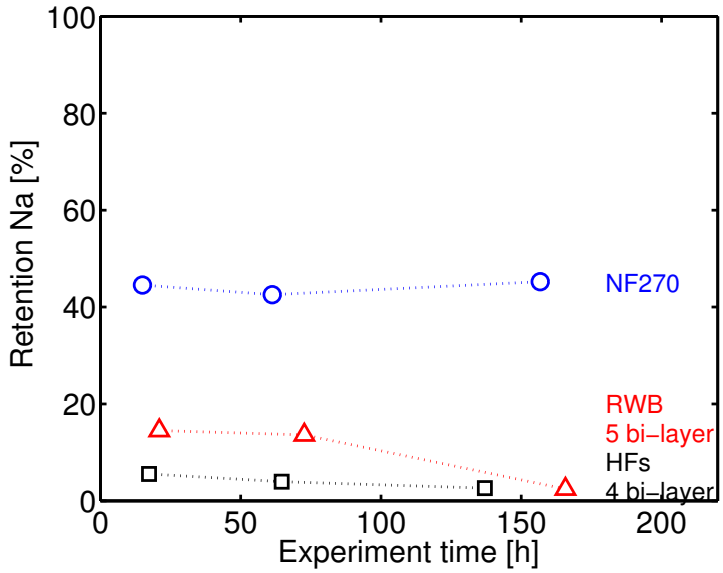

(a) Retention for Na^+

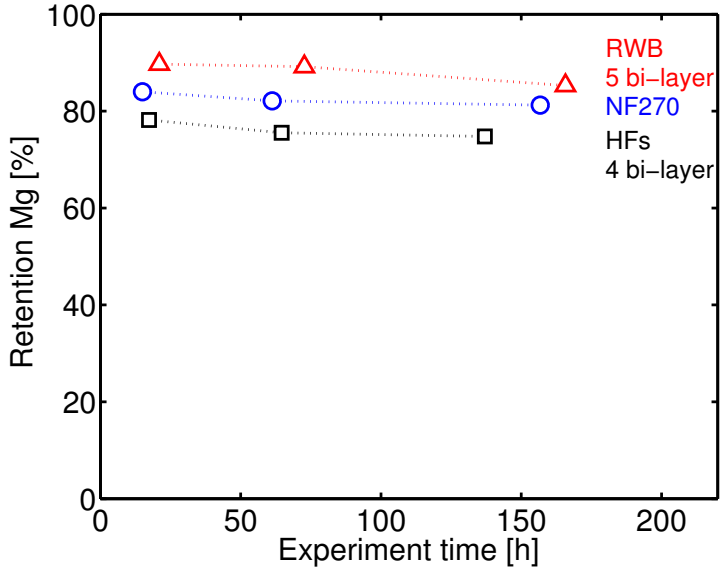

(b) Retention for Mg^{2+}

Figure 8.3: Retention for cations as a function of experiment time: a) Na^+ and b) Mg^{2+}.

Retention of micropollutants Permeate and feed samples were analyzed to detect four different micropollutants. These micropollutants as well as their molecular weight and charge are listed in Ta-

Table 8.2: Molecular weight and charge of the analyzed micropollutants.

	Molecular weight [g/mol]	charge
Benzotriazole	119.13	neutral
Carbamezepine	235.27	neutral
Sulfamethoxazole	253.28	neutral
Diclofenac	296.15	negative

ble 8.2. Given the molecular weight of the micropollutants it is not surprising that Benzotriazole was rejected neither by the NF270 nor by the two LbL membranes (Figure 8.4a). The NF270 retained Carbamezepine even though the cut-off of the membrane is, with 270 Da, higher than the molecular weigth of Carbamezepine. The LbL membranes retained Carbamezepine to only about 20 to 30% (Figure 8.4b). The other two micropollutants are fully retained by the NF270 while the LbL membrane rejected Sulfamethoxazole and Diclofenac to about 50% and 70%, respectively (Figure 8.5a and 8.5b). The highest retention was determined for Diclofenac. It was the compound with highest molecular weight and, in addition, it was negatively charged; thus, the highest retention for Diclofenac was expected.

According to Chapter 5, the MWCO of the applied LbL membranes should have been around 250 Da; thus, the retention for Sulfamethoxazole and Diclofenac should have been higher. The cut-off of 250 Da was determined at turbulent conditions, whereas this study was conducted with a laminar flow pattern and much lower crossflow velocity, leading to worse retention behavior. In addition, the LbL membranes were prepared at an early state of researching this thesis. By now, the coating methods and the handling with the coating device have been optimized, resulting in more reproducible, defect-free, and uni-

form LbL films. Thus, a repetition might show better results for the LbL membranes, though most likely lower retentions than observed for the NF270.

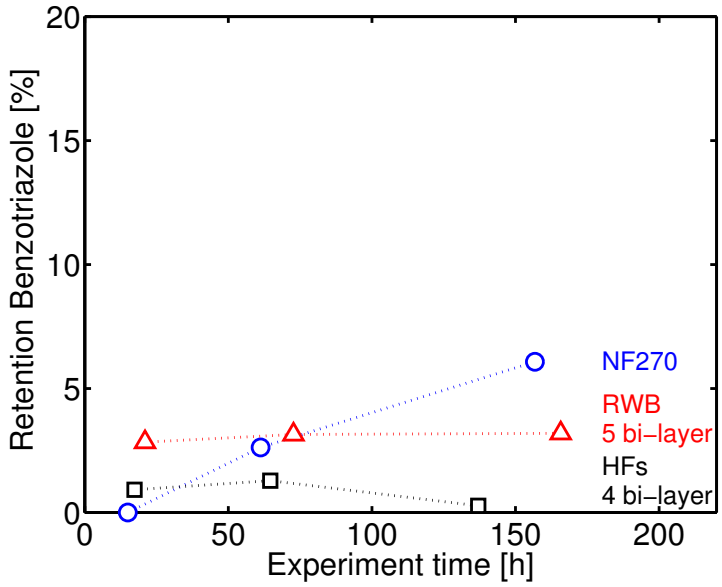

(a) Retention for Benzotriazole

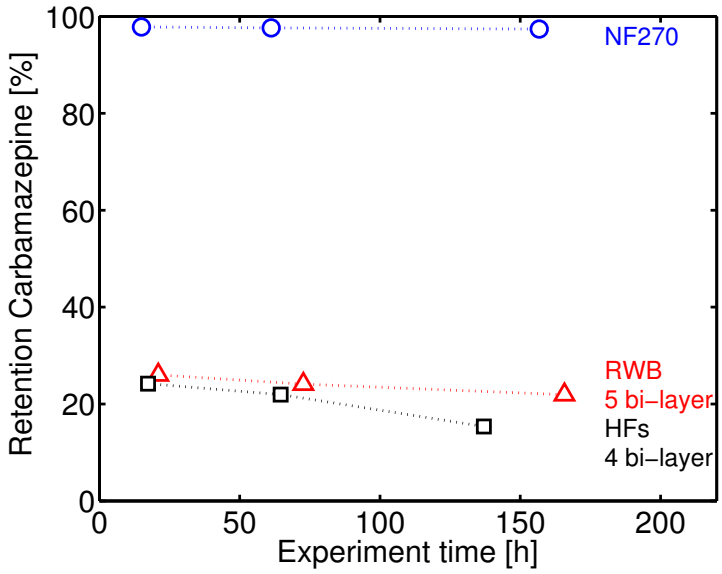

(b) Retention for Carbamezepine

Figure 8.4: Retention for various micropollutants: a) Benzotriazole, and b) Carbamezepine

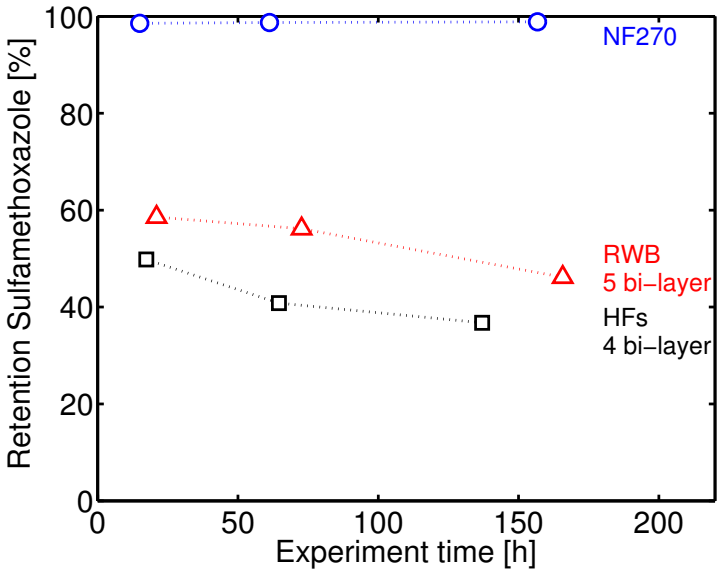

(a) Retention for Sulfamethoxazole

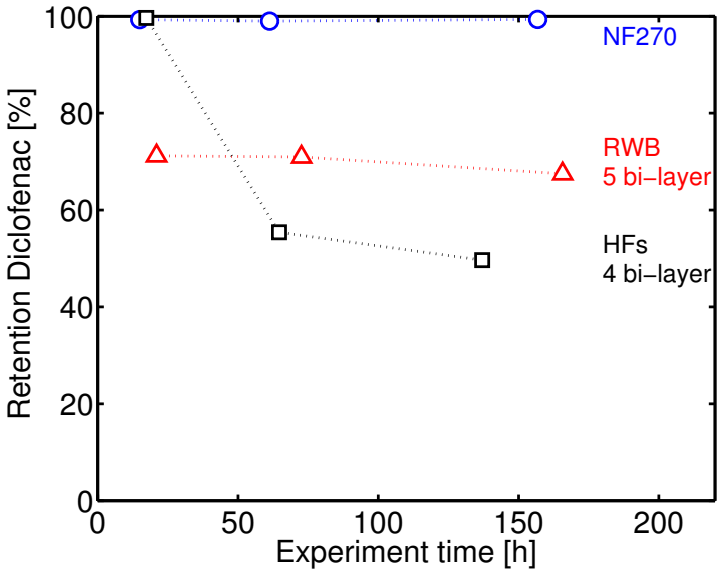

(b) Retention for Diclofenac

Figure 8.5: Retention for various micropollutants: a) Sulfamethoxazole, and b) Diclofenac

Conclusion This benchmark study showed clearly that the NF270 performed better than the LbL membranes tested here. The flux decline was less and the retention was always better than the one deter-

mined for the LbL membranes. Only bivalent cations were retained in a comparable manner by the LbL membranes.

Nevertheless, the flexibility of the LbL system to prepare the right membrane for a certain separation task (Chapter 5) and the good cleaning options (Chapter 7) are advantages of the LbL membranes.

8.2 Tubular ceramic LbL membrane for lignin filtration

Fossil resources, such as oil and gas, will be depleted in the future. Thus, processes based on lignocellulosic biomass as renewable feed stock to synthesise fuels and chemicals are highly desired. A common approach is to fraction lignocellulose into its constituents: cellulose, hemicellulose, and lignin. Cellulose and hemicellulose are converted to platform chemicals, such as malic acid, levulinic acid, and itaconic acid [137] (see Chapter 8.3). In order to achieve an economically feasible process, lignin must be converted into products as well [138]. However, existing techniques process the lignin with expensive catalysts at undesired high temperatures and pressures [139].

Recently, a new process for the electrochemical depolymerization of lignin to vanillin was reported [140, 141]. However, the product yield of this process is rather low and limited due to overoxidation of the product to CO_2. Thus, an *in situ* product recovery with a membrane increases the yield of the product [140]. The process is run at alkaline conditions at a pH of a least 12.5 in order to dissolve lignin. Thus, most commercial nanofiltration membranes are not suited for this task as they are not stable at this high pH. Furthermore, the product (vanillin, MW: 152 Da) should pass the membrane while lignin (MW: $\approx$ 1000-5000 Da) must be rejected and recirculated to the reactor. As the

LbL film is stable even at high pH (Section 7.1) and it can be tailored precisely (Chapter 5), an LbL membrane is well suited to meet the requirements of this process.

A ceramic monolith, as described in Chapter 6, was used as support and coated with six bilayers. As the LbL film should not be too dense to avoid vanillin retention, a coating that does not cover but that constricts the pores was pursued. The coating was conducted without any salt and under low flux conditions of 15 LMH. The resulting membrane showed a pure water permeability of 15 LMH/bar and a retention for $MgSO_4$ of about 25 % (measurements conducted as explained in Section 3.3 and 3.4).

This membrane retained lignin between 75 and 90% (measured with UV-VIS at 283 nm wave length), depending on the applied crossflow velocity (Figure 8.6a). Increasing the crossflow resulted in a higher retention, which is in agreement with theoretical considerations concerning concentration polarization. Size exclusion chromatography revealed complete retention for bigger molecules (>1000 Da) while smaller molecules passed the membrane as desired.

This example shows the potential use of LbL membranes in industrial applications. In particular, niche markets with tailored cut-offs and operations under harsh conditions can be addressed by LbL membranes.

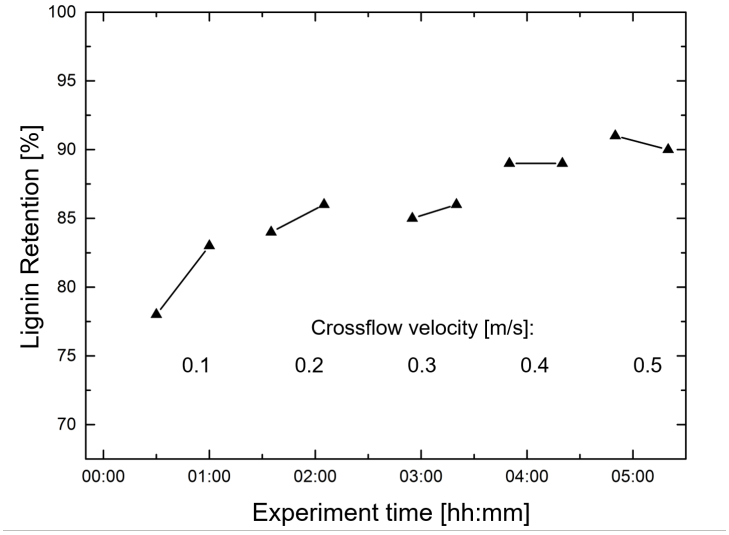

(a) Retention

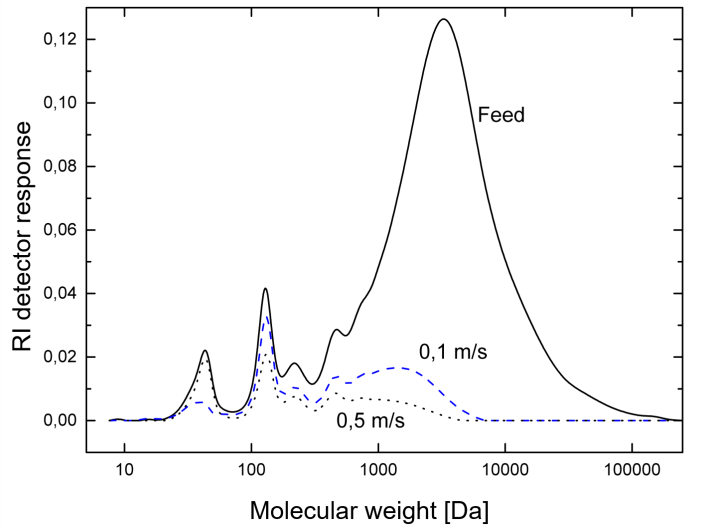

(b) Molecular weight distribution

Figure 8.6: a) Lignin retention measured by UV-VIS as a function of experiment time and crossflow velocity. b) Molecular weight distribution of feed and permeate at two varying crossflow velocities

8.3 Separation of itaconic acid from glucose at various pH

The production of the platform chemical itaconic acid from cellulose and hemicellulose in biorefineries is a promising alternative to fossil fuels as feedstock. After the fractionation of lignocellulose into its constituents – cellulose, hemicellulose and lignin – cellulose and hemicellulose are hydrolyzed to monosaccharides, such as glucose and xylose. In a second step, the monosaccharides are fermented to itaconic acid by microorganisms, e.g. *Aspergillus terreus* or with *Ustilago maydis* [137]. While *Aspergillus terreus* produces itaconic acid at a pH lower than 2 [142], *Ustilago maydis* is most effective at a pH between 4.5 and 6 [143].

After fermentation, unreacted glucose and the produced itaconic acid must be separated. This can be achieved by nanofiltration. Since the molecular weight of itaconic acid (130 Da) does not differ much from that of glucose (180 Da), the retention will be comparable for both components using commercial membranes. As two different microorganisms working at varying pH levels were identified, the separation performance at pH 2 and 6 was investigated. Using a conventional nanofiltration membrane (Desal DL) at pH 2, the glucose and the itaconic acid are retained by 98% and 66%, respectively, while at pH 6 the retention is the same for the both (Table 8.3). The itaconic acid is at least once and partly also twice negatively charged at pH 6; thus, the high retention can be explained by Donnan exclusion as the membrane is negatively charged.

Using a LbL membrane with four bilayers coated on the polymeric support at 30 LMH with 0.5 mol/l NaCl in the coating solution reveals, in general, a lower retention of glucose. Depending on the pH,

Table 8.3: Retention for glucose and itaconic acid for a conventional nanofiltration membrane and an LbL membrane for two different pH values.

	Desal DL		LbL	
	Glucose	Itaconic Acid	Glucose	Itaconic Acid
pH 2	98	66	69	13
pH 6	98	98	67	93

the membrane retained itaconic acid either hardly ever or almost completely (Table 8.3); thus, the retention behavior of the LbL membrane at pH 6 was inverse to that of the conventional nanofiltration membrane at pH 2, i.e. the retention of itaconic acid is higher as for glucose although itaconic acid is smaller the smaller molecule.

These filtrations were conducted at an early stage of this thesis. By now, we understand these membranes much better. As shown in Chapter 5, the cut-off will further increase by adding more layers, while the ion retention remains constant. Thus, a membrane with high retention for itaconic acid and a very low retention for glucose can be prepared. This might result in an interesting new process design. By the use of a conventional nanofiltration membrane, the product itaconic acid will accumulate in the permeate; thus, a second process step to concentrate the itaconic acid is required. With an LbL membrane as described above, the concentration and separation can be merged into a single step as itaconic acid accumulates in the retentate.

9

Conclusion and outlook

In this thesis, the LbL technique with PEs for membrane modification was applied to tailor the separation performance of polymeric hollow fiber membranes. Therefore, a new coating method for precise membrane tuning involving constant flux permeation was developed. It was shown that the PE mass transported convectively to the surfaces determines the properties of the membrane (Chapter 4). The membranes prepared with this new method showed a performance that is equal or even superior to existing nanofiltration membranes. The MWCO was about 240 Da with a permeability of about 15 LMH/bar.

This method was applied to further study the impact of various coating parameters on membrane performance (Chapter 5). It is shown that membrane performance can be precisely tailored with various coating parameters and, thus, the perfect membrane for a certain separation task can be achieved (Figure 9.1). Surprisingly, the MWCO increased with layer number, particularly for the coatings with 0.25 and 0.5 mol/l NaCl in the PE solution. The observations have been associated with the accumulation of PDADMAC in the LbL film and, hence, the strong swelling of the film. While the cut-off increased, the retention for ions remained constant. Thus, the LbL membrane can be tailored to be selective for big organic compounds (M_w >6000) while ions are retained. To the best of our knowledge, this is the first membrane to have this feature.

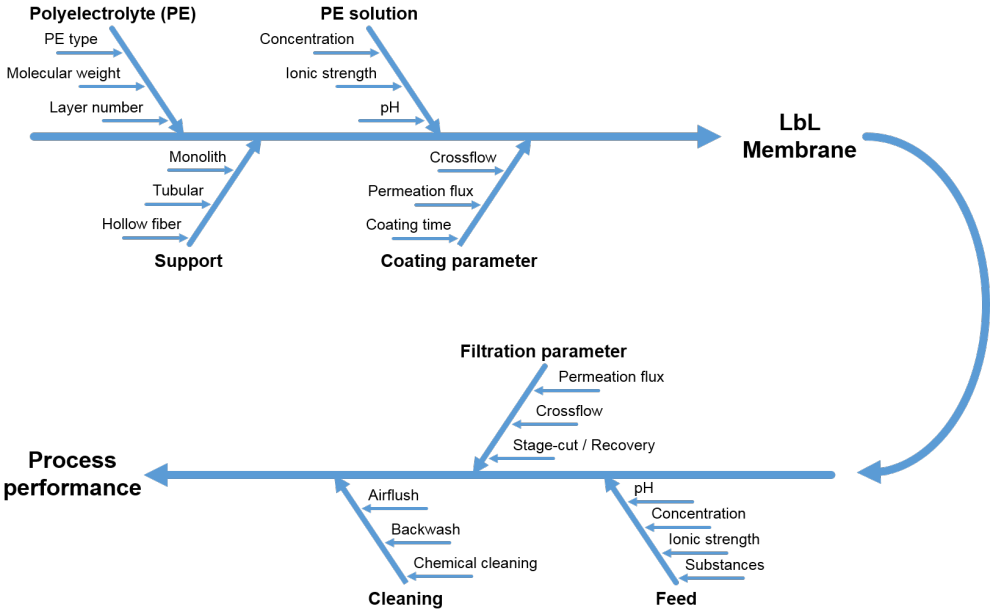

Figure 9.1: Parameter influencing the synthesise of the LbL membrane and the process performance

The coating method was adopted to ceramic membranes (Chapter 6). The rather open pores of about 100 nm could be covered and closed with only three bilayers. Using a supporting layer comprising three bilayers coated at low flux and without salt in the PE solution constricted the pore. Thus, the final separation layers (three bilayers with salt and higher coating flux) did not penetrate that deep into the porous structure, which revealed a higher permeability. The resulting ceramic LbL membrane, irrespective of whether a support layer was used or not, showed performance comparable to existing nanofiltration membranes. Recent developments bear good all-ceramic nanofiltration membranes [123, 124]. However, they are very difficult and cumbersome to prepare in a defect free way, and are too expensive to be competitive to polymeric nanofiltration membranes. Thus, membrane presented here, might be a viable alternative, from the technical and economical, points of view.

The stability with respect to backwashing (using a polymeric and a

ceramic support) and high pH (only the ceramic support as the polymeric support itself is not pH stable) was demonstrated (Chapter 7). The presented membrane showed better stability than today's nanofiltration membranes based on polyamides. The high stability enables good cleaning opportunities. In case of the ceramic support, the membrane can be employed under harsh conditions such as high pH. Even organic solvent nanofiltration might be feasible as the LbL film is stable with respect to organic solvents as presented elsewhere [35, 72, 73]. Using salts diminished the electrostatic interaction of the PEs resulting in irreversible changes in the membrane performance. Thus the membranes cannot be applied for seawater filtration.

However, regeneration – i.e. desired film deconstruction and rebuild – is of great interest. If the membrane performance cuts below a certain threshold due to irreversible fouling, the LbL film can be renewed. The deconstruction was demonstrated on a ceramic membrane as support material by the use of highly concentrated salt solution, ionic surfactants, and hypochlorite. The membrane was regenerated thrice and is, to the best of the author's knowledge, the first regenerable ceramic nanofiltration membrane based on a ceramic multichannel support. Regeneration improves the economic situation as the more expansive and more stable ceramic support is reused. During regeneration, the monolith must not be dismounted, which underlines the potential applicability of the regeneration on-site in a real treatment plant, where dismounting of the membrane is rather elaborate.

This thesis characterized the membranes only in a macroscopic way based on performance parameters such as retention and permeability. Microscopic characterization, except for a few scanning electron microscopy images, could not be conducted due the geometry of the employed membranes (hollow fiber and tubular), as the employed mem-

branes were prescribed by an EU-project (LbLBRANE). Therefore, further studies should focus on the microscopic level for better understanding of the presented coating method and film formation. Although many studies within the last two decades dealing with LbL film characterization have been published, none of them involved the presented coating method, as it is applicable on porous supports only. For real applications, hollow fibers and tubular membranes are much more interesting. Nevertheless, the presented coating method should be adopted to flat geometries. Flat sheet membranes can be much better characterized and, thus, deeper insights into the thickness, structure, and morphology of the LbL film are possible. With these characterizations, the observations of this thesis, for instance the increase of the MWCO with increasing layer number, might be explained.

In terms of applications, the membranes should be tested further within several different processes. For instance, the use of the ceramic LbL membrane for organic solvent nanofiltration is highly promising. Furthermore, the first pretest using the membrane for phosphate recovery together with the University of Applied Sciences and Arts Northwestern Switzerland showed great potential. Moreover, the applications already mentioned here, such as lignin filtration and itaconic acid glucose separation, should be pursued further.

Bibliography

[1] Mark A. Shannon, Paul W. Bohn, Menachem Elimelech, John G. Georgiadis, Benito J. Mariñas, and Anne M. Mayes. Science and technology for water purification in the coming decades. Nature, 452(7185):301–310, 2008.

[2] Bart Van Der Bruggen and Carlo Vandecasteele. Removal of pollutants from surface water and groundwater by nanofiltration: Overview of possible applications in the drinking water industry. Environmental Pollution, 122 (3):435–445, 2003.

[3] Kathleen Moons and Bart Van der Bruggen. Removal of micropollutants during drinking water production from surface water with nanofiltration. Desalination, 199(1-3):245–247, 2006.

[4] Katsuki Kimura, Gary Amy, Jörg E. Drewes, Thomas Heberer, Tae-Uk Kim, and Yoshimasa Watanabe. Rejection of organic micropollutants (disinfection by-products, endocrine disrupting compounds, and pharmaceutically active compounds) by NF/RO membranes. Journal of Membrane Science, 227(1-2): 113–121, 2003.

[5] Long D Nghiem, Andrea I Schäfer, and Menachem Elimelech. Removal of natural hormones by nanofiltration membranes: measurement, modeling, and mechanisms. Environmental science & technology, 38(6):1888–96, 2004.

[6] Long D. Nghiem, Andrea I. Schäfer, and Menachem Elimelech. Pharmaceutical retention mechanisms by nanofiltration membranes. Environmental Science and Technology, 39(19):7698–7705, 2005.

[7] A. I. Schäfer, A. G. Fane, and Thomas D. Waite. Nanofiltration: Principles and Applications. Elsevier Advanced Technology, 2005. ISBN 1856174050.

[8] Jeremy J. Harris, Jacqueline L. Stair, and Merlin L. Bruening. Layered Polyelectrolyte Films as Selective, Ultrathin Barriers for Anion Transport. Chemistry of Materials, 12:1941–1946, 2000.

[9] Chao Cheng, Andriy Yaroshchuk, and Merlin L Bruening. Fundamentals of Selective Ion Transport through Multilayer Polyelectrolyte Membranes. Langmuir, 29:1885–92, 2013.

[10] Ramamoorthy Malaisamy and Merlin L Bruening. High-Flux Nanofiltration Membranes Prepared by Adsorption of Multilayer Polyelectrolyte Membranes on Polymeric Supports. Langmuir, 21:10587–92, 2005.

[11] Lutz Krasemann and Bernd Tieke. Selective Ion Transport across Self-Assembled Alternating Multilayers of Cationic and Anionic Polyelectrolytes. Langmuir, 16:287–290, 2000.

[12] Wanqin Jin, Ali Toutianoush, and Bernd Tieke. Use of Polyelectrolyte Layer-by-Layer Assemblies as Nanofiltration and Reverse Osmosis Membranes. Langmuir, 19:2550–2553, 2003.

[13] Regine v. Klitzing and Bernd Tieke. Polyelectrolyte Membranes. Advances in Polymer Science, 165:177–210, 2004.

[14] Nithya Joseph, Pejman Ahmadiannamini, Richard Hoogenboom, and Ivo. F. J. Vankelecom. Layer-by-Layer Preparation of Polyelectrolyte Multilayer Membranes for Separation. Polymer Chemistry, 5:1817, 2014.

[15] Daniel Menne, Johannes Kamp, John Erik Wong, and Matthias Wessling. Precise tuning of salt retention of backwashable polyelectrolyte multilayer hollow fiber nanofiltration membranes. Journal of Membrane Science, 499: 396–405, 2016.

[16] Daniel Menne, Cagri Üzüm, Arne Koppelmann, John Erik Wong, Chiel van Foeken, Fokko Borre, Lars Dähne, Timo Laakso, Arto Pihlajamäki, and Matthias Wessling. Regenerable Polymer/Ceramic Hybrid Nanofiltration Membrane Based on Polyelectrolyte Assembly by Layer-by-Layer Technique. Journal of Membrane Science, 520:924 – 932, 2016.

[17] G. Decher. Fuzzy Nanoassemblies: Toward Layered Polymeric Multicomposites. Science, 277(5330):1232–1237, 1997.

[18] G. Decher, J.D. Hong, and J. Schmitt. Buildup of Ultrathin Multilayer Films by a Self-Assembly process: III. Consecutively Alternating Adsorption

of Anionic and Cationic Polyelectrolytes on Charged surfaces. Thin Solid Films, 210-211:831–835, 1992.

[19] Zbigniew Adamczyk, Krzysztof Jamroży, Piotr Batys, and Aneta Michna. Influence of ionic strength on poly(diallyldimethylammonium chloride) macromolecule conformations in electrolyte solutions. Journal of Colloid and Interface Science, 435:182–190, 2014.

[20] A.A. Antipov, G.B. Sukhorukov, and H. Möhwald. Influence of the ionic strength on the polyelectrolyte multilayers' permeability. Langmuir, 19(6): 2444–2448, 2003.

[21] Stephan T Dubas and Joseph B Schlenoff. Factors Controlling the Growth of Polyelectrolyte Multilayers. Macromolecules, 32(24):8153–8160, 1999.

[22] Frank Caruso, Kenichi Niikura, D Neil Furlong, and Yoshio Okahata. 1 . Ultrathin Multilayer Polyelectrolyte Films on Gold : Construction and Thickness Determination. Langmuir, 13:3422–3426, 1997.

[23] John E. Wong, Florian Rehfeldt, Peter Hänni, Motomu Tanaka, and Regine V. Klitzing. Swelling behavior of polyelectrolyte multilayers in saturated water vapor. Macromolecules, 37(19):7285–7289, 2004.

[24] Pritesh A Patel, Andrey V Dobrynin, and Patrick T Mather. Combined effect of spin speed and ionic strength on polyelectrolyte spin assembly. Langmuir, 23(25):12589–97, 2007.

[25] Law Yong Ng, Abdul Wahab Mohammad, and Ching Yin Ng. A review on nanofiltration membrane fabrication and modification using polyelectrolytes: effective ways to develop membrane selective barriers and rejection capability. Advances in Colloid and Interface Science, 197-198:85–107, 2013.

[26] Joseph B. Schlenoff and Stephan T. Dubas. Mechanism of Polyelectrolyte Multilayer Growth: Charge Overcompensation and Distribution. Macromolecules, 34:592–598, 2001.

[27] Bastien Seantier and André Deratani. 18. Polyelectrolytes at Interfaces: Applications and Transport Properties of Polyelectrolyte Multilayers in Membranes. In Ionic Interactions in Natural and Synthetic Macromolecules,

pages 683–726. John Wiley & Sons, Inc., Hoboken, NJ, USA, 2012. ISBN 9781118165850.

[28] Matthew D. Miller and Merlin L. Bruening. Correlation of the Swelling and Permeability of Polyelectrolyte Multilayer Films. Chemistry of Materials, 17(21):5375–5381, 2005.

[29] Ramy A Ghostine, Marie Z Markarian, and Joseph B Schlenoff. Asymmetric growth in polyelectrolyte multilayers. Journal of the American Chemical Society, 135(20):7636–46, 2013.

[30] Joris de Grooth, Radek Oborný, Jens Potreck, Kitty Nijmeijer, and Wiebe M. de Vos. The role of ionic strength and odd–even effects on the properties of polyelectrolyte multilayer nanofiltration membranes. Journal of Membrane Science, 475:311–319, 2015.

[31] Danijela Gregurec, Mateusz Olszyna, Nikolaos Politakos, Luis Yate, Lars Dähne, and Sergio Enrique Moya. Stability of polyelectrolyte multilayers in oxidizing media: a critical issue for the development of multilayer based membranes for nanofiltration. Colloid and Polymer Science, 293(2):381–388, 2014.

[32] Sara Llamas, Eduardo Guzmán, Francisco Ortega, Nawel Baghdadli, Colette Cazeneuve, Ramón G. Rubio, and Gustavo S. Luengo. Adsorption of polyelectrolytes and polyelectrolytes-surfactant mixtures at surfaces: A physico-chemical approach to a cosmetic challenge. Advances in Colloid and Interface Science, 222:461–487, 2015.

[33] J. J. Iturri Ramos, I. Llarena, and S. E. Moya. Selective removal of hybrid di-block polyelectrolyte multilayers by means of quaternary ammonium surfactants. Journal of Materials Science, 45(18):4970–4976, 2010.

[34] Orlando J. Rojas, Marie Ernstsson, Ronald D. Neuman, and Per M. Claesson. Effect of polyelectrolyte charge density on the adsorption and desorption behavior on mica. Langmuir, 18(14):1604–1612, 2002.

[35] Xianfeng Li, Steven De Feyter, Dongju Chen, Steliana Aldea, Pieter Vandezande, Filip Du Prez, and Ivo F. J. Vankelecom. Solvent-Resistant

Nanofiltration Membranes Based on Multilayered Polyelectrolyte Complexes. Chemistry of Materials, 20(12):3876–3883, 2008.

[36] G Zhang, H Yan, S Ji, and Z Liu. Self-assembly of polyelectrolyte multilayer pervaporation membranes by a dynamic layer-by-layer technique on a hydrolyzed polyacrylonitrile ultrafiltration membrane. Journal of Membrane Science, 292:1–8, 2007.

[37] Jing Kang and Lars Dähne. Strong Response of Multilayer Polyelectrolyte Films to Cationic Surfactants. Langmuir, 27:4627–4634, 2011.

[38] Baowei SU, Tingting Wang, Zongwen Wang, Xueli Gao, and Congjie Gao. Preparation and performance of dynamic layer-by-layer PDADMAC/PSS nanofiltration membrane. Journal of Membrane Science, 423:324–331, 2012.

[39] Richard a. McAloney, Vyacheslav Dudnik, and M. Cynthia Goh. Kinetics of salt-induced annealing of a polyelectrolyte multilayer film morphology. Langmuir, 19(9):3947–3952, 2003.

[40] a J Milling and K Kendall. Depletion, Adsorption, and Structuring of Sodium Poly(acrylate) at the Water-Silica Interface. 1. An Atomic Force Microscopy Force Study. Langmuir, 16:5106–5115, 2000.

[41] Per M. Claesson, Evgeni Poptoshev, Eva Blomberg, and Andra Dedinaite. Polyelectrolyte-mediated surface interactions. Advances in Colloid and Interface Science, 114-115:173–187, 2005.

[42] Paul Rouster. Layer-by-Layer modification of nanofiltration membranes: development of a regenerable separation layer. PhD thesis, University of Strasbourg, 2015.

[43] Joseph B. Schlenoff, Hiep Ly, and Ming Li. Charge and mass balance in polyelectrolyte multilayers. Journal of the American Chemical Society, 120 (30):7626–7634, 1998.

[44] S. S. Shiratori and M. F. Rubner. pH-dependent thickness behavior of sequentially adsorbed layers of weak polyelectrolytes. Macromolecules, 33(11): 4213–4219, 2000.

[45] Wanqin Jin, Ali Toutianoush, and Bernd Tieke. Size- and charge-selective transport of aromatic compounds across polyelectrolyte multilayer membranes. Applied Surface Science, 246(4):444–450, 2005.

[46] Xiaoyun Liu and Merlin L. Bruening. Size-Selective Transport of Uncharged Solutes through Multilayer Polyelectrolyte Membranes. Chemistry of Materials, 16(2):351–357, 2004.

[47] G Decher and J D Hong. Buildup of Ultrathin Multilayer Films by a Self-Assembly Process, 1. Consecutive Adsorption of Anionic and Cationic Bipolar Amphiphiles on Charged Surfaces. Makromolekulare Chemie-Macromolecular Symposia, 46:321–327, 1991.

[48] Joseph B. Schlenoff, Stephan T. Dubas, and Tarek Farhat. Sprayed polyelectrolyte multilayers. Langmuir, 16(26):9968–9969, 2000.

[49] J. Cho, K. Char, J. D. Hong, and K. B. Lee. Fabrication of highly ordered multilayer films using a spin self-assembly method. Advanced Materials, 13 (14):1076–1078, 2001.

[50] Jinhan Cho, Seung Heon Lee, Huiman Kang, Kookheon Char, Japil Koo, Byoung Hoon Seung, and Ki Bong Lee. Quantitative analysis on the adsorbed amount and structural characteristics of spin self-assembled multilayer films. Polymer, 44(18):5455–5459, 2003.

[51] Jozef Kochan, Thomas Wintgens, John Erik Wong, and Thomas Melin. Properties of polyethersulfone ultrafiltration membranes modified by polyelectrolytes. Desalination, 250(3):1008–1010, 2010.

[52] Jozef Kochan, Marco Scheidle, Joost van Erkel, Matías Bikel, Jochen Büchs, John Erik Wong, Thomas Melin, and Matthias Wessling. Characterization of antibacterial polyethersulfone membranes using the respiration activity monitoring system (RAMOS). Water Research, 46(16):5401–5409, 2012.

[53] Chaoyi Ba, David A. Ladner, and James Economy. Using polyelectrolyte coatings to improve fouling resistance of a positively charged nanofiltration membrane. Journal of Membrane Science, 347(1-2):250–259, 2010.

[54] G Zhang, W Gu, S Ji, Z Liu, Y Peng, and Z Wang. Preparation of Polyelectrolyte Multilayer Membranes by Dynamic Layer-by-Layer Process for Pervaporation Separation of Alcohol/Water Mixtures. Journal of Membrane Science, 280:727–733, 2006.

[55] Haiqi Tang, Shulan Ji, Lili Gong, Hongxia Guo, and Guojun Zhang. Tubular ceramic-based multilayer separation membranes using spray layer-by-layer assembly. Polymer Chemistry, 4(23):5621, 2013.

[56] Farid Fadhillah, S M Javaid Zaidi, Zafarullah Khan, Mazen Khaled, and Paula T Hammond. Reverse osmosis desalination membrane formed from weak polyelectrolytes by spin assisted layer by layer technique. Desalination and Water Treatment, 34(1-3):44–49, 2011.

[57] F. Fadhillah, S. M J Zaidi, Z. Khan, M. M. Khaled, F. Rahman, and P. T. Hammond. Development of polyelectrolyte multilayer thin film composite membrane for water desalination application. Desalination, 318:19–24, 2013.

[58] G Zhang, X Song, S Ji, N Wang, and Z Liu. Self-Assembly of Inner Skin Hollow Fiber Polyelectrolyte Multilayer Membranes by a Dynamic Negative Pressure Layer-by-Layer Technique. Journal of Membrane Science, 325:109–116, 2008.

[59] Chang Liu, Lei Shi, and Rong Wang. Enhanced hollow fiber membrane performance via semi-dynamic layer-by-layer polyelectrolyte inner surface deposition for nanofiltration and forward osmosis applications. Reactive and Functional Polymers, 86:154–160, 2015.

[60] C. Porcel, Ph Lavalle, G. Decher, B. Senger, J. C. Voegel, and P. Schaaf. Influence of the polyelectrolyte molecular weight on exponentially growing multilayer films in the linear regime. Langmuir, 23(4):1898–1904, 2007.

[61] Polina Dobromirova Peeva, Nina Million, and Mathias Ulbricht. Factors affecting the sieving behavior of anti-fouling thin-layer cross-linked hydrogel polyethersulfone composite ultrafiltration membranes. Journal of Membrane Science, 390-391:99–112, 2012.

[62] Sven Frost and Mathias Ulbricht. Thermoresponsive ultrafiltration membranes for the switchable permeation and fractionation of nanoparticles. Journal of Membrane Science, 448:1–11, 2013.

[63] Daniel Menne, Fee Pitsch, John E Wong, Andrij Pich, and Matthias Wessling. Temperature-modulated water filtration using microgel-functionalized hollow-fiber membranes. Angewandte Chemie (International ed. in English), 53(22):5706–10, 2014. doi: 10.1002/anie.201400316.

[64] Irena Gancarz, Gryzelda Pozniak, and Marek Bryjak. Modification of polysulfone membranes 3 . Effect of nitrogen plasma. European Polymer Journal, 36:1563–1569, 2000.

[65] Lu Ouyang, David M. Dotzauer, Seth R. Hogg, Jorge Macanás, Jean Francois Lahitte, and Merlin L. Bruening. Catalytic hollow fiber membranes prepared using layer-by-layer adsorption of polyelectrolytes and metal nanoparticles. Catalysis Today, 156(3-4):100–106, 2010.

[66] Saeid Rajabzadeh, Chang Liu, Lei Shi, and Rong Wang. Preparation of low-pressure water softening hollow fiber membranes by polyelectrolyte deposition with two bilayers. Desalination, 344:64–70, 2014.

[67] Kwun Lun Cho, Anita J. Hill, Frank Caruso, and Sandra E. Kentish. Chlorine Resistant Glutaraldehyde Crosslinked Polyelectrolyte Multilayer Membranes for Desalination. Advanced Materials, 27:2791–2796, 2015.

[68] F van Ackern, L Krasemann, and B Tieke. Ultrathin membranes for gas separation and pervaporation prepared upon electrostatic self-assembly of polyelectrolytes. Thin Solid Films, 327:762–766, 1998.

[69] D Sullivan and M Bruening. Ultrathin, cross-linked polyimide pervaporation membranes prepared from polyelectrolyte multilayers. Journal of Membrane Science, 248(1-2):161–170, 2005.

[70] Nithya Joseph, Pejman Ahmadiannamini, Pulluru Sai Jishna, Alexander Volodin, and Ivo F J Vankelecom. 'Up-scaling' potential for polyelectrolyte multilayer membranes. Journal of Membrane Science, 492:271–280, 2015.

[71] Joris de Grooth, Brian Haakmeester, Carlos Wever, Jens Potreck, Wiebe M. de Vos, and Kitty Nijmeijer. Long term physical and chemical stability of polyelectrolyte multilayer membranes. Journal of Membrane Science, 489: 153–159, 2015.

[72] Xianfeng Li, Ward Goyens, Pejman Ahmadiannamini, Willem Vanderlinden, Steven De Feyter, and Ivo Vankelecom. Morphology and performance of solvent-resistant nanofiltration membranes based on multilayered polyelectrolytes: Study of preparation conditions. Journal of Membrane Science, 358(1):150–157, 2010.

[73] Pejman Ahmadiannamini, Xianfeng Li, Ward Goyens, Nithya Joseph, Boudewijn Meesschaert, and Ivo F.J. Vankelecom. Multilayered polyelectrolyte complex based solvent resistant nanofiltration membranes prepared from weak polyacids. Journal of Membrane Science, 394:98–106, 2012.

[74] Pejman Ahmadiannamini, Merlin L. Bruening, and Volodymyr V. Tarabara. Sacrificial polyelectrolyte multilayer coatings as an approach to membrane fouling control: Disassembly and regeneration mechanisms. Journal of Membrane Science, 491:149–158, 2015.

[75] Shazia Ilyas, Joris de Grooth, Kitty Nijmeijer, and Wiebe M. De Vos. Multifunctional polyelectrolyte multilayers as nanofiltration membranes and as sacrificial layers for easy membrane cleaning. Journal of Colloid and Interface Science, 446:365–372, 2015.

[76] T Melin and R Rautenbach. Membranverfahren: Grundlagen der Modul- und Anlagenauslegung. VDI-Buch. Springer Berlin Heidelberg, 3 edition, 2007. ISBN 9783540343288.

[77] J. Radjenovic, M. Petrovic, F. Ventura, and D. Barcelo. Rejection of pharmaceuticals in nanofiltration and reverse osmosis membrane drinking water treatment. Water Research, 42(14):3601–3610, 2008.

[78] Yunlong Luo, Wenshan Guo, Huu Hao Ngo, Long Duc Nghiem, Faisal Ibney Hai, Jian Zhang, Shuang Liang, and Xiaochang C. Wang. A review on the occurrence of micropollutants in the aquatic environment and their fate and removal during wastewater treatment. Science of the Total Environment, 473-474:619–641, 2014.

[79] Nidal Hilal, H. Al-Zoubi, N. A. Darwish, A. W. Mohammad, and M. Abu Arabi. A comprehensive review of nanofiltration membranes: Treatment, pretreatment, modelling, and atomic force microscopy. Desalination, 170 (3):281–308, 2004.

[80] A. Gorenflo, D. Velázquez-Padrón, and F. H. Frimmel. Nanofiltration of a German groundwater of high hardness and NOM content: Performance and costs. Desalination, 151(3):253–265, 2003.

[81] B. Van Der Bruggen, K. Everaert, D. Wilms, and C. Vandecasteele. Application of nanofiltration for removal of pesticides, nitrate and hardness from ground water: Rejection properties and economic evaluation. Journal of Membrane Science, 193(2):239–248, 2001.

[82] J.C. Schippers and J. Verdouw. The modified fouling index, a method of determining the fouling characteristics of water. Desalination, 32:137–148, 1980.

[83] Stergios G. Yiantsios and Anastasios J. Karabelas. An assessment of the Silt Density Index based on RO membrane colloidal fouling experiments with iron oxide particles. Desalination, 151(3):229–238, 2003.

[84] A. Alhadidi, A.J.B Kemperman, B. Blankert, J.C. Schippers, M. Wessling, and W.G.J. van der Meer. Silt Density Index and Modified Fouling Index relation, and effect of pressure, temperature and membrane resistance. Desalination, 273(1):48–56, 2011.

[85] H.C. van der Horst, J.M.K. Timmer, T. Robbertsen, and J. Leenders. Use of nanofiltration for concentration and demineralization in the dairy industry. Journal of Membrane Science, 104:205 – 218, 1993.

[86] Athanasios K. Goulas, Petros G. Kapasakalidis, Haydn R. Sinclair, Robert A. Rastall, and Alistair S. Grandison. Purification of oligosaccharides by nanofiltration. Journal of Membrane Science, 209(1):321–335, 2002. ISSN 03767388. doi: 10.1016/S0376-7388(02)00362-9.

[87] Andrea Hinkova, Zdenek Bubník, Pavel Kadlec, and Jaroslav Pridal. Potentials of separation membranes in the sugar industry. Separation and

Purification Technology, 26(1):101–110, 2002. ISSN 13835866. doi: 10.1016/S1383-5866(01)00121-6.

[88] Manohar Kalyanpur. Downstream Processing in the Biotechnology Industry. Molecular Biotechnology, 22(3), 2002.

[89] Mika Mänttäri, Teuvo Pekuri, and Marianne Nyström. NF270, a new membrane having promising characteristics and being suitable for treatment of dilute effluents from the paper industry. Journal of Membrane Science, 242 (1-2):107–116, 2004.

[90] Mika Mänttäri, Katja Viitikko, and Marianne Nyström. Nanofiltration of biologically treated effluents from the pulp and paper industry. Journal of Membrane Science, 272(1-2):152–160, 2006.

[91] C. Tang and V. Chen. Nanofiltration of textile wastewater for water reuse. Desalination, 143(1):11–20, 2002. ISSN 00119164.

[92] S. Chakraborty, M. K. Purkait, S. DasGupta, S. De, and J. K. Basu. Nanofiltration of textile plant effluent for color removal and reduction in COD. Separation and Purification Technology, 31(2):141–151, 2003.

[93] W. Richard Bowen, Abdul Wahab Mohammad, Nidal Hilal, and W Richard. Characterisation of nanofiltration membranes for predictive purposes - use of salts , uncharged solutes and atomic force microscopy. Journal of Membrane Science, 126:91–105, 1997.

[94] Pierre Aimar, John A. Howell, Michael J. Clifton, and Victor Sanchez. Concentration polarisation build-up in hollow fibers: a method of measurement and its modelling in ultrafiltration. Journal of Membrane Science, 59(1): 81–99, 1991.

[95] P. Prádanos, J. I. Arribas, and A Hernández. Mass transfer coefficient and retention of PEGs in low pressure cross-flow ultrafiltration through asymmetric membranes. Journal of Membrane Science, 99:1–20, 1995.

[96] Conan J. Fee and James M. Van Alstine. Prediction of the viscosity radius and the size exclusion chromatography behavior of PEGylated proteins. Bioconjugate Chemistry, 15(6):1304–1313, 2004.

[97] W.J.C. van de Ven, K. van't Sant, I.G.M. Pünt, A. Zwijnenburg, A.J.B. Kemperman, W.G.J. van der Meer, and M. Wessling. Hollow fiber dead-end ultrafiltration: Influence of ionic environment on filtration of alginates. Journal of Membrane Science, 308(1-2):218–229, 2008.

[98] W. Kern and D. Puotinen. Layer-by-layer preparation of polyelectrolyte multilayer membranes for separation. RCA Rev., 31:187–206, 2014.

[99] S. Schwarz, H. M. Buchhammer, K. Lunkwitz, and H. J. Jacobasch. Polyelectrolyte adsorption on charged surfaces: Study by electrokinetic measurements. Colloids and Surfaces A: Physicochemical and Engineering Aspects, 140:377–384, 1998.

[100] Akhil K. Sen, Sandip Roy, and Vinay A. Juvekar. On the Importance of Purification of Sodium Polystyrene Sulfonate. ISRN Analytical Chemistry, 2012:1–5, 2012.

[101] Jan-Michael Carrillo and Andrey Dobrynin. Salt Effect on Osmotic Pressure of Polyelectrolyte Solutions: Simulation Study. Polymers, 6:1897–1913, 2014.

[102] Akira Takahashi, Narundo Kato, and Mitsuru Nagasawa. The Osmotic Pressure of Polyelectrolyte in Neutral Salt Solutions. The Journal of Physical Chemistry, 74:944–946, 1970.

[103] Bo Zhang, Dahong Yu, Hong-Lai Liu, and Ying Hu. Osmotic Coefficients of Polyelectrolyte Solutions, Measurements and Correlation. Polymer, 43: 2975–2980, 2002.

[104] Yongwoo Shin, James E Roberts, and Maria M Santore. The relationship between polymer/substrate charge density and charge overcompensation by adsorbed polyelectrolyte layers. Journal of Colloid and iIterface Science, 247:220–230, 2002.

[105] G. Bargeman, J. B. Westerink, O. Guerra Miguez, and M. Wessling. The effect of NaCl and glucose concentration on retentions for nanofiltration membranes processing concentrated solutions. Separation and Purification Technology, 134:46–57, 2014.

[106] Johan Schaep, Bart Van der Bruggen, Carlo Vandecasteele, and Dirk Wilms. Influence of ion size and charge in nanofiltration. Separation and Purification Technology, 14(1-3):155–162, 1998.

[107] Johan Schaep, Carlo Vandecasteele, A. Wahab Mohammad, and W. Richard Bowen. Analysis of the Salt Retention of Nanofiltration Membranes Using the Donnan-Steric Partitioning Pore Model. Separation Science and Technology, 34(15):3009–3030, 1999.

[108] Johan Schaep, Carlo Vandecasteele, A.Wahab Mohammad, and W. Richard Bowen. Modelling the retention of ionic components for different nanofiltration membranes. Separation and Purification Technology, 22-23(1-2): 169–179, 2001.

[109] DOW. Product Information DOW FILMTEC - Membranes DOW FILMTEC NF270-400 Nanofiltration Element.

[110] H. Al-Zoubi, N. Hilal, N.A. Darwish, and A.W. Mohammad. Rejection and modelling of sulphate and potassium salts by nanofiltration membranes: neural network and Spiegler–Kedem model. Desalination, 206(1-3):42–60, 2007.

[111] Margarida Ribau Teixeira, Maria Joao Rosa, and Marianne Nyström. The role of membrane charge on nanofiltration performance. Journal of Membrane Science, 265(1-2):160–166, 2005.

[112] GE Power & Water. DK Series - Industrial High Rejection Nanofiltration Elements, 2010.

[113] GE Power & Water. Hl series - Water Softening NF Elements, 2008.

[114] Ting-Ting Dong, Guo-Hua Chen, and Cong-Jie Gao. Preparation of chitin xanthate/polyacrylonitrile NF composite membrane with cross-linking agent hydrogen peroxide and its characterization. Journal of Membrane Science, 304:33–39, 2007.

[115] Maneesha Adusumilli and Merlin L. Bruening. Variation of ion-exchange capacity, zeta potential, and ion-transport selectivities with the number of layers in a multilayer polyelectrolyte film. Langmuir, 25(13):7478–7485, 2009.

[116] V.N. Mynin and G.V. Terpugov. Purification of waste water from heavy metals by using ceramic membranes and natural polyelectrolytes. Desalination, 119(1-3):361–362, 1998.

[117] Li Xu, Wenping Li, Shuqun Lu, Zhi Wang, Qixin Zhu, and Yi Ling. Treating dyeing waste water by ceramic membrane in crossflow microfiltration. Desalination, 149(1-3):199–203, 2002.

[118] Xiaojiang Fan, Yi Tao, Lingyun Wang, Xihui Zhang, Ying Lei, Zhuo Wang, and Hiroshi Noguchi. Performance of an integrated process combining ozonation with ceramic membrane ultra-filtration for advanced treatment of drinking water. Desalination, 335(1):47–54, 2014.

[119] Xihui Zhang, Jianning Guo, Lingyun Wang, Jiangyong Hu, and Jia Zhu. In situ ozonation to control ceramic membrane fouling in drinking water treatment. Desalination, 328:1–7, 2013.

[120] S. E. Weschenfelder, A. C C Mello, C. P. Borges, and J. C. Campos. Oilfield produced water treatment by ceramic membranes: Preliminary process cost estimation. Desalination, 360:81–86, 2015.

[121] Silvio E. Weschenfelder, Ana M T Louvisse, Cristiano P. Borges, Elena Meabe, Javier Izquierdo, and Juacyara C. Campos. Evaluation of ceramic membranes for oilfield produced water treatment aiming reinjection in offshore units. Journal of Petroleum Science and Engineering, 131:51–57, 2015.

[122] Patricia Meyer, Alexander Mayer, and Ulrich Kulozik. High concentration of skim milk proteins by ultrafiltration: Characterisation of a dynamic membrane system with a rotating membrane in comparison with a spiral wound membrane. International Dairy Journal, 51:75–83, 2015.

[123] Stefanie Zeidler, Petra Puhlfürß, Uwe Kätzel, and Ingolf Voigt. Preparation and characterization of new low MWCO ceramic nanofiltration membranes for organic solvents. Journal of Membrane Science, 470:421–430, 2014.

[124] Sareh Rezaei Hosseinabadi, Kenny Wyns, Anita Buekenhoudt, Bart Van der Bruggen, and Dominic Ormerod. Performance of Grignard functionalized ceramic nanofiltration membranes. Separation and Purification Technology, 147:320–328, 2015.

[125] Lu Ouyang, Ramamoorthy Malaisamy, and Merlin L. Bruening. Multilayer polyelectrolyte films as nanofiltration membranes for separating monovalent and divalent cations. Journal of Membrane Science, 310(1-2):76–84, 2008.

[126] Seong Uk Hong, Matthew D. Miller, and Merlin L. Bruening. Removal of Dyes, Sugars, and Amino Acids from NaCl Solutions Using Multilayer Polyelectrolyte Nanofiltration Membranes. Industrial & Engineering Chemistry Research, 45(18):6284–6288, 2006.

[127] Mag Dahlgren and Asa Waltermo. Salt effects on the interaction between adsorbed cationic polyelectrolyte layers: theory and experiment. The Journal of Physical Chemistry A, 97:11769–11775, 1993.

[128] Oded Nir, Tony Trieu, Sebastian Bannwarth, and Matthias Wessling. Microfiltration of deformable microgels. Soft Matter, 12(31):6512–6517, 2016.

[129] M Frank, G Bargeman, A Zwijnenburg, and M Wessling. Capillary hollow fiber nanofiltration membranes. Separation and Purification Technology, 22–23:499 – 506, 2001.

[130] Wenqian Shan, Patrice Bacchin, Pierre Aimar, Merlin L. Bruening, and Volodymyr V. Tarabara. Polyelectrolyte multilayer films as backflushable nanofiltration membranes with tunable hydrophilicity and surface charge. Journal of Membrane Science, 349(1-2):268–278, 2010.

[131] Changyou Gao, Stefano Leporatti, Sergio Moya, Edwin Donath, and Helmuth Möhwald. Swelling and shrinking of polyelectrolyte microcapsules in response to changes in temperature and ionic strength. Chemistry, 9(4): 915–20, 2003.

[132] Joseba Irigoyen, Nikolaos Politakos, Richard Murray, and Sergio E. Moya. Design and Fabrication of Regenerable Polyelectrolyte Multilayers for Applications in Foulant Removal. Macromolecular Chemistry and Physics, 215 (16):1543–1550, 2014.

[133] M. Kallioinen, T. Sainio, J. Lahti, A. Pihlajamäki, H. Koivikko, J. Mattila, and M. Mänttäri. Effect of extended exposure to alkaline cleaning chemicals on performance of polyamide (PA) nanofiltration membranes. Separation and Purification Technology, 158:115–123, 2016.

[134] Mayur Dalwani, Gerrald Bargeman, Seyed Schwan Hosseiny, Marcel Boerrigter, Matthias Wessling, and Nieck E. Benes. Sulfonated poly(ether ether ketone) based composite membranes for nanofiltration of acidic and alkaline media. Journal of Membrane Science, 381(1-2):81–89, 2011.

[135] Kurosch Rezwan, Lorenz P. Meier, and Ludwig J. Gauckler. A prediction method for the isoelectric point of binary protein mixtures of bovine serum albumin and lysozyme adsorbed on colloidal titania and alumina particles. Langmuir, 21(8):3493–3497, 2005.

[136] Ingmar H. Huisman, Gun Trägårdh, Christian Trägårdh, and Arto Pihlajamäki. Determining the zeta-potential of ceramic microfiltration membranes using the electroviscous effect. Journal of Membrane Science, 147(2): 187–194, 1998.

[137] Tobias Klement and Jochen Büchs. Itaconic acid - A biotechnological process in change. Bioresource Technology, 135:422–431, 2013.

[138] Pooya Azadi, Oliver R. Inderwildi, Ramin Farnood, and David A. King. Liquid fuels, hydrogen and chemicals from lignin: A critical review. Renewable and Sustainable Energy Reviews, 21:506–523, 2013.

[139] Charles M. Cai, Taiying Zhang, Rajeev Kumar, and Charles E. Wyman. Integrated furfural production as a renewable fuel and chemical platform from lignocellulosic biomass. Journal of Chemical Technology and Biotechnology, 89(1):2–10, 2014.

[140] Serafin Stiefel, Jonas Lölsberg, Lukas Kipshagen, Robin Müller-Gulland, and Matthias Wessling. Controlled depolymerization of lignin in an electrochemical membrane reactor. Electrochemistry Communications, 61:49–52, 2015.

[141] S. Stiefel, C. Marks, T. Schmidt, S. Hanisch, G. Spalding, and M. Wessling. Overcoming lignin heterogeneity: reliably characterizing the cleavage of technical lignin. Green Chem., 18:531, 2016.

[142] Mario Batti and Leonard B Schweiger. Process for the production of itaconic acid, 1963.

[143] Tobias Klement, Sofia Milker, Gernot Jager, Philipp M Grande, Pablo Dominguez de Maria, and Jochen Buchs. Biomass pretreatment affects *Ustilago maydis* in producing itaconic acid. Microbial Cell Factories, 11: 43, 2012.